

การพัฒนาเทคนิคอย่างง่ายสำหรับการตรวจวัดการกระจายขนาดของฝุ่นกัมมันตรังสีของธาตุลูก
เรดอนและโทรอนเพื่อใช้ในการประเมินปริมาณรังสี

นางสาว ชุติมา กรานรอด

วิทยานิพนธ์นี้เป็นส่วนหนึ่งของการศึกษาตามหลักสูตรปริญญาวิทยาศาสตรดุษฎีบัณฑิต

สาขาวิชาวิศวกรรมนิวเคลียร์ ภาควิชานิวเคลียร์เทคโนโลยี

คณะวิศวกรรมศาสตร์ จุฬาลงกรณ์มหาวิทยาลัย

ปีการศึกษา 2553

ลิขสิทธิ์ของจุฬาลงกรณ์มหาวิทยาลัย


**DEVELOPMENT OF A SIMPLE TECHNIQUE FOR MEASURING
THE ACTIVITY SIZE DISTRIBUTION OF ATTACHED RADON
AND THORON PROGENY FOR DOSE ASSESSMENT**

Miss Chutima Kranrod

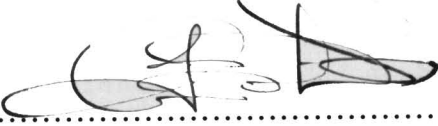
**A Dissertation Submitted in Partial Fulfillment of the Requirements
for the Degree of Doctor of Engineering Program in Nuclear Engineering
Department of Nuclear Technology
Faculty of Engineering
Chulalongkorn University
Academic year 2010
Copyright of Chulalongkorn University**

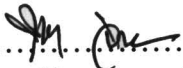
Thesis Title DEVELOPMENT OF A SIMPLE TECHNIQUE
FOR MEASURING THE ACTIVITY SIZE
DISTRIBUTION OF ATTACHED RADON AND
THORON PROGENY FOR DOSE ASSESSMENT
By Miss Chutima Kranrod
Field of Study Nuclear Engineering
Thesis Advisor Associate Professor Supitcha Chanyotha, Ph.D.
Thesis Co-Advisor Professor Shinji Tokonami, Ph.D.,
 Associate Professor Nares Chankow, M.Eng.

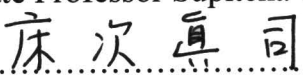
Accepted by the Faculty of Engineering, Chulalongkorn University in
Partial Fulfillment of the Requirements for the Doctoral Degree



..... Dean of the Faculty of Engineering
(Associate Professor Boonsom Lerdkhironwong, Dr.Eng.)

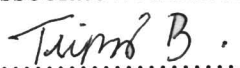
THESIS COMMITTEE



..... Chairman
(Associate Professor Sunchai Nilsuwankosit, Ph.D.)



..... Thesis Advisor
(Associate Professor Supitcha Chanyotha, Ph.D.)


..... Thesis Co-Advisor
(Professor Shinji Tokonami, Ph.D.)


..... Thesis Co-Advisor
(Associate Professor Nares Chankow, M.Eng.)


..... Examiner
(Associate Professor Tripob Bhongsuwan, Ph.D.)


..... Examiner
(Mr. Phongphaeth Pengvanich, Ph.D.)


..... External Examiner
(Mrs. Wanna Wimolwattanapun, Ph.D.)

ชุติมา กรานรอด : การพัฒนาเทคนิคอย่างง่ายสำหรับการตรวจวัดการกระจายขนาดของฝุ่นกัมมันตรังสีของธาตุลูกเรดอน และโทรอนเพื่อใช้ในการประเมินปริมาณรังสี. (DEVELOPMENT OF A SIMPLE TECHNIQUE FOR MEASURING THE ACTIVITY SIZE DISTRIBUTION OF ATTACHED RADON AND THORON PROGENY FOR DOSE ASSESSMENT) อ. ที่ปรึกษาวิทยานิพนธ์หลัก : รศ. ดร. สุพิชชา จันทโรยธา, อ. ที่ปรึกษาวิทยานิพนธ์ร่วม : ศ. ดร. ชินจิ โทโกนามิ, รศ. ดร. นเรศร์ จันทน์ขาว, 106 หน้า.

การพัฒนาเทคนิคใหม่สำหรับการตรวจวัดการกระจายขนาดของฝุ่นกัมมันตรังสีของธาตุลูกเรดอน และ โทรอน อย่างมีประสิทธิภาพและเหมาะสมกับสภาวะแวดล้อม ได้เลือกและปรับปรุง impactor สำหรับเก็บตัวอย่างฝุ่นขนาดพวกพา ที่ประกอบด้วยชั้นแยกเก็บตัวอย่างตามขนาดจำนวน 4 ชั้น และชั้นสำหรับกระดาศกรอง 1 ชั้น โดยสามารถคัดแยกขนาดอนุภาคของฝุ่นได้ในช่วง 0.5-10 ไมโครเมตร ที่ flow-rate 4 ลิตรต่อนาที และได้ใช้ CR-39 วัสดุรังสีแอลฟาจากฝุ่นรังสีของธาตุลูกหลานเรดอน และโทรอน และในการตรวจวัดเพื่อคัดแยกธาตุลูกเรดอนและโทรอนนั้นจะใช้ แผ่นไมลาอลูมิเนียมตามความหนาที่เหมาะสมกับพลังงานของแอลฟาที่ถูกปลดปล่อยจากธาตุลูกเรดอน และโทรอนให้ทำอันตรกิริยาบน CR-39 และได้ติดตั้งสกิน (ตารางเหล็ก) ขนาด 400 mesh ไว้ตรงทางเข้าของอากาศ ด้านบน impactor เพื่อป้องกัน unattached fraction ของลูกหลานเรดอนและโทรอน

นอกจากนี้ได้ทำการหาประสิทธิภาพการจับกับฝุ่นกัมมันตรังสีของ impactor โดยผลิตฝุ่นในช่วงขนาดตั้งแต่ 0.1 - 1.23 ไมโครเมตร และได้พบว่าการที่ได้มีลักษณะเป็นรูปดาวเอส และคล้ายคลึงกันในชั้นที่สาม และสี่

จากนั้น ได้ศึกษาปัจจัยต่าง ๆ ที่มีอิทธิพลต่อการวัดการกระจายขนาดของฝุ่นกัมมันตรังสีของธาตุลูกเรดอนและโทรอน ได้แก่ ความชื้นสัมพัทธ์ ($\approx 30-90\%$), อุณหภูมิ ($\approx 5-30\text{ }^{\circ}\text{C}$), unattached progeny และการเปลี่ยนแปลงของ air flow-rate ($\approx 12-75\%$) ผลจากการศึกษาพบว่ามีแนวโน้มของการสะสมตัวของ unattached radon progeny บน impactor ชั้นที่ 1 และ 2 สำหรับปัจจัยอื่น เช่น ความชื้นสัมพัทธ์, อุณหภูมิ, และการเปลี่ยนแปลงของ air flow-rate ที่ประมาณ 20-40% นั้นแทบไม่มีผลต่อการเปลี่ยนแปลงของค่า Activity Median Aerodynamic Diameter (AMAD).

ได้ตรวจสอบความถูกต้องของเทคนิคที่พัฒนาขึ้นนี้กับเครื่องมือที่นิยมใช้ในการตรวจวัดการกระจายขนาดของฝุ่นกัมมันตรังสี และผลจากการตรวจสอบทำให้มั่นใจได้ว่าค่าการกระจายตัวของฝุ่นกัมมันตรังสีของธาตุลูกเรดอน และโทรอนที่ได้จากเทคนิคที่พัฒนาขึ้นสามารถนำไปใช้ในการประเมินปริมาณรังสีได้จริง นอกจากนี้ยังได้มีการทดสอบเทคนิคที่พัฒนาขึ้นในการตรวจวัดภาคสนามเพื่อใช้ในการประเมินปริมาณรังสีที่คนงานได้รับภายในโรงงานอุตสาหกรรมที่เกี่ยวข้องกับการใช้สารกัมมันตรังสีตามธรรมชาติแห่งหนึ่งในจังหวัดภูเก็ต

ภาควิชาวิศวกรรมเทคโนโลยี.....ลายมือชื่อนิสิต.....ชุติมา กรานรอด
 สาขาวิชาวิศวกรรมนิวเคลียร์.....ลายมือชื่อ อ.ที่ปรึกษาวิทยานิพนธ์หลัก.....สุพิชชา จันทโรยธา
 ปีการศึกษา 2553.....ลายมือชื่อ อ.ที่ปรึกษาวิทยานิพนธ์ร่วม.....ชินจิ โทโกนามิ
 ลายมือชื่อ อ.ที่ปรึกษาวิทยานิพนธ์ร่วม.....นเรศร์ จันทน์ขาว

4971809021 : MAJOR NUCLEAR ENGINEERING

KEYWORDS : ACTIVITY SIZE DISTRIBUTION /IMPACTOR/ ATTACHED RADON PROGENY / ATTACHED THORON PROGENY / ACTIVITY MEDIAN DIAMETER / DOSE ASSESSMENT

CHUTIMA KRANROD : DEVELOPMENT OF A SIMPLE TECHNIQUE FOR MEASURING THE ACTIVITY SIZE DISTRIBUTION OF ATTACHED RADON AND THORON PROGENY FOR DOSE ASSESSMENT. THESIS ADVISOR : ASSOC. PROF. SUPITCHA CHANYOTHA, Ph.D., THESIS CO-ADVISOR : PROF. SHINJI TOKONAMI, Ph.D., ASSOC. PROF. NARES CHANKOW, 106 PP.

A new portable type cascade impactor has been developed to determine the activity size distribution of radon and thoron progeny in a natural environment more efficiently. The modified impactor consists of 4 stages with a back up filter stage for the collection of aerosol samples. The aerosol cut points in the impactor are set for 10, 2.5, 1 and 0.5 μm at a flow rate of 4 L min^{-1} . Five CR-39 chips were used as alpha detectors for each stage. In order to separate α particles emitted from radon and thoron progeny, CR-39 detectors are covered with aluminum-vaporized Mylar films. Thickness of each film is properly adjusted to allow α particles emitted from radon and thoron progeny to reach the CR-39 detectors. In addition, a 400-mesh metal wire screen is mounted as diffusion collector at the air inlet of the impactor to remove the unattached fraction of radon and thoron decay products. Furthermore, the particle cutoff characteristics of each stage was determined by mono-disperse aerosols particle size ranging from 0.1-1.23 μm from the collection efficiency curve. The cutoff characteristics were found to be similar for stage 3 and 4 only. We have investigated the influence of relative humidity (30-90%), temperature (5-30°C), unattached progeny, and air sampling at different flow-rates (\approx 12-75%) for the sensitivity of the developed technique whereas activity median aerodynamic diameter (AMAD) is not much affected due to change in relative humidity, temperature and air flow-rate from 20-40%. The results showed that high-unattached radon progeny enhanced deposition effect at stage 1 and 2 of impactor. Validation of the technique was performed with the commercial devices and results confirmed that the developed technique can provide significant information to estimate the activity size distribution of attached radon and thoron progeny for dose assessment.

The develop technique has been successfully tested in field studies especially inside a NORM industry in Phuket to estimate doses at working environment.

Department : Nuclear Technology

Field of Study : Nuclear Engineering

Academic Year : 2010

Student's Signature Chutima Kranrod.

Advisor's Signature [Signature]

Co-Advisor's Signature [Signature]

Co-Advisor's Signature Nares Chankow

Acknowledgment

The author would like to express her deepest gratitude to Associate Professor Dr. Supitcha Chanyotha, for her kind academic guidance, support and warm encouragement throughout the entire period of doctoral dissertation studies.

Earnest gratefulness is also attributed to co-advisors Professor Dr. Shinji Tokonami and Associate Professor Nares Chankow, for their understanding, expert suggestions and sincere support throughout the study period.

The author also would like to gratefully articulate her heartfelt appreciations to Dr. Tetsuo Ishikawa, National Institute Radiological Science (NIRS), Japan for his support and advices throughout the research period in Japan. Sincere thanks are also due to Dr. Atsuyuki Sorimachi and Mr. Yoshio Ohuchi (NIRS) for their help and co-operations while conducting experiments and for solving many problems during the research period in Japan.

The author also likes to convey her hearty appreciations to Dr. Sarat Sahoo (NIRS), for his scientific suggestions and supportive guidance during her stay at NIRS.

I am thankful to the Japanese Government (MEXT) Scholarship program for which I could visit Japan to pursue my higher studies. My special thanks are also offered to “National Institute of Radiological Sciences” for providing the radon facilities which is unique in the world to continue my doctoral studies with collaborating with Chulalongkorn University.

The author also likes to extend her thanks Ms. Rawiwan Kritsananuwat, Mrs. Tharawadee Takahashi, Ms. Sawwanee Asavaphatiboom, Mr. Nabil Hassan, Dr. Norbert Kavashi, Dr. Mirek Janik and his family, Mrs. Setsuko Endo and her family, for their constant support and friendly attitude throughout the study.

Finally, it is impossible to express gratitude to one's kith and kin but it is no exaggeration for the author to say that without the invaluable moral support, patient understanding, encouragement and continuous co-operations from her father Mr. Boonchoo Kranrod, mother Mrs. Supa Kranrod, younger brother Mr. Theerawut Kranrod, and all close relatives, this piece of research work would never have been completed.

Contents

	Page
Abstract (Thai).....	iv
Abstract (English).....	v
Acknowledgement.....	vi
Contents.....	vii
List of tables.....	x
List of figures.....	xi
Chapter	
I INTRODUCTION.....	1
1.1 Background on problems of interest.....	1
1.2 Thesis objective.....	3
1.3 Scope and limitation of the study.....	3
1.4 Expected benefit.....	4
1.5 Research methodology.....	4
1.6 Organization and chapter contents.....	4
II THEORY AND LITERATURE REVIEW.....	6
2.1 Radon, thoron and their progeny	6
2.2 Particle size: A significant parameter of radioactive aerosol.....	9
2.2.1 Activity size distribution for radioactive aerosol.....	11
2.2.2 Activity size distribution determination techniques.....	12
2.3 Alpha detector.....	15
2.3.1 Nuclear track detector as radiation detector.....	16
2.3.2 Stopping power, restricted energy loss.....	17
2.4 Dose assessment.....	19
2.4.1 The new ICRP lung model and LUDEP.....	20
2.4.2 Description of LUDEP.....	20
2.4.3 Mathematical approaches used in LUDEP.....	21
2.4.4 Best estimated parameters for calculating dose using LUDEP.....	24
2.4.5 Dependence of dose on radon/thoron progeny.....	25
III PRELIMINARY WORK.....	29
3.1 Study Location.....	29
3.2 Measurement Techniques.....	29
3.3 Measurement Conditions.....	31
3.4 Results and Discussion.....	31

Contents (Continue)

Chapter	Page
3.4.1 Measurement Results.....	31
3.4.2 Estimation of Effective Dose.....	35
3.5 Conclusions.....	36
IV DESIGN AND MODIFICATION OF IMPACTOR, PERFORMANCE TEST AND VALIDATION OF DEVELOPMENT TECHNIQUE.....	38
4.1 Impactor design.....	38
4.1.1 Manufacture of portable cascade impactor.....	40
4.1.2 Modification of the Collection media.....	41
4.2 Performance test of portable impactor.....	42
4.2.1 Discrimination of ^{220}Rn and ^{222}Rn progeny on CR-39 detectors with aluminum-vaporized Mylar films.....	45
4.2.2 Detector efficiency calibration.....	48
4.2.3 Impactor collection efficiency calibration.....	50
4.3 Evaluation parameter that might affect the sensitivity of development technique	56
4.3.1 Humidity.....	60
4.3.2 Temperature.....	61
4.3.3 Unattached progeny.....	61
4.3.4 Changing of air sampling flow rate.....	62
4.4 Validation of development technique.....	63
V FIELD EVALUATION ON ATTACHED RADON AND THORON PROGENY SIZE DISTRIBUTION AND DOSE ASSESSMENT IN THE MINERAL TREATMENT INDUSTRY....	66
5.1 Study location.....	66
5.2 Method and measurement setup.....	66
5.2.1 Determination of attached radon and thoron progeny activity size distribution.....	66
5.2.2 Determination of radon, thoron and their progeny concentration	68
5.3 Results of field survey.....	69
5.3.1 Attached radon and thoron progeny activity size distribution	69
5.3.2 Determination of Equilibrium factor	71

Contents (Continue)

	Page
Chapter	
5.4 Dose assessment.....	71
5.5 Conclusions.....	73
VI SUMMARY AND CONCLUSIONS.....	75
6.1 Conclusions and discussion.....	75
6.2 Suggestions and future studies.....	78
6.3 List of publications.....	79
Reference.....	81
Appendices	
Appendix A: Particle Sizing Method.....	89
Appendix B: Impactors in Particle Size Distribution.....	94
Appendix C: Radiation Detectors.....	102
Biography.....	106

List of Tables

	Page
Table 2-1 The best estimated parameter values for this study.....	25
Table 3-1 Mean (\pm standard deviation) concentrations of radon and its progeny.....	32
Table 3-2 Mean (\pm standard deviation) concentrations of the unattached and total activity concentrations (ranges are given in parentheses).....	34
Table 3-3 Mean values of the activity median aerodynamic diameter (AMAD _i), the geometric standard deviation (σ_{gi}), and the activity fraction (f_i) of log-normal activity size distribution of attached progeny (ranges are given in parentheses).....	35
Table 4-1 Design parameters for portable cascade impactor.....	39
Table 4-2 Film area densities absorber for each channel.....	48
Table 4-3 The average counting efficiency of CR-39.....	49
Table 4-4 The collection efficiency of portable impactor.....	52
Table 4-5 Cut point diameters of each impaction substrate for impactor Stage 3 and 4.....	52
Table 4-6 Sharpness of collection efficiency for stage 3 and 4 of portable impactor as a function of substrate.....	56
Table 4-7 AMAD and σ_g at various relative humidity.....	60
Table 4-8 AMAD and σ_g at various temperature.....	61
Table 4-9 Experimental results for the effect of unattached progeny.....	62
Table 4-10 Experimental resultd for effect of air flow-rate change.....	62
Table 4-11 Verification results of development technique.....	64
Table 4-12 A comparison of dose conversion factor from dosimetric approach..	65
Table 5-1 Sizing information of attached radon and thoron progeny at different places in Thaisarco characterized by the activity median aerodynamic diameter (AMAD) and geometric standard deviations.....	69
Table 5-2 Activity concentration of radon, thoron and their progeny concentration.....	71
Table 5-3 Dose Conversion Factor (DCFs) of attached radon and thoron progeny by LUDEP.....	72
Table 5-4 Annual effective doses at Thaisarco due to exposure of radon thoron and their progeny.....	73

List of Figures

	Page
Figure 2-1 Natural decay series: Uranium-238.....	7
Figure 2-2 Natural decay series: Thorium-232.....	7
Figure 2-3 a) Basic processes of radon decay product behavior in air defining “unattached” and “aerosol-attached” particle activities. b) Processes of ^{218}Po and ^{214}Pb in air.....	8
Figure 2-4 Variation of dose conversion factor from radon progeny (DCF_{RnP}) as a function of AMAD.....	27
Figure 2-5 Variation of dose conversion factor from thoron progeny (DCF_{ThP}) as a function of AMAD.....	28
Figure 3.1 The schematic diagram of unattached radon progeny measuring system.....	31
Figure 3-2 Temporal variations of (a) radon and EECRn , (b) temperature and relative humidity, and (c) air pressure.....	33
Figure 3-3 The activity size distribution of radon progeny (averaged over the study period).....	34
Figure 4-1 Cross-section view of portable cascade impactor	40
Figure 4-2 Picture of portable impactor sampler.....	41
Figure 4-3 Arrangement of the detection channel on the impaction plate.....	41
Figure 4-4 The illustration of reference chambers at NIRS: a) Radon chamber and b) Thoron chamber.....	43
Figure 4-5 Experiment set-up for performance test: a) Radon chamber b) Thoron Chamber.....	44
Figure 4-6 Alpha spectrum results: a) Attenuation of 5.5 MeV from Am-241 b) Attenuation of 7.7 MeV from Pb-214.....	46
Figure 4-7 Relationship between track density and area density of film for cut-off alpha energy 4.2, 6.1 and 7.7 MeV: a) Measuring the alpha particles emitted from aerosols and impinge on CR-39. b) Measuring the alpha particles emitted from the surface of the glass fiber filter and impinges on the CR-39 through an air layer of 22.5 mm.....	47
Figure 4-8 The illustration of detector channel at each impactor plate geometry.	48
Figure 4-9 Experiment procedure for alpha track registration a) Measuring the alpha particles emitted from aerosols and impinge on CR-39. b) Measuring the alpha particles emitted from the surface of the glass fiber filter and impinges on the CR-39 through an air layer of 22.5 mm.....	50
Figure 4-10 A block diagram of aerosol generator.....	52
Figure 4-11 Sampling system for collection efficiency of attached radon progeny.....	53
Figure 4-12 The illustration of instruments for collection efficiency calibration.	54

List of Figures (Continue)

	Page
Figure 4-13 Collection efficiency of stage 3 (1 μm).....	54
Figure 4-14 Collection efficiency of stage 4 (0.5 μm).....	55
Figure 4-15 The illustration of etch pits on the surface of CR-39 at each detection channel of stage 3 (Magnification: 100 \times). Sampling at radon concentration 5000 kBqm-3 and aerosol size 1 mm was generated: a) CH1, b) CH2, c) CH3 and d) CH4.....	57
Figure 4-16 The activity size distribution of radon progeny: a) ELPI, b) MOUDI and c) 4-stage impactor. Sampling at radon concentration 5000 kBqm-3 and aerosol size 1 mm was generated.....	65
Figure 5-1 Location of measurement points at Thaisarco, Phuket, Thailand. a) HSE office, b) Ore sampling area, and c) Production storage area.....	67
Figure 5-2 Illustration of the particle size distribution: a) attached radon progeny size distribution b) attached thoron progeny size distribution.....	70

Chapter I

INTRODUCTION

1.1 Background and problems of interest

The risks to human health posed by ionizing radiation are well known. UNSCEAR [1] reports that the most important sources of ionizing radiation are radon and its decay products because they contribute about 50% of the annual dose received by population. Two isotopes of radon are more concerned for the hazard by inhalation. First is the ^{222}Rn isotope that is commonly known as radon, which arises from the radioactive decay chain of uranium-238. Second is the ^{220}Rn isotope that is usually called thoron, which arises from decay chain of thorium-232. Uranium and thorium are common elements in the earth's crust, rocks and soils. Some fraction of the radon and thoron produce in rocks and soils escape to air. Therefore, radon and thoron are present in the atmosphere. Radon and thoron progeny are generated in the atmosphere in two steps as follow;

I) The formation of their progeny from the radon and thoron gas by decay. The freshly generated radionuclides, mostly positively charged, are neutralized and become small particles called clusters through reaction with atmospheric trace gases and water vapor in air.

II) The cluster formation. These radionuclides attach to existing aerosol particles in the atmosphere within 1-100 s, forming radioactive aerosol of the radon and thoron progeny.

Thus, simply by breathing, people everywhere are exposed to radiation from radon, thoron and radioactive aerosol of their decay products.

When radon, thoron and radioactive aerosol of their decay products are inhaled, densely ionizing alpha particles emitted by deposited short-lived decay products of radon (^{218}Po , ^{214}Po and ^{214}Bi) and thoron (^{212}Pb) can interact with biological tissue in the lungs leading to cancer [1]. Health effects of radon, thoron and their decay products, most notably lung cancer, have been investigated for several decades. Initially, investigations focused on underground miners exposed to high concentrations of radon, thoron and their decay products in occupational environment. Recently, risk assessment for radon, thoron and their decay products both in mines

and in residential settings have provided clear insights into the health risks due to radon, thoron and their decay products [2]. Radon, thoron and their decay product are now recognized as the second most important cause of lung cancer after smoking in the general population.

Over the past two decades, sophisticated dosimetric models have been developed which enable assessment of dose to sensitive tissue in the lung resulting from inhalation of radon and thoron decay products. These models take into account the special physical properties of radon and thoron decay product aerosols which give rise to non-uniform irradiation of lung tissue by alpha particles. These include exposure concentration, exposure duration, respiratory tract anatomy, ventilator parameters, and particle properties e.g., particle size, hygroscopicity, particle shape, and density in airway fluids and cellular components. The attached and unattached radon decay products deposit in different regions of the human respiratory tract and lung, based on the aerosol size distribution [3]. The probability of deposition in the respiratory tract and lung is dependent on aerosol diameter since it influences diffusion coefficient and inertia of the particle. Therefore, the activity size distribution is one of the major parameter to estimate the dose.

The cascade impactors are widely used for measuring the size distribution of aerosol particles in environmental pollution [4] and health physics. Measurement of activity size distribution of radon and thoron decay products using several kinds of low pressure cascade impactors (e.g. Andersen, Berner, Davis, MOUDI etc) have been reported elsewhere [5-8]. The cascade impactors have more advantages due to the collection efficiency curves have steeper slope and give better cut-off characteristics. In addition, the collector plate separation has less effect on their collection efficiency and leakage is seldom a problem. On the other hand, most of the cascade impactors are expensive to assemble and require equipments that make them unsuitable for use in the field studies where no direct power supply is available.

Commercial instruments, used for the measurement of activity of alpha particle from the aerosols on impactor substrates, are expensive, too large and cumbersome to handle during field experiments. In most of studies, the activity of alpha particles is analyzed using a traditional ZnS (Ag) scintillation detector. These detectors are sensitive if exposed to light through the Aluminized Mylar window. Zinc sulfide scintillation counters are prone to window punctures. Scintillation counters can be affected by

magnetic fields, adversely affecting the instrumental response. The photomultiplier tubes are fragile, require a well regulated power supply, and degrade over time. In addition, these instruments are also mechanically affected by humidity and temperature [9]. The solid state nuclear track detectors (SSNTDS), especially allyl diglycol carbonate (commercially known as CR-39) are widely used for radon and thoron measurement to overcome above limitations [10]. In some cases, CR-39 has been used as alpha spectrometer for radon and thoron progeny monitoring. They studied the relationship between track size and energy for alpha particles. However, this technique takes much time to analyze the etched pit [11-14]. On the other hand, some researchers used the Aluminum-Mylar with various thicknesses to discriminate between radon and thoron progeny, and the results were quite encouraging [15-17].

Therefore, it is necessary to develop a portable aerosol sampler for the air sampling, and to measure the activity of attached radon and thoron progeny in field survey from the view point of dose assessment.

1.2 Objectives

The main of the dissertation are:

1.2.1 To development of a device that can evaluate particle size distribution of attached radon and thoron progeny.

1.2.2 Rapid measurement of the activity concentration of attached radon and thoron progeny aerosols effectively.

1.3 Scope and limitation of the study

1.3.1 Modification of a 4th-stage portable impactor sampler and CR-39 detector as an alpha spectrometer for measurement of radon and thoron progeny.

1.3.2 Test the performance of the developed technique on radon and thoron in a standard laboratory to find out alpha energy discrimination of radon and thoron progeny using aluminium-Mylar film, detector efficiency calibration, collection efficiency in the size range of 0.3-10 μm .

1.3.3 Evaluation of parameters that affect sensitivity of the developed technique including humidity, temperature, unattached progeny and air flow-rate.

1.3.4 Validation of the developed technique with the commercial device such as MOUDI (Micro Orifice Uniform Deposit Impactor) and ELPI (Electrical Low Pressure impactor).

1.3.5 Field tests of the developed technique for dose assessment.

1.4 Benefits

1.4.1 The new developed technique simultaneously measure the activity size distribution of both radon and thoron progeny in the ambient air.

1.4.2 The new technique can be used as a portable device for field studies use without AC power supply.

1.5 Research methodology

1.5.1 Modification of 4th-stages portable impactor sampler using CR-39 as alpha detector to measure radon and thoron progeny

1.5.2 Experimental set up to test the performance of detector.

1.5.3 Sensitivity test of the developed technique

1.5.4 Verification of the developed technique with the commercial device.

1.5.5 To carry out the activity size distribution of the attached radon and thoron progeny measurement in ambient air for dose assessment.

1.6 Organization and chapter contents

This dissertation consists of five chapters. The chapters are organized principally to focus on the assessment of dose from radon and thoron progeny exposure with an emphasis on the characteristics of activity median aerodynamic diameter determined using modification of a 4th-stage portable impactor sampler, and CR-39 as a radiation detector.

Chapter I deals with background and problem of interest, objective, scope, expected benefits and research methodology of the study.

Chapter II presents the previous work on mitigation of the effective dose of radon decay products through the use of an air cleaner in a dwelling in Okinawa, Japan.

Chapter III provides about radon and thoron decay product aerosol, the significant parameter of radioactive aerosol, measurements technique for activity size distribution, and dose assessment.

Chapter IV describes the modifications of the cascade impactor and the associated experiments to test the performance of the developed technique on radon and thoron. Parameters that might affect sensitivity and reliability of the technique have been evaluated. The findings of experiments with modified cascade impactor are also reported to obtain the most desirable results.

Chapter V describes the experimental result of attached radon and thoron progeny size distribution using developed technique which was obtained at Thailand smelting and refining Co. Ltd. The experimental results support for dose calculation using the particle size those play a significant role.

Finally in Chapter VI, the overall findings of the studies are summarized and discussed.

CHAPTER II

THEORY AND LITERATURE REVIEW

Chapter II describes about the theory and literature review of radon, thoron and their decay products, particle size of aerosols, its activity size distribution as well as determination techniques, alpha radiation detectors and dose assessment.

2.1 Radon, thoron and their decay products

Radon (^{222}Rn) is a decay product from the ^{238}U decay series (Figure 2-1). It is an inert gas having a half-life of 3.8 d, which is long enough to enter the human respiratory system. Another member of radon isotope family is thoron, ^{220}Rn , having a half life of 56 s and chemical properties thensame as that of radon. Thoron is a part of the ^{232}Th decay series (Figure 2-2). The decay products of radon and thoron are solid and act as airborne particles. Mostly of the decay products are ^{218}Po ($T_{1/2} = 3.05$ m), ^{214}Pb (26.8 m) and ^{212}Pb (10.64 h). A long lived radioisotope, ^{210}Pb (22 y), is produced in the ^{222}Rn decay chain within one hour from ^{218}Po . Initially, decay products are free atoms in the air and "unattached" to other aerosol particles. But these decay products are very small that they easily attach to aerosol particles. The fraction that attach depends strongly on the size and concentration of carrier aerosol particles. The basic processes of radon decay product behavior in air as show in Figure 2-3a and 2-3b.

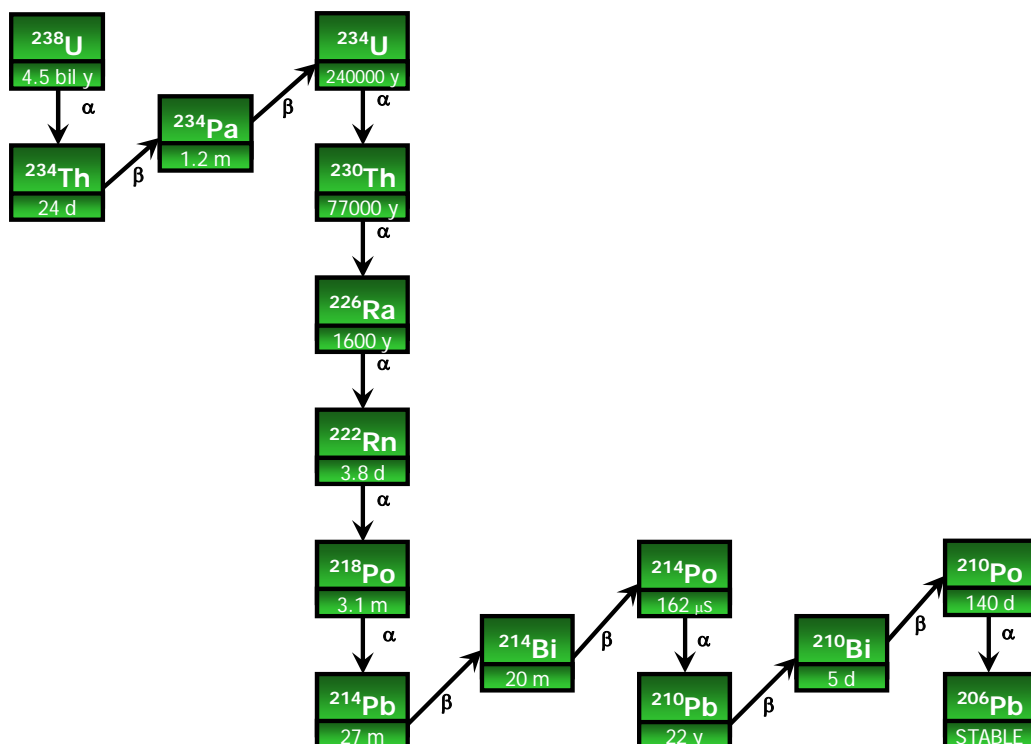


Figure 2-1 Natural decay series: Uranium-238.

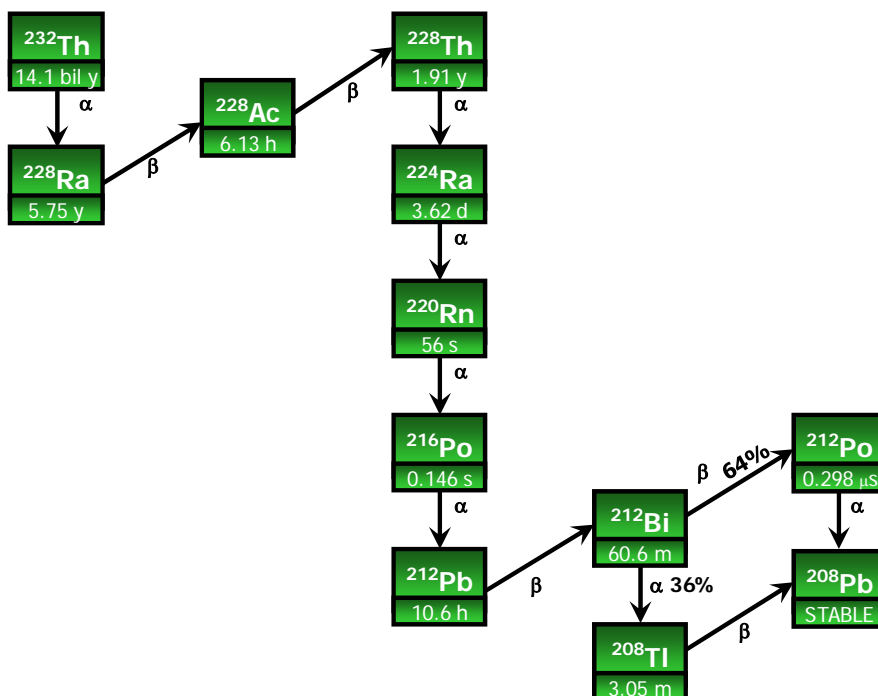


Figure 2-2 Natural decay series: Thorium-232.

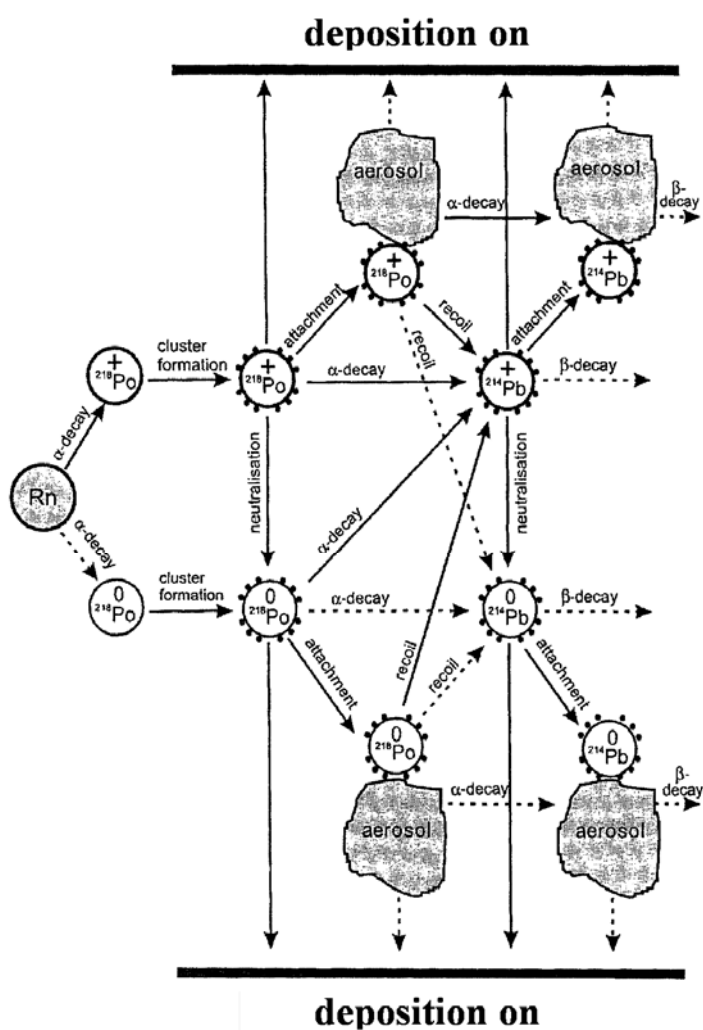
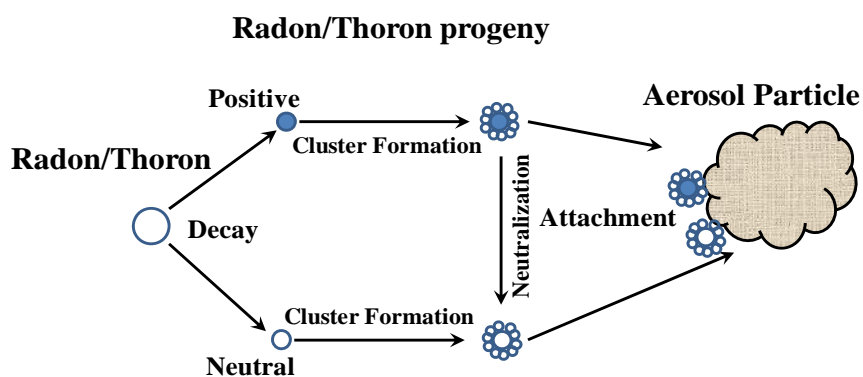


Figure 2-3 a) Basic processes of radon decay product behavior in air defining “unattached” and “aerosol-attached” particle activities. b) Processes of ^{218}Po and ^{214}Pb in air [5].

2.2 Particle Size: A significant parameter of radioactive aerosol

Particle size is the most important attribute characterizing the properties and behavior of aerosols. Most aerosols have a wide range of sizes and their properties depend strongly on particle size. Particle size commonly refers to the dimension which is determined by its geometry. For spherical particles, it is their diameter. For irregularly shaped particle it is the volumetric equivalent diameter or light scattering equivalent diameter, electric mobility equivalent diameter and diffusion equivalent diameter. Airborne aerosol particles have irregular shapes, and their aerodynamic behavior is expressed in terms of the diameter of an idealized spherical particle known as aerodynamic diameter. The aerodynamic equivalent diameter (AED) (also called aerodynamic diameter) is the diameter of a sphere, with density = 1 g cm^{-3} , that has the same terminal settling velocity under gravity as the airborne particle considered. Particles are sampled and described on the basis of their aerodynamic diameter. Particles having the same aerodynamic diameter may have different dimensions and shapes.

In dosimetry and inhalation toxicology it is often more important to describe the size distribution of aerosols rather than individual particle size. Particle size distribution (PSD) is a description of how much of the aerosol is in each set (or continuum) of size intervals. One can count the number of particles in the size interval or one can weigh them (these are the two most common approaches). The PSD is most properly means the functional relation between the number of particles and some measure of the particle size. Size is usually taken to mean the diameter, so the PSD is often presented as a graph of the logarithm of the total number of particles smaller than particle diameter “d”. The PSD can be monodisperse or polydisperse. Monodisperse means all the particles are of the same size and polydisperse refers that particles are of more than one size.

Most size distributions require two parameters: one that identifies the location or center of the distribution and another that characterizes the width or spread of the distribution. The most commonly used quantities for defining the location of distribution are the mean, mode, median and geometric mean. The distribution of mass and the distribution of count for the same sample of particles have different

means, medians, geometric means, graphical representations and probability density functions. The median of the distribution of mass is called the mass median diameter (MMD), while the median of the distribution of count is called the count median diameter (CMD). These two parameters are frequently encountered in size distribution discourse. In discussing about the size distribution of radioactive aerosol, another entity that frequently comes across is the activity median aerodynamic diameter (AMAD).

AMAD is used when deposition depends mainly on sedimentation and inertial impaction, typically when the AMAD is greater than about 0.5 μm . Fifty percent of the activity in an aerosols is associated with particles of aerodynamic diameter greater than or smaller than the AMAD. A lognormal distribution of particle sizes is assumed. The AMAD refers to the entire distribution. The AMAD is the aerodynamic equivalent diameter (AED) for which one-half of the radioactivity in a distribution has an AED smaller than the AMAD and one-half of the radioactivity in a distribution has an AED larger than the AMAD. The AMAD, along with the associated the geometric standard deviation (σ_g), is the most useful diameter for characterizing the behavior of the aerosol in air, in sampling instruments, and the respiratory tract.

Aerosols are defined as a suspension of solid or liquid in a gas. The term aerosol includes both the particles and the suspending gas, which is usually air. Thus an aerosol is a two-phase system, consisting of the particles and the gas they are suspended in. A complete description of the atmospheric aerosol would include an accounting of the chemical composition, morphology, and size of each particle as well as the relative abundance of each particle type as a function of particle size [18]. Most of the airborne radionuclides attach on the surface of aerosol particles and form radioactive aerosol. The majority of these aerosols present in natural and work environments are polydisperse.

The distribution of aerosol particles with respect to size is a very important physical parameter governing particle behavior. Aerodynamic size, rather than geometric size, determines the trajectory of the particle in a gas stream because it accounts for all three major aerodynamic factors: size, shape and mass density. The aerodynamic size distribution of aerosol particle captured by the sampler can be represented by the lognormal distribution. Thus the lognormal distribution (i.e., the

situation in which the logarithms of particle diameter (d_p) are distributed normally) are in use for describing size distributions of aerosols. The geometric mean is the median of the distribution and the metric of variability around this central tendency is the geometric standard deviation (σ_g). The σ_g , is a dimensionless term, is the ratio of particle size at the 84th (or 16th) percentile to the 50th percentile [19]. Thus, the only two parameters needed to describe a lognormal distribution of particle sizes for the radioactive aerosol are the median diameter and the geometric standard deviation (σ_g). However, the actual size distribution may be obtained in various ways. The discussion in this dissertation will be focus on AMAD because it is the most commonly used measurement of radioactive aerosol distribution. However, alternative descriptions are also used for particles with actual physical sizes below 0.5 μm because in such a case, aerodynamic properties become less important. Due to their instability as an aerosol depends mainly on their interaction with air molecules. Like particles in Brownian motion, they are caused to "diffuse". For these small particles and especially for ultrafine particles, this interaction is independent of the particle density and varies only with geometric particle diameter. Very small particles are not expressed in aerodynamic equivalency, but instead to a thermodynamic-equivalent size. The thermodynamic particle diameter is the diameter of a spherical particle that has the same diffusion coefficient in air as the particle of interest. The activity median thermodynamic diameter (AMTD) is the diameter associated with 50 percent of the activity for particles classified thermodynamically.

2.2.1 Activity size distribution of radioactive aerosol

Usually the activity size distribution of radon decay products can be determined by two approaches. By calculation, if the number size distribution $Z(d)$ of the atmospheric aerosol is known by measurement, then the activity size distribution $C(d)$ can be obtained by the correlation expression between $C(d)$ and $Z(d)$ as follows:

$$C(d) = \frac{c}{x} \beta(d) Z(d) \quad (2-1)$$

where c is the activity concentration, x is the attachment rate and $\beta(d)$ is the attachment probability [20]. While the other one is the direct measurement of the activity size distribution of the decay products. The activity size distribution of

radioactive aerosol can be obtained directly using impactors or impingers, multi-channel graded wire screen diffusion batteries.

At present, cascade impactors are the instruments of choice for measuring the particle size distribution of aerosol. The cascade impactors are widely used for measuring the size distribution of aerosol particles in the area of environmental pollution [3], health physics and in atmospheric electricity. The inertial impactors are devices widely used for sampling and size-selective collection of aerosol particles. There are two classes of inertial impactors: single stage impactors and multiple stage impactors that are popularly known as cascade impactors. The cascade impactor is an instrument used for the classification of aerosols in terms of AED and for possible subsequent chemical analysis.

2.2.2 Activity size distribution determination techniques

Airborne particle size varies from molecular clusters measuring approximately 1 nanometer to cloud droplets and dust particles measuring around 100 micrometers, five to six orders of magnitude larger. Size is an important particle property, because it largely determines particle behavior in gas suspension. Particles at different ends of the size range behave in completely different ways and are even governed by different physical laws. As there is no single measurement technique capable of handling this range of sizes, the most appropriate method needs to be selected on a case-by-case basis. There are various methods for aerosol size measurement. These are mobility analyzers, diffusion batteries, optical particle counters, optical microscopes, time of flight methods, inertial methods, impactors, scanning electron microscope, transmission electron microscope etc. The main features of these methods are discussed in Appendix A.

Particle shape is another important parameter. Particle diameter is an unambiguous measure of particle size only for spherical particles, in contrast, is difficult to define for non-spherical particles, such as agglomerates, fibrous, and crystals. As a result, particle size is usually defined by the chosen measurement method, and particle size given in equivalent diameter, most commonly aerodynamic equivalent diameter, electrical mobility equivalent diameter, light scattering equivalent diameter, optical equivalent diameter and diffusion equivalent diameter.

Aerodynamic diameter is useful for characterizing particle settling and inertial behavior, and can be used to describe the behavior of particles in the human respiratory tract, filters, cyclones, and impactors. The most common instrument used here is impactor. Mobility equivalent diameter provides information on how particles respond to external forces, and is important when diffusion or electrical forces govern the behavior of particles. Mobility equivalent diameter is usually measured using electrical mobility analyzers, such as differential mobility analyzers (DMA) [21] and scanning mobility analyzers (SMPS) [22]. Optical diameter, for its part, depends on the interaction of light with particles. In practice, data is reported in terms of an equivalent diameter for particles with the same refractive index as that of the calibration aerosol of the instrument employed. Diffusion equivalent diameter is usually measured using diffusion battery. Diffusion battery devices separate radon decay products into size fractions using differential mobility to capture the higher-mobility particles. Often these devices draw the air sample through one or more fine mesh screens that precede a "collect-all" filter.

Of all the techniques, inertial impactors are devices widely used for the sampling and size-selective collection of aerosol particles. Their principle of operation is simple: an aerosol stream passes through a nozzle and impinges upon a collection plate. Particles in the aerosol stream having large enough inertia will impact upon the collection plate while the other particles will follow the airflow out of the impaction region. There are two classes of inertial impactors: single stage impactors and multiple stage impactors (also called cascade impactors). The cascade impactors are commonly used to determine the aerosol size distribution. They have sharp cut-point characteristics, low internal particle holdup, and are easy to operate. Particles can be collected on substrates for microscopic analysis or additional measurements of mass or composition. They are designed for applications where wide size-range coverage and fast response are required. The theoretical principle and construction details of a cascade impactor are presented in Appendix B.

In general, there are advantages and disadvantages for every particle sizing technique and for every particular instrument. It stands to reason that certain techniques are better suited for certain tasks, and that no instrument will be able to solve all problems. There are several publications using different methods for particle size characteristics by various researchers. There has been significant progress in

techniques for the determination of the activity size distribution in the recent days. Despite the progress, many inconsistencies/differences still exist with respect to the activity distribution, especially in the range of smaller particle size.

Porstendörfer et al. [20] studied the activity size distribution of short-lived radon decay products in ambient air continuously for several hours. They used two different measurement techniques: direct measurements with a low pressure on-line alpha cascade impactor (OLACI) and an indirect determination based on measurement with a differential mobility analyzer (5~200nm) or a laser aerosol spectrometer (100~5000nm). The results of both measurement techniques show that the greatest activity fraction of the radon decay products is adsorbed on aerosol particles in the accumulation size range.

The size distribution studies of radon/thoron decay products have also been performed in the open air by Becker et al. [23]. A high volume cascade impactor was used and the gamma activity on were measured by a well type Ge detector. The impactor data were evaluated by means of an improved computer program taking into account the effect of inter stage losses on the measured precipitation values of the impactor.

Yamada et al. [24] measured the aerosol size information using a commercial cascade impactor i.e. electrical low pressure impactor (ELPI). The impactor covered a wide diameter range from 0.03 to 10 μm , gave number weighted size distribution in real time by an electrical detection method. ELPI allowed size distribution data on aerosol number and activity to be independently determined for the same impactor sample.

Rahman, et al. [25] evaluated the size characteristic of low pressure cascade impactor using imaging plate technique for radon decay products. The radon aerosol-particle size distribution was obtained by drawing air sample through a 13 stage low pressure Anderson cascade impactor. The impactor, which covers a wide diameter from 0.05 to 12 μm . The air sample was collected on 47 mm diameter of stainless steel plates with a coating of silicon grease of 7.5 $\text{mg}\cdot\text{cm}^{-2}$ taken as collection media.

The activity size distributions of both unattached and attached fractions of short lived radon decay products (^{218}Po , ^{214}Pb and ^{214}Bi) were measured in indoor air by Mohammed [26]. The measurements were performed with a wire screen diffusion

battery and a low pressure cascade impactor (Berner type). In addition, the collected activity on each impactor stage was measured with a germanium detector. Most of the attached activities were associated with the aerosol particles of accumulation mode.

Knutson and Tu [27] improved particle size data for reconstructing the radiation dose by combining data from an impactor with data from a diffusion-based sampler. It was possible to cover the particle size range from 0.5 to 5000 nm. In case of attached radon progeny, a micro-orifice uniform deposit impactor (MOUDI) was used. After sampling, each sampling substrate was simultaneously counted the alpha particles by ZnS(Ag) alpha scintillation counters and the weighted least squares method was used to calculate the activity of ^{218}Po , ^{214}Pb and ^{214}Bi on each substrate. The expectation-maximization algorithm was used to calculate particle size distributions from the activities measured each substrate of the MOUDI.

A new technique for measuring the activity size distribution of radon progeny were developed by Tokonami, et al [28]. This activity size distribution instrument incorporates both impactor and wire screen method. The wire screen prevents the invasion of unattached fractions into the cascade impactor. After that, attached fractions are introduced into the four-stage low pressure cascade impactor, which covers a diameter range from 0.07 to 2.1 μm . The silicon photodiodes, while the ceramic windows were removed, were installed in each stage of the impactor for measuring alpha particles of radon progeny. This instrument can determine the size distribution of radon progeny and the aerosol in a normal environment within 90 minutes.

All these studies support the fact that cascade impactors are convenient as particulate size distribution measuring instrument for indoor as well as for outdoor sources. The reviewing of the earlier research works provided a helpful suggestion to ensue the present study using the impactors described in Appendix A.

2.3 Alpha radiation detectors

A number of different techniques are used for radon measurements at home or at workplaces. These range from collection of radon decay products on an air filter and counting, exposing a charcoal canister for several days and performing gamma spectroscopy for absorbed decay products, exposure of an electret ion chamber and readout, and long-term exposure of CR-39 plastic with subsequent chemical etching

and alpha track counting. All these approaches have different advantages and disadvantages which need to be evaluated prior to use. The most commonly used radon measurement devices are Charcoal Canisters, Solid state nuclear track detector or SSNTD, scintillation counter, liquid scintillation counters (LSC), Proportional counter and multi channel analyzer (MCA) etc. The main features of all these devices are described in Appendix C.

All commercial instruments, to measure the activity of the alpha particles from the aerosols on impactor substrates, are expensive, too large and cumbersome to conduct experiments in the normal environment. Generally, is analyzed either with a solid state detector or with a traditional ZnS (Ag) scintillation detector. These detectors are sensitive to light leaks through the Aluminized Mylar window in case of alpha scintillators. Zinc sulfide scintillation counters are prone to window punctures. Scintillation counters can be affected by magnetic fields, adversely affecting the instrument response. The photomultiplier tubes that they contain are fragile, require a well-regulated power supply, represent a shock hazard, and operationally degrade over time. In addition, these instruments are also mechanically affected by humidity and temperature [9].

So in this study the solid state nuclear track detectors (SSNTDS), namely CR-39 has been widely used for radon and thoron measurements, was proposed with the potential to overcome above limitations of ZnS (Ag) scintillation detector [10].

2.3.1 Nuclear track detector as radiation detector

Operation of the solid-state nuclear track detector is based on the fact that a heavy charged particle will cause extensive ionization of the material when it passes through a medium. For example, an alpha particle with energy of 6 MeV creates about 150,000 of ion pairs in cellulose nitrate. Since the range of a 6 MeV alpha particle in this material is only about 40 mm that means on average 3700 ion pairs are created per μm , or 3–4 ion pairs per nm. An alpha particle ionizes almost all molecules close to its path. This primary ionizing process triggers a series of new chemical processes that result in the creation of free chemical radicals and other chemical species. Along the path of the alpha particle, a zone enriched with free chemical radicals and other chemical species is then created. This damaged zone is called a latent track.

If a piece of material containing latent tracks is exposed to some chemically aggressive solution, chemical reactions would be more intensive along the latent tracks. Aqueous solutions of NaOH or KOH are the most frequently used chemical solutions. The overall effect is that the chemical solution etches the surface of the detector material, but with a faster rate in the damaged region. In this way, a “track” of the particle is formed, which may be seen under an optical microscope. This procedure is called “detector etching” or track visualization, and the effect itself is called the “track effect”.

The track effect is relatively well known, and the technique is rather simple and straightforward, there is not a unique theory that explains track formation. The basic physical processes after the initial charged particle loses its energy are the ionization and excitation of molecules of the material. This first “physical” phase in which the initial particle delivers its energy to the atoms surrounding its path is very short in time; stopping of the particle occurs within a time of the order of picoseconds. The free electrons created in these primary interactions will slow down through a series of ionizations and excitations, and will create more and more free electrons. Some of these may go further away from the initial particle path creating the so-called delta (δ) rays. A large number of free electrons and damaged molecules are created close to the particle track.

In the second physiochemical phase, new chemical species are created by interactions of the damaged molecules. During etching, the interactions of these new chemical species with the etching solution are stronger than that with the undamaged detector material. However, it is not known which chemical species are formed after the particle passage through the material, and the nature of damage is also not entirely known.

2.3.2 Stopping power, restricted energy loss

The primary process of charged-particle interaction with the detector material is ionization and excitation of the molecules in the detector. The initial charged particle loses its energy through the many interaction processes. Theoretically, it interacts through Coulomb force with charged particles (electrons and nuclei) in the material. Of course, distal interactions may be neglected and we focus on the particle interactions with atoms and molecules that are close to its path. The majority of the

interactions occur with electrons and only a small number of interactions are with nuclei. Since the initial heavy charged particle (only such particles can produce tracks) is much heavier than electrons, the direction of the particle effectively does not change and the path is almost completely a straight line. This may not be true if the particle interacts with a nucleus, where a significant deviation from the initial direction may occur. However, such interactions are relatively rare. Some deviations from the straight line can happen close to the end of the particle range, when the energy of a particle becomes very low.

The particle loses its energy in many small interaction processes, so the energy loss each time is usually very small when compared to its energy. For example, ionization of one molecule in air on average needs about 32 eV, which is 10^{-5} to 10^{-6} of the particle energy (assuming that the particle energy is in the MeV region). As a result of these many small interaction processes, the particle will continuously slow down in the detector material. The physical quantity that describes the slowing down of charged particles in mater is the stopping power $-dE/dx$ (or the stopping force), where dE is the energy lost in the distance dx . Stopping power is given in J/m or in keV/mm. The energy lost by a particle in the distance dx is the energy transferred to the material so this quantity is also called the linear energy transfer (LET).

The first expression for the stopping power was given by Bohr [29]. That was a classical consideration of the particle interaction with a free electron, where the energy lost in the collision with one electron was integrated in some assumed limits of interaction and the expression for the stopping power was derived. This was modified by taking into account the quantum effects by Bethe [30], and the relativistic effects by Bloch [31], and finally the well-known Bethe–Bloch expression for the stopping power was given as:

$$-\frac{dE}{dx} = \frac{Z^2 e^4}{4\pi\epsilon_0^2 m_0 v^2} N \left[\ln \frac{2m_0 v^2 W_{max}}{\bar{I}^2 (1-\beta^2)} - 2\beta^2 - \delta - U \right] \quad (2-2)$$

where Z was the charge of the incident particle, v its velocity, $\beta = v/c$, m_0 the rest mass of the electron, N the number of electrons per unit volume, \bar{I} the average excitation potential of electrons in the stopping material, W_{max} the maximal value of transferred energy of electron, δ the correction for polarization of the material and U takes into account non-participation of inner electrons in the collision. The stopping

power given in the above equation takes into account only collisions with electrons. Events with nuclei are not considered.

Equation 2-2 has been from perturbation theory and the first Born approximation. The drawback of this equation is that in the low-energy region, this approximation may not be valid, i.e., the function inside the logarithm may become less than 1, thus the whole expression becomes negative in the low-energy region. In addition, this formula does not take into account some effects that appear when the energy of particles falls below some limits. Slowly moving charged particles can experience the charge exchange process, viz. capture of an electron in a collision with an atom of the stopping medium, and lose it in subsequent collisions. The charge of ions is not equal to Z and the effective charge Z_{eff} should be introduced to describe the process. However, such a simple change of the formula is not sufficient to describe the complicated process of charge exchange.

When the particle loses energy in the material, part of the energy is taken by energetic electrons which can then go far away from the initial particle path and are called δ rays. This energy is spent far away from the particle path and does not take part in the formation of the particle track. For this reason, a new quantity called the restricted energy loss (REL) was introduced $(-dE/dx)_{Eb}$. Only energy transfers smaller than E_b are considered for calculations of dE . Here, for collisions with energy transfer larger than E_b , δ electrons are assumed to be formed, which do not take place in track formation. As we will see later, there is not a unique value for E_b .

The concept of REL is also used in other fields of physics. However, this quantity is not unique, and may be different for various materials. For this reason, a microdosimetric quantity called linear energy, which does not have such shortcomings, is used.

Nowadays, some computer softwares are available for the calculation of stopping power and range of charged particles in different media. The most well-known one is the SRIM (Stopping and Range of Ions in Matter) program developed by Ziegler et al. [32].

2.4 Dose assessment

There are two approaches for the dose assessment due to radon and thoron progeny inhalation: (i) dosimetric approach that developed by the International

Commission on Radiological Protection (ICRP) [33] to calculate dose and (ii) epidemiological approach that derived directly from studies on cohorts of miners.

In this study, the dosimetric approach will be used to calculate the dose conversion factors of radon and thoron decay products. The dose calculations were conducted using a computer program LUDEP (Lung Dose Evaluation Program) [34].

2.4.1 The new ICRP lung model and LUDEP

LUDEP and the new ICRP respiratory tract model were developed for dose assessment over the past ten years. To implement new models, there were extensive period of consultation with interested parties and several papers have been reported describing its progress from time to time. ICRP adopted version 1.0 as its first model to implement structurally. However, version 1.1 was the first to be fully compatible with ICRP Publication 66 [33].

2.4.2 Description of LUDEP

LUDEP is a suite program using Turbo and Power Basic and have been compiled for the IBM1 - compatible personal computer. It enables the user to calculate doses and dose rates to the respiratory tract regions and other body organs for a wide range of user-defined conditions. The software has been designed to be as flexible as possible, permitting the user to change most of the parameters used in the dose calculation and display the results obtained at each stage of the calculation. Although flexibility can be useful, it requires the user to make more decisions and in some situations this can increase the probability of errors. In the majority of situations, the user will not wish to deviate from ICRP-recommended parameter values, and so LUDEP has been designed to select these default values automatically when loaded.

The program has been designed in a modular form, with each module called automatically by a central program, over which the user has direct control. The upper part of the screen contains the menu for selecting the modules which enable the various parameters to be specified and the dose calculations to be performed; the lower part of the screen displays the values of several of the more important parameters already chosen by the user. The necessary parameters are entered using the options contained in the 'Input Parameters' menu, described below.

The first option, INTAKE REGIME, allows details of the intake or exposure to the radionuclide to be entered.

The next, TIME, enables the user to specify the time at which the dose rate or cumulative dose is to be calculated.

DEPOSITION permits the fractional deposition in each region of the respiratory tract to be specified directly, or calculated from specific particle size parameters and/or physiological parameters.

In PARTICLE TRANSPORT, the rates at which deposited particles move from one region of the respiratory tract to another, and the rates at which particles are cleared from the respiratory tract, can be altered.

In ABSORPTION, the rates of particle dissolution and subsequent uptake to blood are specified.

RADIONUCLIDES enable the radionuclide of interest to be selected from one of two databases. The first incorporates decay data from ICRP Publication 38, and is recommended to the user. The second is included for comparison purposes.

BIOKINETIC MODEL allows the user either to enter a biokinetic model directly or to select one of the models specified in Publication 30 [35].

The calculations menu contains options for calculating dose to the body organs.

The option, DOSE CALCULATION, accesses the modules in which the doses or dose rates to the regions of the respiratory tract and to the body organs are calculated, using an internal database of specific absorbed fractions for photons. The user is given the choice of using either the ICRP Publication 26 tissue weighting factors, or those given in ICRP Publication 60 [36].

The final menu option, LUDEP UTILITIES, contains some useful facilities, including those for saving all the parameters into a disk file and entering the DOS environment with LUDEP stored in memory.

2.4.3 Mathematical approaches used in LUDEP

In ICRP Publication 66 [33] the deposition of a mono-disperse aerosol in the different regions of the respiratory tract is modeled by treating the regions as a series of filters. Deposition occurs in all regions of the HRT (Human Respiratory Tract), but with different efficiencies. The deposition pattern depends on the aerosol diameter as

well as airflow characteristics. The behavior of small-size particles which are deposited by diffusion is described in terms of the thermodynamic diameter d_{th} and the diffusion coefficient D . Deposition of larger particles is described by the aerodynamic diameter d_{ae} .

The aerodynamic diameter is defined in terms of the equivalent particle volume diameter d_e i.e., the diameter of a spherical particle with the same volume as the considered particle. Each region of HRT has deposition efficiency, η , which denotes the fraction of the number of particles that enter a single region of the respiratory tract that is deposited in that region. The deposition efficiency, η depends on both the thermodynamic and the aerodynamic diameters of the particles. Algebraic expressions for η are given in ICRP Publication 66 as,

$$\eta = \sqrt{\eta_{th}^2 + \eta_{ae}^2} \quad (2-3)$$

where, η_{th} is the thermodynamic deposition efficiency and η_{ae} , is the efficiency of the aerodynamic deposition process which includes both “impaction”, η_i and “sedimentation”, η_s components and can be related by the following expression:

$$\eta_{ae} = 1 - (1 - \eta_i)(1 - \eta_s) \quad (2-4)$$

LUDEP implements above equations directly for monodisperse aerosols and treats polydisperse aerosols as a convolution of 100 monodisperse aerosol of appropriate particle size.

The LUDEP dose calculation module combines the respiratory tract model with the ICRP gastrointestinal (GI) tract model [34] and the biokinetic models to form one large non-recycling compartment model. The deposition fractions are combined with the intake to determine the initial number of atoms in each compartment. The remaining activity and integrated disintegrations in each compartment are then calculated using a very fast algorithm.

Dosimetry for body organs is treated in the conventional manner [34]. First, the dose to each of the target organs from one disintegration in each source organ is calculated by combining decay information for chosen radionuclide with the appropriate absorbed fractions [34] to form a matrix of specific effective energy SEE values. The dosimetric formulation of ICRP Publication 30 [35], in which the committed equivalent dose, H_T in a target organ T is determined by the energy

absorbed per unit mass from the radiation emitted from a source organ, can be expressed as:

$$H_{(t,t_0)} = c \sum_S \sum_t q_{S,t}(t) SEE(T \leftarrow S; t) \quad (2-5)$$

where, $q_{s,j}(t)$ is the activity of radionuclide j present in source organ S at age t ; $SEE(T \leftarrow S; t)$ is the total energy absorbed per unit mass in the target T ; the contribution of each radiation emitted by the radionuclide are weighted by their radiation weighting factor, per nuclear transformation of radionuclide in source region S ; and c is any numerical constant required by the units of q and SEE .

The SEE matrix is then multiplied by the array containing the number of disintegrations in each source organ to give the dose to each target organ. Dosimetry of the respiratory tract is treated by using algebraic approximations [34] for the energy-dependent absorbed fractions from the various sub-regions of the respiratory tract to the sensitive cells.

To calculate regional doses in the ICRP dosimetric system, it is necessary to sum doses those for extrathoracic airways and those for the thoracic regions. Since the regions of respiratory tract vary greatly in radiation sensitivity, therefore the regional doses must be adjusted for their relative sensitivity to sum up finally. The regional doses, weighted with factors assigned for the partitions of radiation detriment, are summed to give a value of committed equivalent dose for extrathoracic region and another for the thoracic regions, as follows:

$$H_{ET} = H_{ET_1} A_{ET_1} + H_{ET_2} A_{ET_2} + H_{LN_{ET}} A_{LN_{ET}} \quad (2-6)$$

$$H_{TH} = H_{BB} A_{BB_1} + H_{bb} A_{bb} + H_{AI} A_{AI} + H_{LN_{TH}} A_{LN_{TH}} \quad (2-7)$$

where, H represents the committed equivalent dose,

A represents the assigned fractions of tissue weighting factors, w_T ,

ET_1 represent the anterior nose, ET_2 is the posterior nasal passages, larynx and mouth,

LN_{ET} represents the lymphatics of the extrathoracic region,

BB is the bronchial, bb is the bronchiolar, AI is the alveolar-interstitial and

LN_{TH} is the lymphatics of the thoracic region.

The appropriate ICRP tissue weighted factor, T_w can then be applied to these two values in calculating effective dose as described in ICRP 60 [36].

2.4.4 Best estimated parameters for calculating dose using LUDEP

The ICRP 66 lung dose model offers the ability to input data characteristic of specific material. The ICRP 66 model employs ten input parameters for determination of regional deposition fraction [37]. Thus the program package LUDEP has also been designed to be as flexible as possible, permitting the user to change all these ten parameters. These input parameters were varied according to their characteristic distributions, in an effort to perform uncertainty analysis of regional deposition fraction.

The sensitivity of the weighted equivalent dose to lung per unit exposure of radon decay products to HRTM was verified and cited in literatures. The parameters considered to be the most influential are: (i) aerosol parameter, (ii) breathing rate, fraction breathed through nose and the age and gender of subject itself, (iii) target cell parameters, and (iv) the parameters that define the absorption rates of radon & thoron decay products from lung to blood.

While considering all these sensitive parameters, best estimated input parameter values were taken for LUDEP to calculate dose for the present study and these values are presented in Table 2-1.

These parameter values were the best representation for the radon and thoron decay products measured indoor and workplace and were recommended by Ishikawa et al. [38, 39], Porstendörfer et al. [40, 41], Marsh et al. [42], Nuccetelli, and Bochicchio [43] and by Kranrod et al. [44]. The best estimated parameter values used for the lung model are the HRTM default values for a male adult at indoor environment.

Table 2-1 The best estimated parameter values for the this study

Input category	Parameter	Input value
Time	Time for dose calculation (years)	50
Deposition	Nose/mouth breathing	Nose breathing
	Breathing rate ($\text{m}^3 \text{h}^{-1}$)	0.78
	Particle density (g cm^{-3})	1
	Particle shape factor	1
Absorption	Half-time for absorption into blood (h)	10
	Fraction cleared by rapid dissolution (d^{-1})	1
	Rapid dissolution rate (d^{-1})	1.65
Radionuclides	—	RnP: ^{218}Po , ^{214}Pb , ^{214}Bi TnP: ^{212}Pb , ^{212}Bi
Bio-kinetic model	—	ICRP 30
Dose calculation	Radiation weighting factor (alpha particles)	20
	Tissue weighting factor	ICRP 60
	Assigned partition for tissue weighting factor among thoracic region (BB:bb:AI)	0.333:0.333:0.333
	Equilibrium factor	RnP:0.4, TnP:0.02

2.4.5 Dependence of dose on radon/thoron decay products particle size

The particle size distribution of radon/thoron aerosols characterized by AMAD is an important attribute for dose assessment. When radon thoron and their decay products are inhaled, only a minor portion of radon and thoron decays in the lungs, whereas radon and thoron decay products appear in the form of clusters and aerosols deposited on the walls of airways in the mouth, nose and lungs, where they further decay and damage the nearby tissue. For this reason, the main concern for radon and thoron dose assessment are not radon and thoron themselves rather their decay products ^{218}Po , ^{214}Pb , ^{214}Bi , ^{212}Pb and ^{212}Bi . Therefore, it is important to comprehend the dependency of dose on radon and thoron decay products particle characteristics. This dependency was evaluated in the study by calculating “Dose Conversion Factor” (DCF) for radon and thoron decay products with different activity median diameter (AMAD). The dose conversion factor for radon thoron and their decay product can be calculated using the following equation [38].

$$DCF_{RnP} = \frac{BH \times \left(\sum_i C^u(i) D^u(i) + \sum_i C^A(i) D^A(i) \right) \times 3700}{F} \quad (2-8)$$

$$DCF_{ThP} = \frac{BH \times \left(\sum_i C^u(i) D^u(i) + \sum_i C^A(i) D^A(i) \right) \times 276}{F} \quad (2-9)$$

where, B , breathing rate ($0.78 \text{ m}^3 \text{ h}^{-1}$)

$D(i)$, Effective dose per unit intake of ^{218}Po , ^{214}Pb and ^{214}Bi in the case of Radon decay products and ^{212}Pb and ^{212}Bi in the case of thoron decay products (Sv Bq^{-1})

H , Exposure hours per month (170 h)

$C(i)$, Activity concentration ratios of ^{218}Po , ^{214}Pb , ^{214}Bi , ^{212}Pb and ^{212}Bi to ^{222}Rn and ^{220}Rn , respectively. (Bq m^{-3})

U , Unattached fraction; A , Attached fraction and F , Equilibrium factor.

The dose conversion factor for each radon decay products can be calculated as function of activity median diameter (AMD) according to the following equations:

$$DCF^M(^{218}\text{Po}) = B \times \left[\frac{PD^M(^{218}\text{Po})}{A_p} \right] \quad (2-10)$$

$$DCF^M(^{214}\text{Pb}) = B \times \left[\frac{PD^M(^{214}\text{Pb})}{B_p} \right] \quad (2-11)$$

$$DCF^M(^{214}\text{Bi}) = B \times \left[\frac{PD^M(^{214}\text{Bi})}{C_p} \right] \quad (2-12)$$

$$DCF^M(^{212}\text{Pb}) = B \times \left[\frac{PD^M(^{212}\text{Pb})}{D_p} \right] \quad (2-13)$$

$$DCF^M(^{212}\text{Bi}) = B \times \left[\frac{PD^M(^{212}\text{Bi})}{E_p} \right] \quad (2-14)$$

Where, DCF^M , is the dose conversion factor each decay products at particle diameter M , $\text{mSv (Bq m}^{-3} \text{ h)}^{-1}$,

D^M , is the effective dose per unit intake for each decay products at particle diameter M , $\text{mSv (Bq}^{-1}\text{)}$

B , is the breathing rate $0.78 \text{ m}^3 \text{ h}^{-1}$,

P , is the value of PAEC that equals 1 Bq i.e. $1.3 \times 10^5 \text{ MeV}$

A_p , B_p , C_p , D_p and E_p are values of PAEC for unit radioactivity of ^{218}Po , ^{214}Pb , ^{214}Bi , ^{212}Pb and ^{212}Bi , i.e. $3673.6 \text{ MeV}(\text{Bq}^{-1})$, $17832.7 \text{ MeV}(\text{Bq}^{-1})$, $13241.5 \text{ MeV}(\text{Bq}^{-1})$, $431042.4 \text{ MeV}(\text{Bq}^{-1})$ and $40916.6 \text{ MeV}(\text{Bq}^{-1})$, respectively.

The effective dose per unit exposure for each radon and thoron decay product were estimated by LUDEP, assuming the equilibrium factor 0.4 for aerosol attached particles and 0.1 for unattached particles and the best input parameter shown in Table 2-1 were also used. The dependence of dose per unit exposure DCF on AMAD of radon and thoron decay products were thus evaluated and are illustrated in Figure 2-4 and 2-5, respectively.

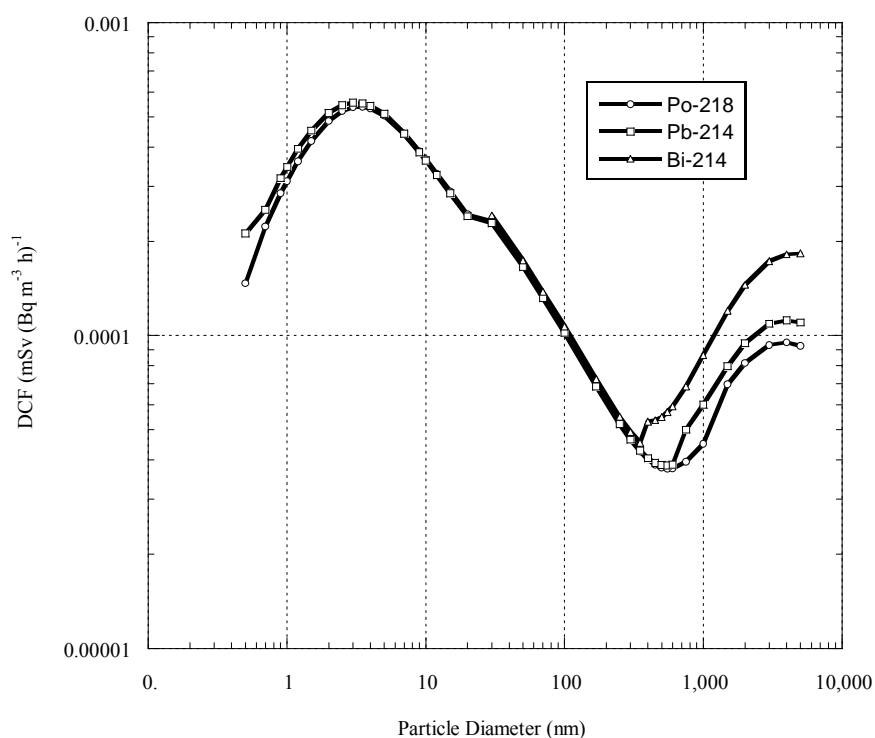


Figure 2-4 Variation of dose conversion factor from radon progeny (DCF_{RnP}) as a function of AMAD.

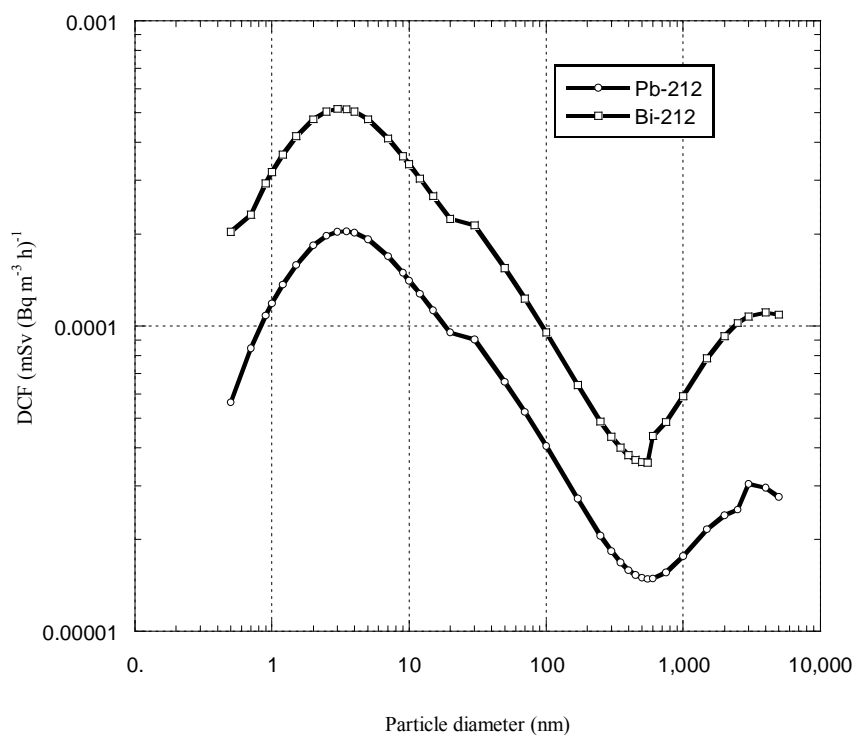


Figure 2-5 Variation of dose conversion factor from thoron progeny (DCF_{TnP}) as a function of AMAD.

The DCF for all decay products of radon and thoron exhibit almost identical dependency on median diameters of radon/thoron aerosols particles. A reduction of DCF was observed below the range of 100 nm. The highest DCF was noticed around 3.5 nm and the lowest value appeared at 550 nm.

Chapter III

PRELIMINARY WORK

Chapter III presents the previous work on mitigation of the effective dose of radon decay products through the use of an air cleaner in a dwelling in Okinawa, Japan [45]. The concentration of radon and its decay products and the activity size distribution of attached aerosol particles were measured with and without the use of an air cleaner in a dwelling with a high radon concentration.

3.1 Study Location

Concentrations of indoor radon and its decay progeny were measured in the first-floor bedroom of a dwelling in Yomitan village, Okinawa prefecture, Japan. The study took place from 19 to 21 November 2007. The volume and surface area of the room are about 72 m³ and 24 m², respectively. The walls and the floors are made from gypsum board and wood, respectively. The bedroom was selected for experiments because relatively high levels of radon concentration had been previously recorded in this room [46].

3.2 Measurement Techniques

Indoor radon concentration and equilibrium equivalent concentration of radon (EECRn) were measured continuously at every one hour with a pulse ionization chamber (AlphaGUARD, Genitron Instruments GmbH, Germany) and a Working Level monitor (Pylon Electronics Inc., Canada), respectively.

The total activity concentration of radon progeny was measured after sampling radon progeny on a glass microfiber filter (47 mm diameter, Whatman[®], England) that had been operated at a flow rate of 10 L min⁻¹ for 5 min. Gross alpha particles were counted with a ZnS(Ag) scintillation detector (Ludlum Instrument Inc., USA) for a period of 40 min at 5-min intervals. The concentrations of ²¹⁸Po, ²¹⁴Pb, and ²¹⁴Bi were calculated with the method described by Thomas [47].

The unattached fraction of radon progeny was measured by using an alpha spectrometry method. Unattached progeny was collected on a 400-mesh metal wire screen (47 mm diameter, TETKO Inc., USA), and they were considered as a single type for convenience. The diffusion coefficient was assigned to be 0.065 cm² s⁻¹ [48].

The alpha activities were detected during and after air sampling by a continuous air monitoring PIPS detector (Model CAM1700, Canberra Inc., USA), which was set opposite to the metal wire screen [49]. The measurement system was set up as shown in Figure 3-2. ^{241}Am was used as a calibration source, and the counting efficiency was found to be $30.1 \pm 0.5\%$. The detector has an active area of 1700 mm^2 (46.5 mm diameter) and an alpha energy resolution of about 70 keV. This resolution enables the discrimination between the alpha particle energies of 6.0 MeV from ^{218}Po and 7.8 MeV from ^{214}Po . To determine the activity concentration of unattached radon progeny (^{218}Po , ^{214}Pb and ^{214}Po), the measurements were performed in two steps. First, the alpha spectrum was acquired during a sampling period of 20 min. Second, after waiting for a period of 5 min without sampling, the alpha spectrum was measured again (during decay) for a period of 15 min. The air flow rate during the measurement was 4 L min^{-1} . From the measured alpha-counts of ^{218}Po and ^{214}Po during the sampling period and the ^{214}Po counts during the decay period, the activity concentrations of ^{218}Po , ^{214}Pb , and ^{214}Bi could be calculated by using the build-up and decay method [50]

For the determination of the particle size distribution of the attached radon progeny, a Micro Orifice Uniform Deposit Impactor (Model 110 MOUDITM, USA) was used. Efficiency curves and interstage losses of the impactor stages were determined [51]. The impactor consisted of eight size fractionating stages and a back-up filter holder, and it was operated at a flow rate of 30 L min^{-1} for 10 min. The measured 50% cut-off diameters for the eight stages were 0.056, 0.10, 0.18, 0.32, 0.56, 1.0, 1.8, 3.2, and $18 \mu\text{m}$. A 400-mesh metal wire screen was set at the top of the MOUDI to prevent invasion of unattached progeny, and the collection efficiency was estimated to be 89.1%, based on fan model filtration theory [52]. After sampling, the collected activity on each impactor stage was simultaneously measured with the ZnS(Ag) scintillation detectors. The activity concentrations of radon progeny for each stage were analyzed by using the decay method. The particle size distributions were described in terms of a log-normal distribution, defined by the activity median aerodynamic diameter (AMAD) and geometric standard deviation (σ_g). In addition to this numerical evaluation, the impactor data were also evaluated by the Expectation-Maximization algorithm [53].

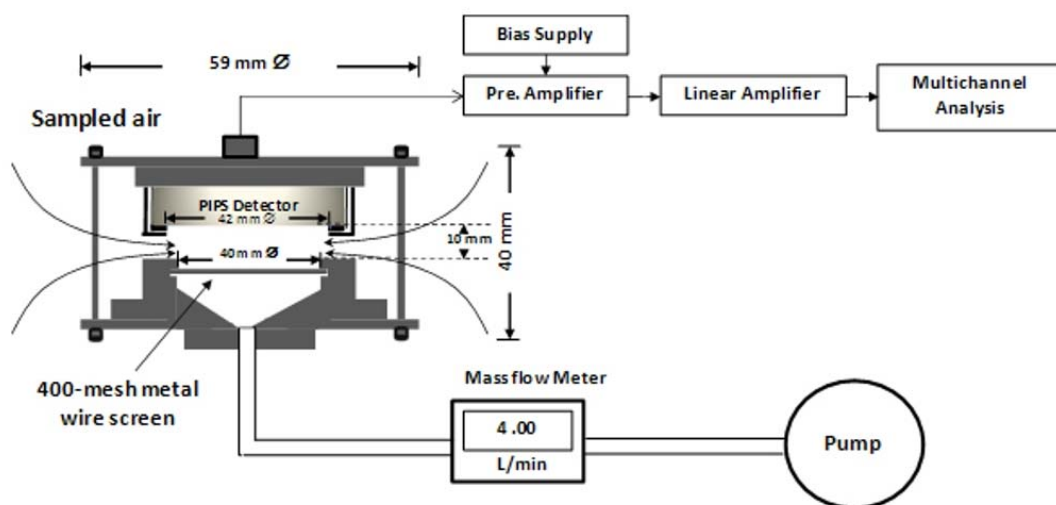


Figure 3.1 The schematic diagram of unattached radon progeny measuring system.

3.3 Measurement Conditions

The air cleaner (Hitachi model EP-X31, Japan) was equipped with a HEPA filter and a deodorizing activated carbon filter, and was set at the highest flow rate ($6.5 \text{ m}^3 \text{ min}^{-1}$) for faster and more powerful room cleaning. The air cleaner is suitable for a room of up to about 50 m^2 in size, according to its specifications. Measurements were conducted without the operation of the air cleaner (case I, 16:00 on 19/11/07 to 16:00 on 20/11/07) and with it (case II, 16:00 on 20/11/07 to 16:00 on 21/11/07). Human activities were kept as a minimum as possible during the measurement periods.

Ambient conditions in the room, including temperature, relative humidity, and air pressure were continuously measured, along with the radon concentration, by the AlphaGUARD monitor.

3.4 Results and Discussion

3.4.1 Measurement Results

Figure 3-2 shows the temporal variations for radon concentration and EECRn (Figure 3-2a), temperature and relative humidity (Figure 3-2b), and air pressure (Figure 3-2c) for cases I and II. The radon concentration level and EECRn show the same tendencies in both cases. In this measurement, the differences in temperature

and air pressure between indoor and outdoor were about 2-5 °C and 1-3 hPa, respectively. These differences were not so significant. However, the mean radon concentration in case II (373 Bq m⁻³) was higher than in case I (229 Bq m⁻³) (Table 3-1), whereas the mean EECRn was lower by about 57%. A possible explanation is that the difference resulted from the human activities in the experimental room and from the indoor-outdoor air exchange process on radon entry into or escape from the experimental room. The air exchange process is the results of a complex interplay of many factors, such as wind velocity and indoor-outdoor temperature and air pressure differences. In addition, these factors are time-varying [54]. The cause of difference in radon concentration could not be specified from our short-term survey. Long-term measurements of radon concentration and related parameters will be necessary. The mean radon concentration during the measurement was more than 300 Bq m⁻³ (Table 3-1), much higher than the average annual indoor radon concentration in Japan (15.5 Bq m⁻³). The effectiveness of the air cleaner in reducing exposure can be observed from the values for the equilibrium factor (F , the ratio of EECRn to radon concentration): it was about one-third the size of case I in case II (decreased by about 71%). Li and Hopke [55] also reported that the radon concentration was unchanged but F was reduced by about 50-60 % when the air cleaning system was operated.

Table 3-1 Mean (\pm standard deviation) concentrations of radon and its progeny.

Case	Radon (Bq m ⁻³)	EECRn (Bq m ⁻³) ^{a,c}	F ^b
I	229 \pm 15	33.1 \pm 3.1	0.14 \pm 0.01
II	373 \pm 17	14.4 \pm 0.7	0.04 \pm 0.01
Mean	301 \pm 17	23.8 \pm 1.6	0.08 \pm 0.01

^aEECRn is the equilibrium equivalent concentration of radon, that was calculated using “Correction Factor (CF)”, and the CF was estimated assuming a certain activity concentration ratio: ²¹⁸Po, ²¹⁴Pb and ²¹⁴Bi = 1:1:1. However, in actual environment, the concentration ratio of ²¹⁸Po, ²¹⁴Pb and ²¹⁴Bi is always different from it.

^b F is the equilibrium factor as a ratio of EECRn to radon concentration.

A summary of radon progeny concentrations is shown in Table 3-2. The unattached progeny of ²¹⁸Po and ²¹⁴Bi increased by about 50% during the operation of the air cleaner, and the attached progeny decreased as compared with case I. The potential alpha energy concentration (PAEC) of unattached progeny increased by about 87 %, while the air cleaner was operated (case II). The unattached progeny

increased because aerosol particles were removed from the room air by the air cleaner. Thus, newly formed radon decay products have fewer particles to which they can attach, and the concentration of unattached progeny can increase during the operation of an air cleaner with a high-efficiency filter [56]. Consequently, there is also a high value for f_p in case II, which increased by about 174% as compared with case I. However, the activity concentrations of ^{218}Po and ^{214}Pb and the PAEC of the whole fraction (attached and unattached fractions) in case II are lower than in case I. This resulted in a low F value for case II (Table 3-1).

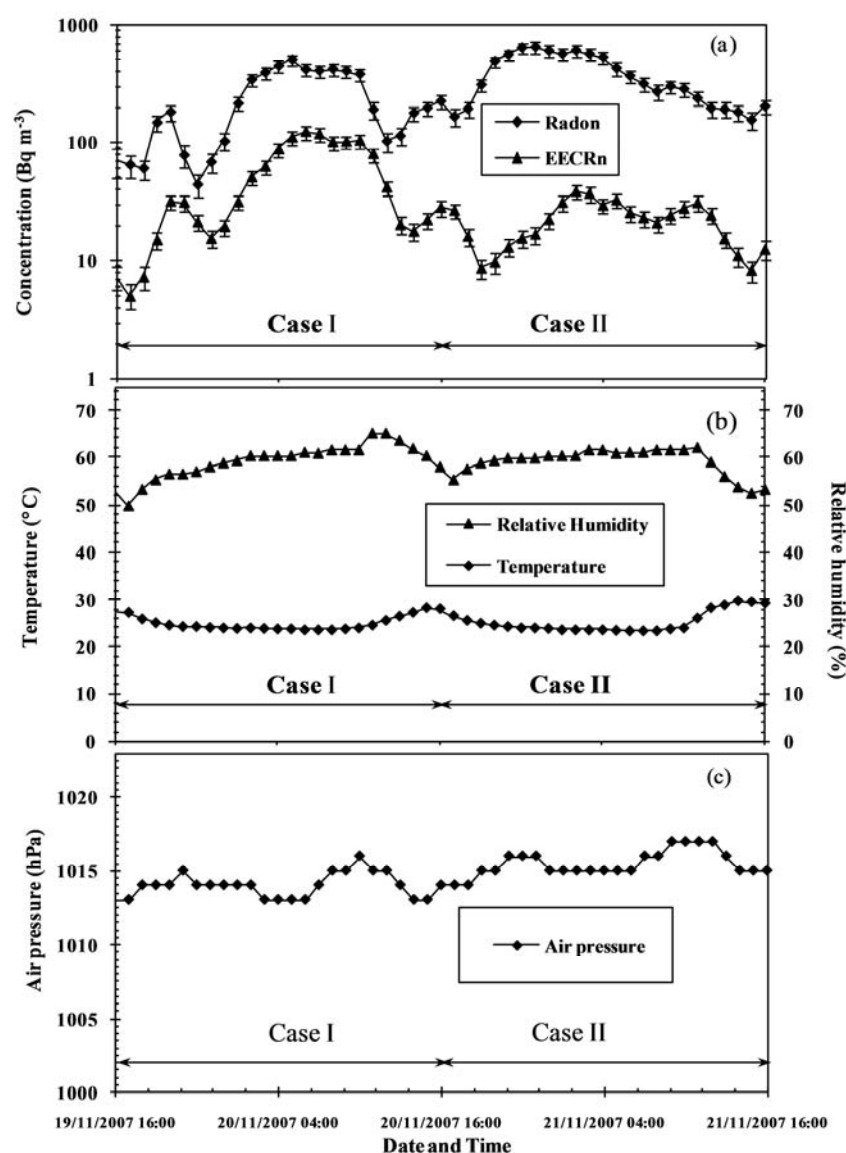


Figure 3-2 Temporal variations of (a) radon and EECRn, (b) temperature and relative humidity, and (c) air pressure.

Table 3-2 Mean (\pm standard deviation) concentrations of the unattached and total activity concentrations (ranges are given in parentheses)^{a, b}.

Case	Number of measurement	C_1^{un} (Bq m ⁻³)	$C_1^{\text{att+un}}$ (Bq m ⁻³)	C_2^{un} (Bq m ⁻³)	$C_2^{\text{att+un}}$ (Bq m ⁻³)	C_3^{un} (Bq m ⁻³)	$C_3^{\text{att+un}}$ (Bq m ⁻³)	PAEC ^{un} (nJ m ⁻³)	PAEC ^{att+un} (nJ m ⁻³)	f_p^{c}
I	5	26.4 \pm 1.4 (3.3–51.7)	75.4 \pm 2.9 (46.5–88.2)	0.9 \pm 0.4 (0–3.0)	23.0 \pm 0.8 (13.7–33.6)	2.1 \pm 0.3 (0–5.9)	5.7 \pm 1.0 (0.04–11.3)	22.3 \pm 1.3 (7.6–42.2)	119.7 \pm 3.5 (65.2–161.1)	0.19 (0.05–0.21)
II	6	52.2 \pm 0.4 (37.6–63.7)	60.0 \pm 1.8 (48.2–90.1)	0.8 \pm 0.2 (0–3.8)	12.8 \pm 0.5 (5.8–20.4)	4.4 \pm 0.1 (2.5–5.8)	4.8 \pm 0.6 (1.5–9.1)	41.7 \pm 0.6 (37.6–47.8)	80.6 \pm 2.1 (62.6–125.6)	0.52 (0.30–0.71)

^a“un” and “att+un” refer to unattached progeny and total progeny, respectively.

^b C_1 , C_2 and C_3 refer to the activity concentrations of ²¹⁸Po, ²¹⁴Pb and ²¹⁴Bi, respectively.

^c f_p is the unattached fraction, which was calculated using the equation $f_p = \text{PAEC}^{\text{un}} / (\text{PAEC}^{\text{att+un}})$.

Figure 3-3 shows the activity size distribution of radon progeny for the two cases. The parameters for the activity size distributions of the attached radon progeny are summarized in Table 3-3, where it can be seen that σ_g is the same for both cases in the nucleation, accumulation, and coarse modes. The lowest activity fractions of the coarse mode in both cases are observable. In addition, the activity concentration of attached radon progeny (Figure 3-3) in the accumulation mode (50–2000 nm) in case II was obviously decreased by about 42% as compared with that of case I. This decrease is related to the EECRn level (Figure 3-2a), which was lower in case II than in case I. Furthermore, the deposition velocity of accumulation mode particles is less than that of nucleation and coarse mode particles [57]. Particles in the accumulation mode can therefore no longer be in suspension in air. Thus, it is feasible that the decreased EECRn in case II is a result of a reduction of particles in the accumulation mode.

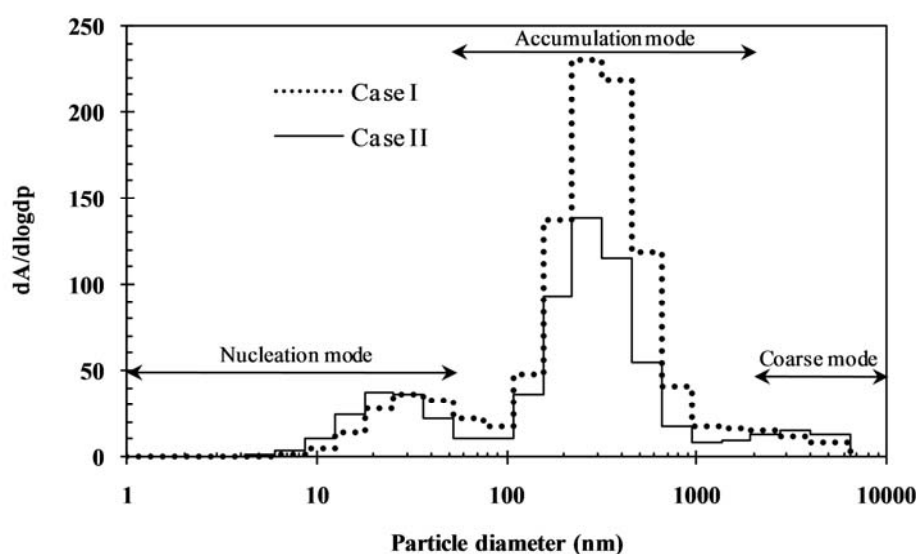


Figure 3-3 The activity size distribution of radon progeny (averaged over the study period).

Table 3-3 Mean values of the activity median aerodynamic diameter ($AMAD_i$), the geometric standard deviation (σ_{gi}), and the activity fraction (f_i) of log-normal activity size distribution of attached progeny (ranges are given in parentheses). The nucleation mode (aerosol particle size range: < 50 nm), accumulation mode (50–2000 nm), and coarse mode (> 2000 nm) are represented by Mode 1, Mode 2, and Mode 3, respectively [58].

Case	Number of measurements	Radon progeny								
		Mode 1			Mode 2			Mode 3		
		$AMAD_1$ (nm)	σ_{g1}	f_1	$AMAD_2$ (nm)	σ_{g2}	f_2	$AMAD_3$ (nm)	σ_{g3}	f_3
I	4	29 (23–42)	1.6 (1.5–1.7)	0.14 (0.09–0.21)	267 (234–308)	1.7 (1.6–1.9)	0.81 (0.73–0.86)	2082 (1858–2520)	1.5 (1.4–1.6)	0.05 (0.05–0.07)
II	3	23 (17–28)	1.6 (1.5–1.7)	0.20 (0.05–0.32)	249 (217–275)	1.7 (1.6–1.8)	0.71 (0.73–0.86)	2576 (2170–3143)	1.5 (1.4–1.6)	0.08 (0.03–0.17)

i refer to the mode of particles.

These results show that the air cleaner used in this study is effective in removing particles in the accumulation mode, that in agreement with the Trust Science Innovation [59], that reported the mechanisms of HEPA filter is high efficiency (99.97%) for 300 nm particles at a flow rate of $0.085 \text{ m}^3 \text{ min}^{-1}$. Therefore, F (Table 3-1) decreased and f_p (Table 3-2) increased in case II as a result of the removal of particles in the accumulation mode. Several studies [55, 60, 61] have shown that air cleaners are effective in reducing total radon progeny, although the concentration of unattached radon progeny can increase.

3.4.2 Estimation of Effective Dose

To estimate the effective dose from radon progeny, the effective dose per unit exposure to radon progeny (the dose conversion factor, DCF) is needed. The DCF can be derived by using either a dosimetric or an epidemiological approach. Although the International Commission on Radiation Protection (ICRP) recommends that the DCF should be based on epidemiological studies, it also states that a dosimetric approach is useful for comparing the doses that result from different exposure conditions [33]. In the present study, aerosol conditions are quite different between the two cases. Thus, the effective dose was compared between the two cases, using the ICRP 66 dosimetric model.

Porstendörfer [41] proposed that a dominant factor affecting the DCF is f_p , and that it can be expressed as the following function of f_p :

$$DCF = DCF_{ae} + C f_p \quad (3-1)$$

where DCF_{ae} is the DCF for the attached fraction and C is a constant derived from DCF for the unattached fraction (DCF_{un}).

Ishikawa et al. [38] calculated DCF values for reference conditions in places that have different aerosol characteristics. Using these values, the DCF_{ae} was calculated to be $20.2 \text{ nSv}/(\text{Bq h m}^{-3})$ for case I and $26.1 \text{ nSv}/(\text{Bq h m}^{-3})$ for case II. Also, the DCF_{un} was calculated to be $86.6 \text{ nSv}/(\text{Bq h m}^{-3})$ for cases I and II, assuming that AMAD and σ_g of a typical particle size distribution for the unattached fraction are 1 nm and 1.3, respectively [38]. On the basis of these values, DCF can be expressed as the following functions of f_p :

$$\text{Case I: } DCF = 20.2 + 66.4f_p \text{ nSv}/(\text{Bq h m}^{-3}) \quad (3-2)$$

$$\text{Case II: } DCF = 26.1 + 60.5f_p \text{ nSv}/(\text{Bq h m}^{-3}) \quad (3-3)$$

Using the above formulas and the unattached fraction (Table 3-2), the DCF of case I was calculated to be $32.8 \text{ nSv}/(\text{Bq h m}^{-3})$ and that of case II was $57.6 \text{ nSv}/(\text{Bq h m}^{-3})$. That is, the DCF for case II is about 1.8 times the size of that for case I.

The Radiological Protection Regulation [33] recommends that the minimum exemption level for exposure situations to radon in dwellings is 200 Bq m^{-3} . Using this radon concentration and estimated equilibrium factors (Table 3-1), the EECRn was assumed to be 28 in case I and 8 in case II. Consequently, the effective dose (rate) for the two cases can be compared as follows:

$$\text{Case I: } 28 \text{ Bq m}^{-3} \times 32.8 \text{ (nSv}/(\text{Bq h m}^{-3})) = 918 \text{ nSv/h}$$

$$\text{Case II: } 8 \text{ Bq m}^{-3} \times 57.6 \text{ (nSv}/(\text{Bq h m}^{-3})) = 461 \text{ nSv/h}$$

Therefore, operation of the air cleaner decreased the effective dose by 50%. This result was in general agreement with the 39% dose reduction found by Li and Hopke [55].

3.5 Conclusions

This study was conducted to investigate the effects of an air cleaner on radon mitigation, including the dose mitigation effects. The air cleaner was operated at the highest flow rate ($6.5 \text{ m}^3 \text{ min}^{-1}$) in the room of 72 m^3 in volume. The results show that the EECRn and the equilibrium factor decreased, but the unattached fraction increased. According to our dose calculations, the effective dose resulting from the radon

progeny was reduced by operating the air cleaner. Hence, the use of an air cleaner was found to be an effective method for mitigating the health hazards of exposure to indoor radon.

Chapter IV

DESIGN AND MODIFICATION OF THE IMPACTOR, PERFORMANCE TEST AND VALIDATION OF DEVELOPMENT TECHNIQUE

In this chapter, describes about the modifications of the cascade impactor and the associated experiments to test the performance of the developed technique on radon and thoron. Parameters that might affect sensitivity and reliability of the technique have been evaluated. The findings of experiments with modified cascade impactor are also reported to obtain the most desirable results.

4.1 Impactor design

A portable air sampler for this study has been designed to measure particulate matter (PM) exposure studies due to its sharp cut-point diameter characteristic. The design of a portable impactor is expected to be able to handle the size distribution of aerosols which would be represented by log-normal size distribution mode. A four fractionating size-selective impactor has been selected on the basis of deposition and retention of aerosol from the human respiratory tract. For most people during breathing air enters respiratory tract and aerosol particles are deposited in various regions of the human lung; extratrathoracic region (inhalable aerosol: 10-2.5 μm), tracheobronchial region (thoracic aerosol; 2.5-1 μm) and alveolar region (respirable aerosol; 1-0.5 μm). It operates in conjunction with a small, battery-operated mini-pump (MP- Σ 500, SIBATA, Japan). It is a made-to-order impactor from Tokyo Dylec Corp, which manufactures several types of particle size instruments in Japan. A cross-section view of the portable cascade impactor is shown in Figure 4-1. The four nozzle array was selected to collect radon and thoron progeny on detection channel of impaction plates. The nozzles for each stage were determined by the manufacture using the Reynolds number. Marple and Liu [62] recommended a Reynold number from 300 to 3000. Moreover, the nozzle plate plays the most important role among the impactor components in terms of determining the particle collection efficiency. The number of nozzles (N) and the nozzle diameter (W) are major design parameters in a multi-nozzle impactor as reported by Marple and Willeke [63]. In this studies, we

have used four nozzle-plate and impactor plate-section for aerodynamic cut-off sizes 0.5, 1.0, 2.5 and 10 μm at a flow rate $Q = 4 \text{ L min}^{-1}$. The initial (approximate) design parameters included the selection of the jet width and number to give the Reynolds number (Re) through the nozzle. The final design parameters presented in Table 4-1 were calculated assuming the following physical properties: temperature $T=20 \text{ }^\circ\text{C}$; pressure $P=101.3 \text{ kPa}$; density of aerosol particles $\rho_p=1 \text{ g cm}^{-3}$; density of air $\rho=1.205 \times 10^{-3} \text{ g cm}^{-3}$; and dynamic viscosity of air $\mu=1.82 \times 10^{-4} \text{ g cm}^{-1} \text{ s}^{-1}$. The impactor d_{50} values were calculated using the relationship, defined as follows:

$$d_{50} \cong \sqrt{\frac{9\pi n\mu W^3 S_{tk50}}{4\rho_p Q C}} \quad (4-1)$$

where the square root of the Stokes number $\sqrt{S_{tk50}} = 0.54$ and Cunningham slip correction factor C was approximated using the following equation [64].

$$C \cong 1.00 + \frac{0.16 \times 10^{-4}}{d_{50}} \quad (4-2)$$

Table 4-1 Design parameters for portable cascade impactor

Parameter	Symbol (units)	Design			
		Stage 1	Stage 2	Stage 3	Stage 4
Particle diameter at 50% impactor collection efficiency	$d_{50}(\mu\text{m})$	10	2.5	1	0.5
Square root Stokes number at 50% collection efficiency	$\sqrt{S_{tk50}}$	0.54	0.54	0.54	0.54
Reynolds number	Re	396	987	1765	2657
Number of impactor nozzles	n	4	4	4	4
Width of impactor nozzles	W(mm)	3.59	1.45	0.81	0.53
Jet-to-plate distance of impactor	S(mm)	11	8	4.5	4
Throat length of impactor nozzle	T(mm)	5.05	2.05	1.55	1.50

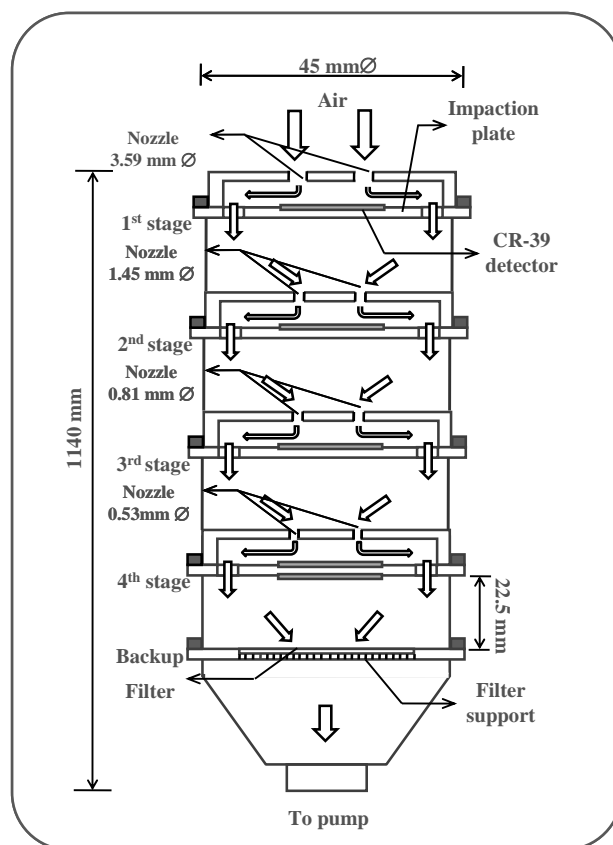


Figure 4-1 Cross-section view of portable cascade impactor.

4.1.1 Manufacture of portable cascade impactor

Each impactor stage consists of the identical stage wall, 4 round jets of nozzles and the impaction plate but differs in terms of nozzle diameter, and the thickness of the nozzle throat (T). This impactor is a round four-jet type with 4-size fractionating stages and a backup filter holder as shown in Figure 4-2. It is known that particles tend to focus toward the center in a straight orifice [65] which may result in their enrichment near the axis of the nozzle. Therefore, T was adjusted by modifying the thickness of the nozzle plate. In the absence of a gradual entrance region, strong aerodynamic focusing occurs which is responsible for the particle concentration enrichment that occurs in the axial region of the nozzle. To prevent an air leak from the inter-stage, O-rings were used. Fully assembled impactors were tightened in the impactor housing. In this design, aerosol particles are drawn through a series of progressively narrowing nozzles, each of which is followed by an impaction plate. After traversing the last stage (stage 4th), the stream is drawn through a backup filter

as it exits the device. Each impactor stage and a backup filter stage were tightened to prevent air leakage from the system.

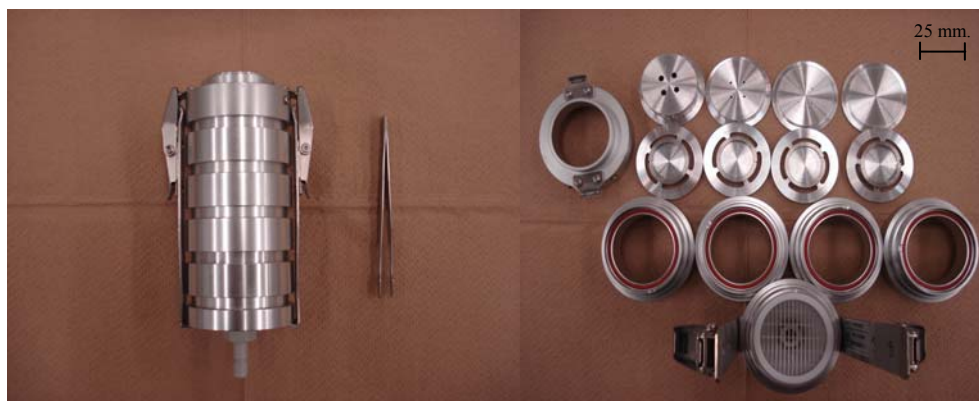


Figure 4-2 Picture of portable impactor sampler.

4.1.2 Modification of the collection media

In this study, the impactor has been slightly modified by inserting a CR-39 detector on the impactor plate as the collection substrate of stage 1st to 4th and on the ceiling of the backup filter holder, facing the glass microfiber filter. Figure 4-3 shows arrangement of the detection channel (CH1-CH4) on the impactor plate. In addition, each CR-39 is covered with proper aluminum vaporized Mylar films to detect the target nuclides as follows; CH1 is for ^{218}Po , ^{214}Po , ^{212}Bi and ^{212}Po , CH2 is for ^{214}Po and ^{212}Po , CH3 is for ^{212}Po and CH4 is for all radionuclides. Each thickness of film is properly adjusted to let their alpha particles reach CR-39 detectors. The film thickness of each channel was evaluated in the laboratory. This technique gives information on the activity of attached radon and thoron progeny with size separation.

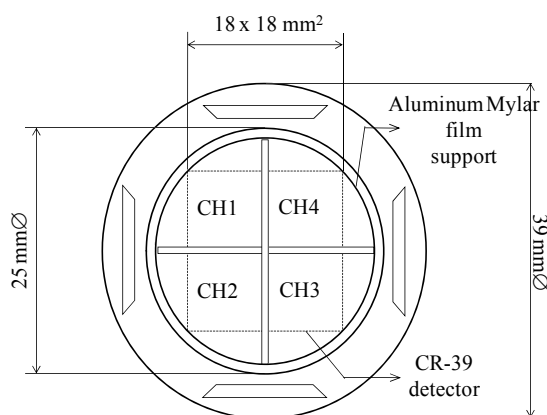


Figure 4-3 Arrangement of the detection channel on the impaction plate.

4.2 Performance test of impactor

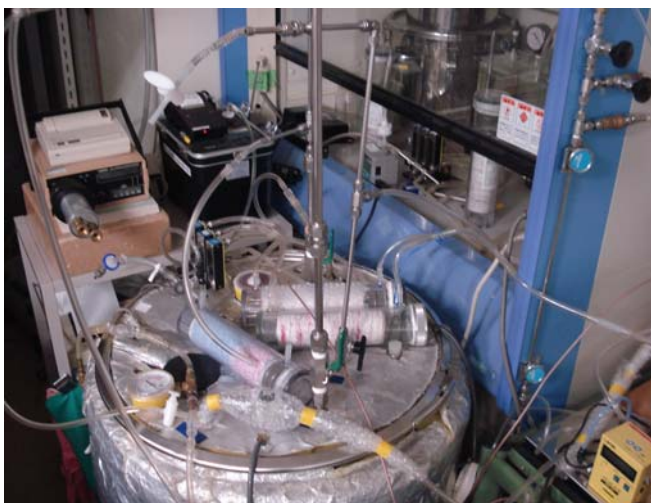
In order to test the performance of impactor for radon progeny, we have used a standard radon chamber at National Institute of Radiological Sciences (NIRS). The capacity of chamber is about 25,000-L inner volume and has been shown in Figure 4-4 a). Radon concentration in the chamber was continuously monitored with an interval of 10 min by a commercially available AlphaGUARD (Genitron GmbH, Germany) ionization chamber, which was calibrated by Physikalisch Technische Bundesanstalt (PTB), Germany. Radon concentration in the chamber was maintained at about 5 kBq m⁻³ in this study. For thoron progeny, a 150-L stainless steel chamber system made in NIRS as shown in Figure 4-4 b) was used. The ²²⁰Rn concentration in the chamber was measured continuously every 1 h using a RAD7 electrostatic collection method (Durridge Co. Inc., USA) and set at about 4 kBq m⁻³. The experimental set-up is shown schematically in Figure 4-5.

In order to test the influence of the detection response of the impactor on the presence of ambient aerosols, a condensation monodisperse aerosol generator Model 3472S (TSI Inc., USA) was used; aerosol particles were generated by the evaporation-condensation method and supplied into the chamber through the sampling port. Carnauba wax was used as the aerosol material in this study. The continuous particle size distribution was monitored by an ELPI, (Dekati Ltd., Finland) for the particle size bigger than 500 nm (it is operated at a flow rate of 30 L min⁻¹). The measured 50 % cut-off diameters for the thirteen stages were 0.029, 0.060, 0.105, 0.166, 0.255, 0.373, 0.637, 0.99, 1.61, 2.46, 3.98, 6.60 and 10.20 μm, while the aerosol particles smaller than 500 nm were measured by scanning mobility particle sizer Model 3936 (TSI Inc., USA).

The CR-39 detector was etched for 24 h at 60°C in 6.25 N NaOH solution. The etch-pits were counted by optical microscope.



a) Radon chamber



b) Thoron chamber

Figure 4-4 The illustration of reference chambers at NIRS.

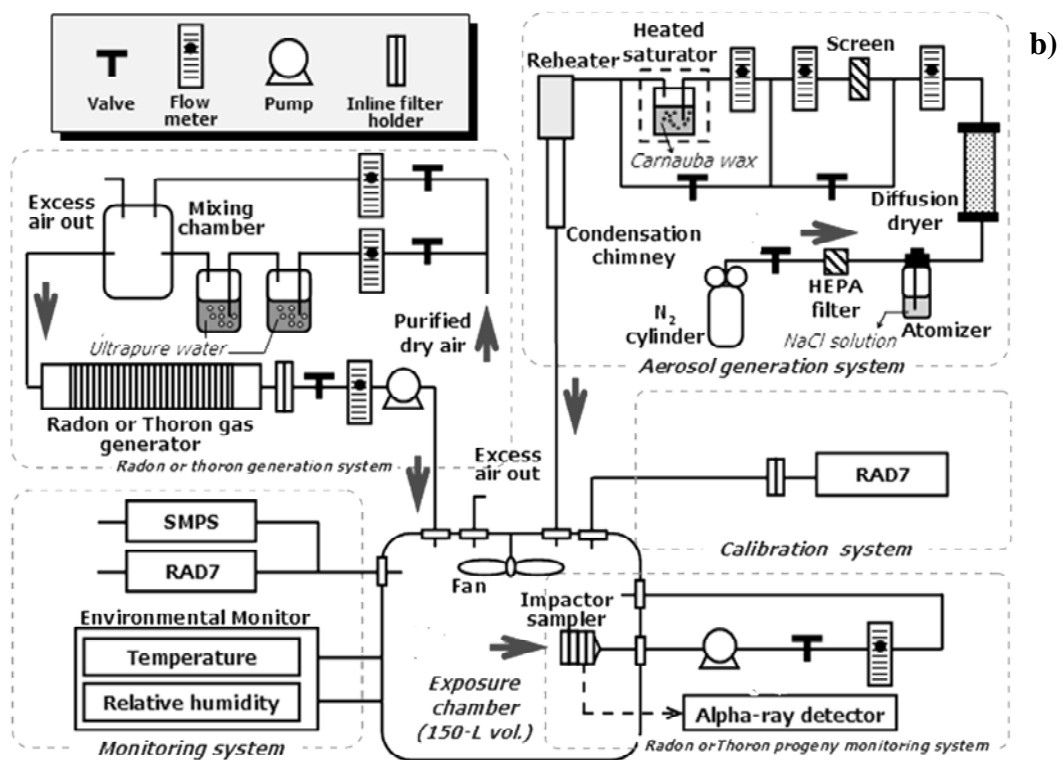
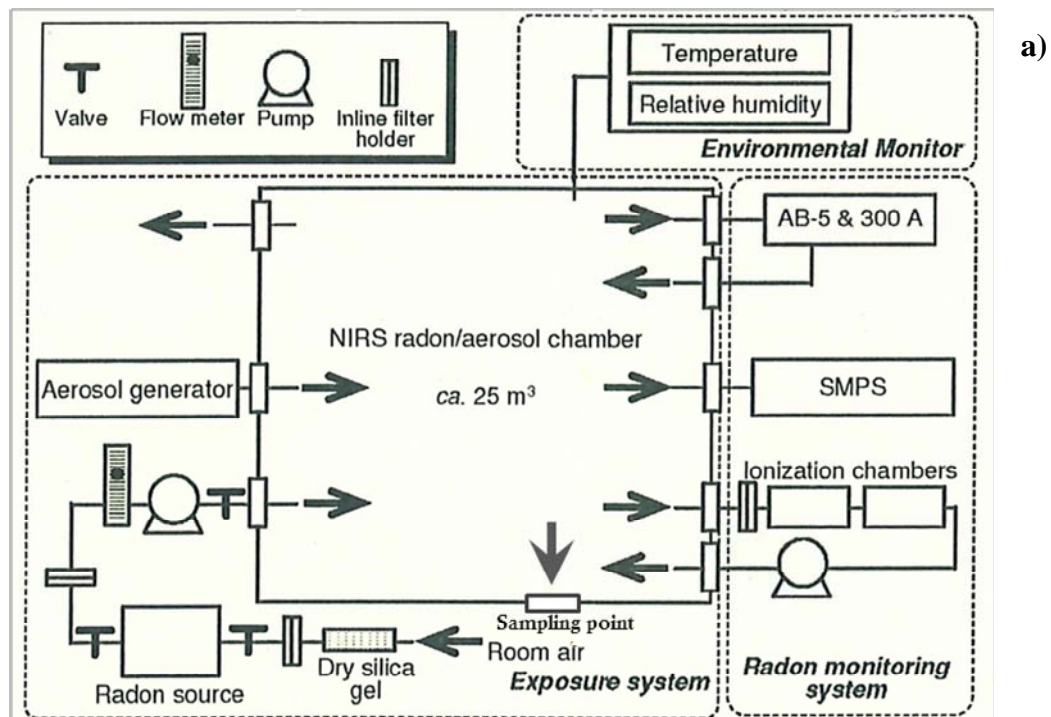


Figure 4-5 Experiment set-up for performance test: a) Radon chamber b) Thoron Chamber.

4.2.1 Discrimination of ^{222}Rn and ^{220}Rn progeny on CR-39 detectors with aluminum-vaporized Mylar films

In order to test the proper film area density for CH1, CH2 and CH3, the various area densities of aluminum-vaporized Mylar film corresponding to alpha particle energy of uranium-thorium and radon progeny to impinge on CR-39 were investigated. CH1, CH2 and CH3 are designed for cut-off alpha energies of about 4.2, 6.1 and 7.7 MeV from uranium-thorium, ^{218}Po and ^{214}Po , respectively.

For making energy of uranium and thorium, an aluminum-vaporized Mylar film with density about 1.34 mg cm^{-2} was used to attenuate α -energy of 5 MeV to 4.2 MeV. It has been tested using a ^{241}Am disc source (activity 974 Bq) and can be seen in Figure 4-6 a).

Short-lived alpha source of energy 7.7 MeV with reference to ^{214}Po was obtained from ^{222}Rn progeny by taking a sample on the 47 mm glass fiber filter. Afterward, it has been attenuated to 6.1 MeV with 1.19 mg cm^{-2} aluminum-vaporized Mylar film as shown in figure 4-6 b) for using as an α -particle source.

The proper film area density for above attenuation were calculated by SRIM program [32] and carried out experiment to confirm the energy of alpha after attenuated by Alpha spectrometry system (Canberra, USA). This detector has an alpha efficiency of approximately 33% at 5.5 MeV.

In the case of proper film area density for discrimination of ^{220}Rn progeny from ^{222}Rn progeny were also calculated by SRIM program and carried out experiment to confirm the energy cutoff by CR-39.

For impactor sampler, there are two measurement geometries of alpha particles that impinge on CR-39; (A) measuring the alpha particles emitted from aerosols and impinge on CR-39 (1st – 4th of impactor stages), and (B) measuring the alpha particles emitted from the surface of the glass fiber filter and impinge on the CR-39 through an air layer of 22.5 mm (back up filter holder impactor stage).

Results of triplicate measurements of the proper film area density for discrimination of ^{220}Rn progeny from ^{222}Rn progeny on CR-39 are shown in Table 4-2 and Figure 4-7.

Figure 4-8 is illustration of detector channel at each impactor plate geometry.

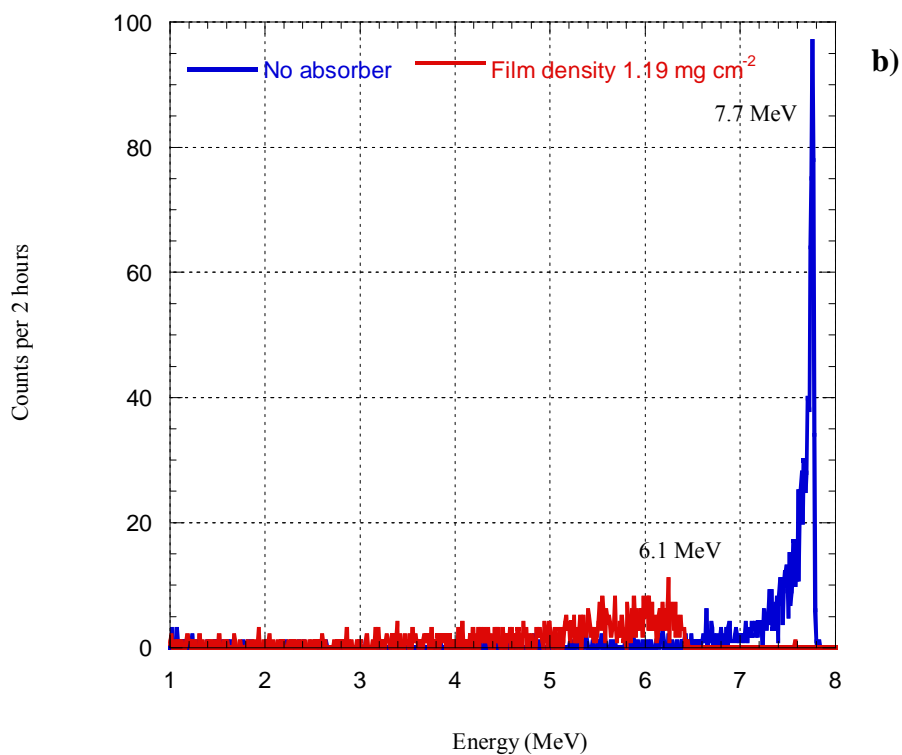
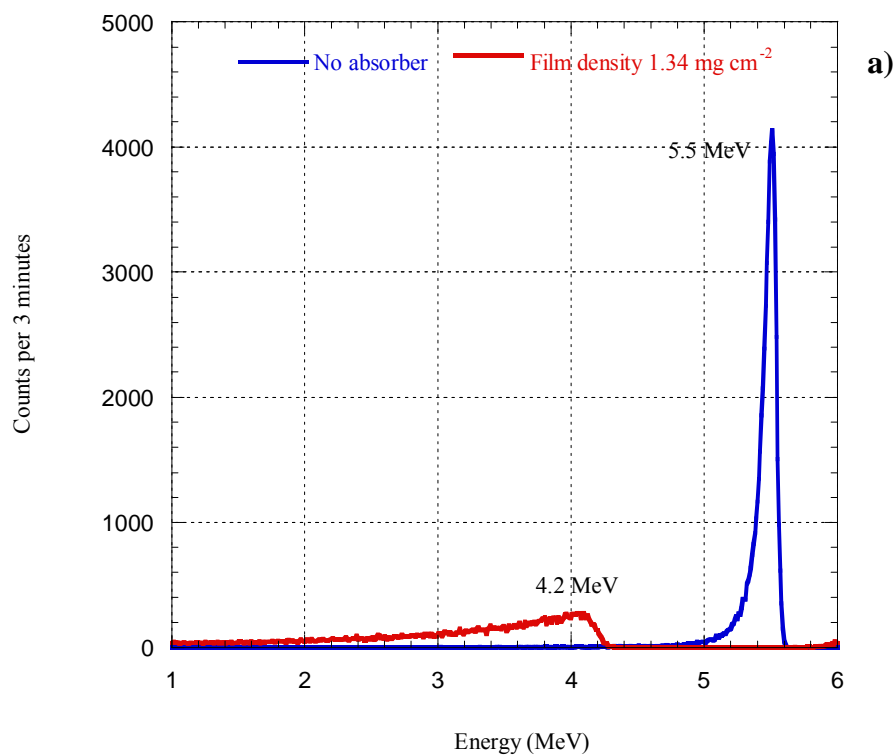


Figure 4-6 Alpha spectrum results: a) Attenuation of 5.5 MeV from Am-241
b) Attenuation of 7.7 MeV from Pb-214.

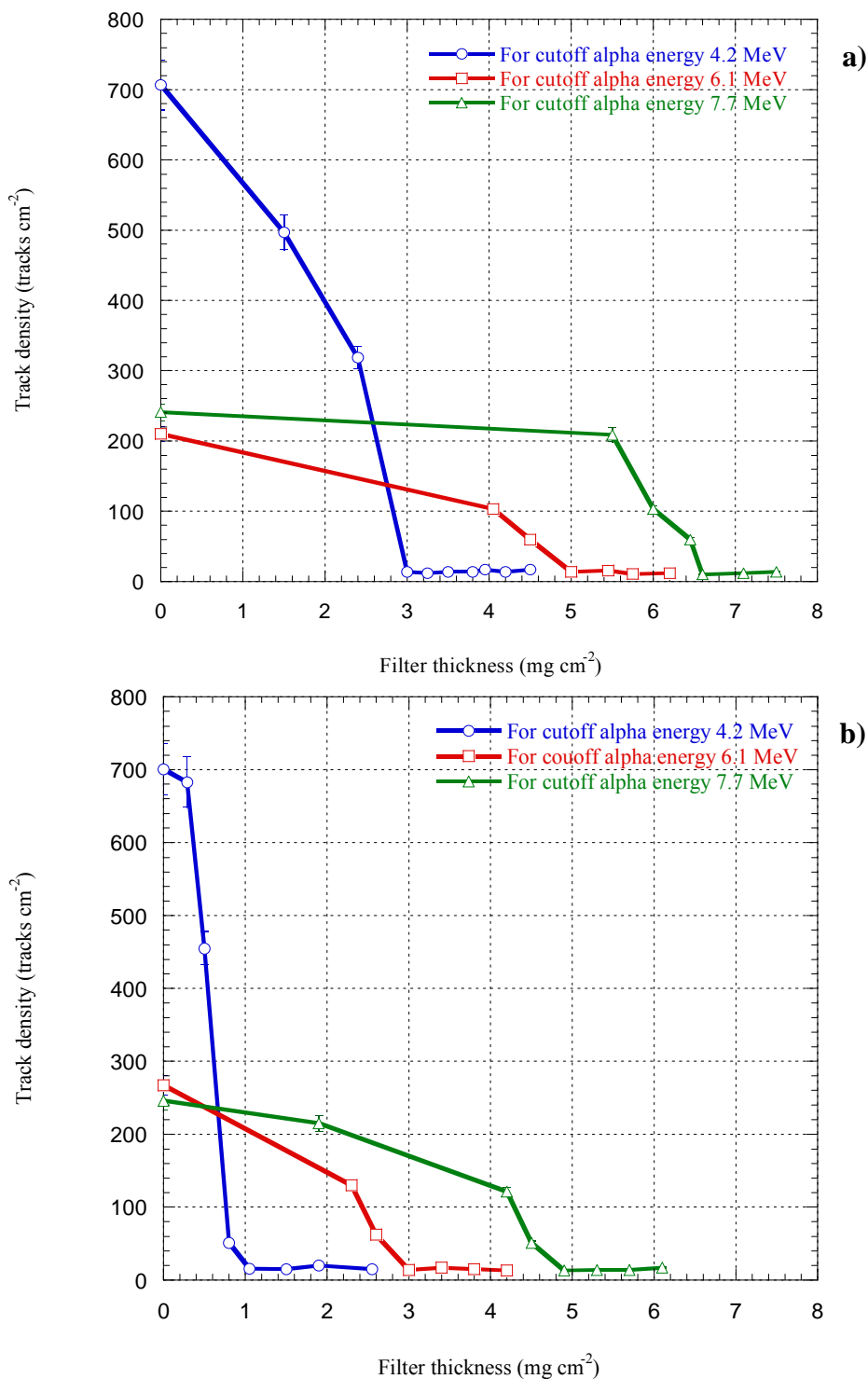


Figure 4-7 Relationship between track density and area density of film for cut-off alpha energy 4.2, 6.1 and 7.7 MeV: A) Measuring the alpha particles emitted from aerosols and impinge on CR-39. B) Measuring the alpha particles emitted from the surface of the glass fiber filter and impinges on the CR-39 through an air layer of 22.5 mm.

Table 4-2 Film area densities absorber for each channel

Channel	Film Thickness (mg cm ⁻²)		Cut-off of alpha energy (MeV)	Radionuclide collection
	(A)	(B)		
CH1	3.00	1.05	4.2	²¹⁸ Po-, ²¹⁴ Po, ²¹² Bi, ²¹² Po
CH2	5.00	3.00	6.1	²¹⁴ Po, ²¹² Po
CH3	7.10	5.00	7.7	²¹² Po
CH4	0.54	0.29	-	Blank

Remark: (A) Measuring the alpha particles emitted from aerosols and impinges on CR-39. (B) Measuring the alpha particles emitted from the surface of the glass fiber filter and impinges on the CR-39 through an air layer of 22.5 mm.



Figure 4-8 Illustration of detector channel at each impactor plate geometry.

4.2.2 Detector efficiency calibration

The efficiency of this impactor is made up of two parts; (A) the counting efficiency of CR-39 at measuring the alpha particles emitted from aerosols and impinge on CR-39 through the proper aluminum-vaporized Mylar films and (B) the counting efficiency of CR-39 at measuring the alpha particles emitted from the surface of the glass fiber filter and impinge on the CR-39 through an air layer of 25 mm and the proper aluminum-vaporized Mylar films. Figure 4-9 shows the experiment for alpha-track registration in this study.

In the experiment, when evaluating counting efficiencies of alpha particles emitted from radon and thoron progeny, a part of the filter was used for alpha

registration with CR-39 detectors (size 18 x 18 mm²) after air sampling. The rest was used for the alpha spectroscopic measurement to obtain an original alpha emission rate.

The collection efficiency could be calculated approximately by the following equation;

$$\eta = \frac{(N - N_{Bg})A_b \times 100}{t \times I \times A_a} \quad (3-3)$$

Where N = alpha-track density (track mm⁻²)

N_{Bg} = background alpha-track density (track mm⁻²)

A_a = effective area of filter that used for alpha track registration (mm²)

A_b = effective area of a part filter that measured by alpha spectrometry (mm²)

I = activity of source which measured by alpha spectrometry (Bq)

t = exposure time of track registration (s)

The value of counting efficiency is shown in Table 4-3.

Table 4-3 The average counting efficiency of CR-39

Geometry	Counting efficiency at various film area density (%)		Average Counting efficiency (%)
	Radon Progeny	Thoron Progeny	
1. measuring the alpha particles emitted from aerosols and impinge on CR-39 through the proper Al film	13.11	10.57	11.84
2. measuring the alpha particles emitted from the surface of the glass fiber filter and impinge on the CR-39 through an air layer of 22.5 mm and the proper Al film	10.12	9.90	10.01

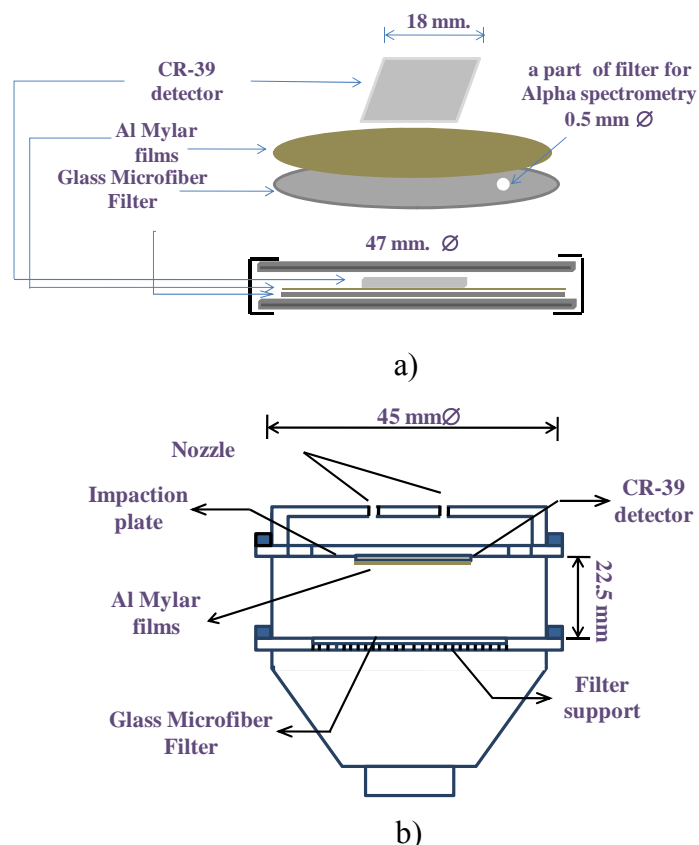


Figure 4-9 Experiment procedure for alpha track registration a) Measuring the alpha particles emitted from aerosols and impinge on CR-39. b) Measuring the alpha particles emitted from the surface of the glass fiber filter and impinges on the CR-39 through an air layer of 22.5 mm.

4.2.3 Impactor collection efficiency calibration

The particle collection efficiency as a function of particle size for each impactor cutpoint stages was determined using a condensation monodisperse aerosol generator (Model 3472S, TSI Inc., USA). Figure 4-10 shows a block diagram of the aerosol generator. After generation of the aerosols was mixed with room air (relative humidity: 60%, Temperature 20°C) in radon chamber (concentration 5 kBq m⁻³) for 2 h. Collection efficiency was determined by measuring total activity of attached radon progeny simultaneously on a reference filter (with impactor nozzle and impactor plate) and on the filter at downstream of the impactor (without impactor nozzle and impactor plate). Sampling system for collection efficiency of attached radon progeny is shown in Figure 4-11. Attached radon progeny samples were taken through sampling port settled on the side of chamber. After 10 min sampling, alpha particles

on each filter were counted using Ludlum Scintillation Model 43-1 counters (Ludlum Measurements Inc., USA). Alpha counts were registered in 1 min increments for a period of 40 min. The counting data were analyzed by the decay method [66], yielding the Equilibrium Equivalent Radon Concentration (EERC).

In addition, the SMPS and ELPI were used to evaluate the particles in size 0.3–0.5 μm range and 0.5-10 μm range, respectively. The SMPS could not be used for particles larger than approximately 0.6 μm since they are removed by the impactor that placed in the inlet of the instrument. Each impactor stage was evaluated using the following surfaces as impaction substrates:

- (a) 22.5 mm Glass fiber filter (GF/F, Whatmam)
- (b) 22.5 mm Aluminum-vaporized Mylar film disk

Impaction surfaces (a) and (b) were used without any coating or adhesive material for all impactor stages.

Figure 4-12 shows the illustration of instruments which were used in this study.

The particle collection efficiency of the impactor stage (E_c) was calculated as

$$E_c = \frac{(C_{w/o} - C_w)}{C_{w/o}} \times 100 \quad (3-4)$$

where C_w and $C_{w/o}$ are the activity of attached radon progeny with and without the impactor nozzle and impactor plate, respectively.

The result from collection efficiencies of portable impactor stage 3rd (1 μm) and stage 4th (0.5 μm) are presented in Table 4-4 and Figure 4-13 ~14. Particle collection efficiency data for each stage are plotted as a function of particle diameter. The collection efficiencies using two different materials as impaction substrates are shown in the same graph for direct comparison. The experiment data were fitted using a sigmoidal function. The cut point diameters of each impaction substrate are summarized in Table 4-5.

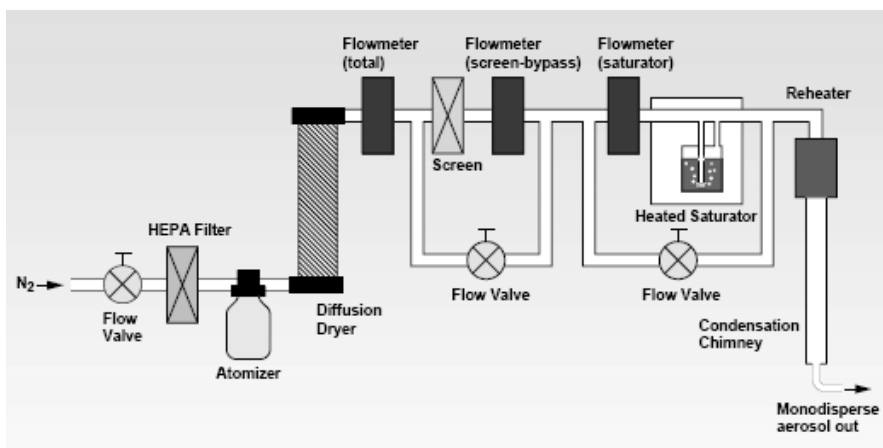


Figure 4-10 A block diagram of aerosol generator.

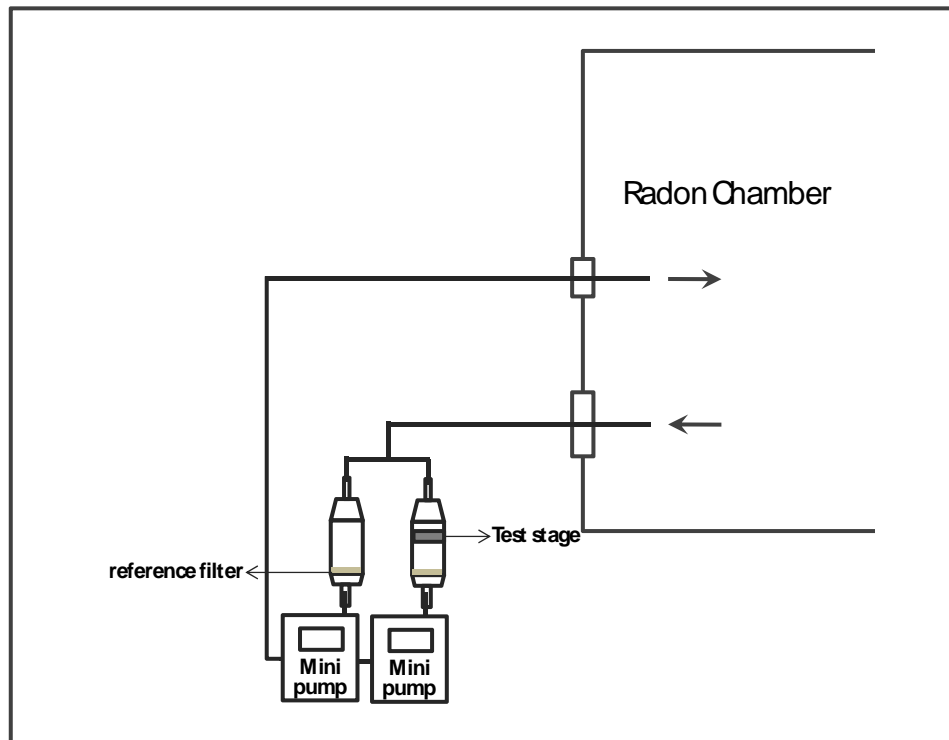
Table 4-4 The collection efficiency of portable impactor

Impactor Stage	Aerosol size (μm)	C_w (Bq m^{-3})		$C_{w/o}$ (Bq m^{-3})		E_C (%)	
		filter	Al disk	filter	Al disk	filter	Al disk
3	0.546	1239	1269	1283	1274	3.413	0.39
	0.637	995	1187	1208	1269	17.63	6.46
	0.715	920	1299	1182	1502	22.16	13.52
	0.905	193	259	690	619	72.03	58.16
	1.230	6	92	641	621	99.06	85.18
4	0.384	234	272	293	286	20.14	4.89
	0.458	813	1120	1403	1520	42.05	25.43
	0.546	499	572	1265	1253	60.55	54.35
	0.637	207	290	1182	1501	82.49	80.67
	0.715	176	237	1283	1322	86.28	82.07

Table 4-5 Cut point diameters of each impaction substrate for impactor stage 3 and 4

Stage No.	Cut-point diameter (μm) ^a	
	GF/F filter	aluminum vaporized Mylar films
3	0.95±0.04	1.00±0.03
4	0.50±0.17	0.53±0.06

^aDetermined by sigmoidal function



a) Sampling system block diagram



b) Illustration of sampling system

Figure 4-11 Sampling system for collection efficiency of attached radon progeny.

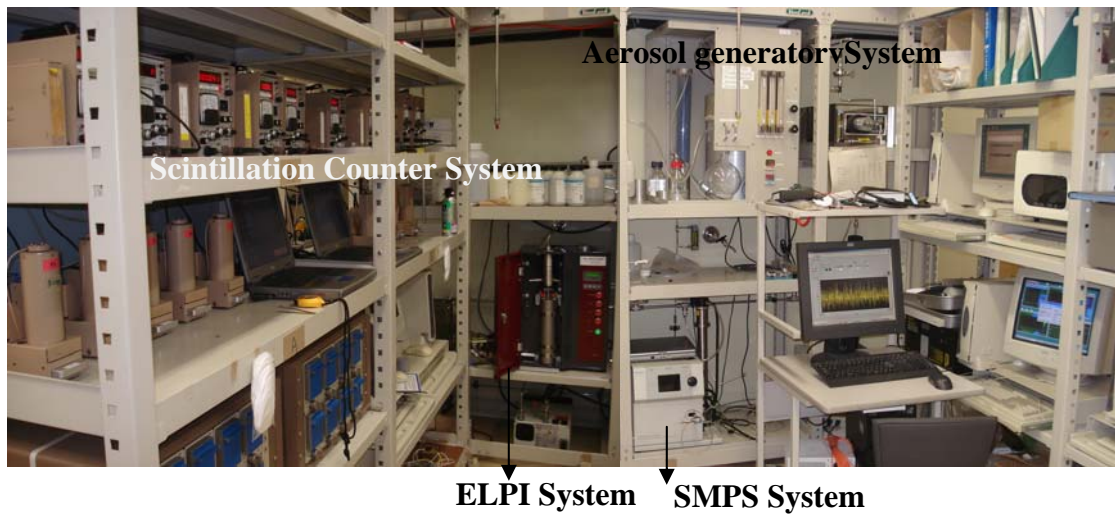


Figure 4-12 The illustration of instruments for collection efficiency calibration.

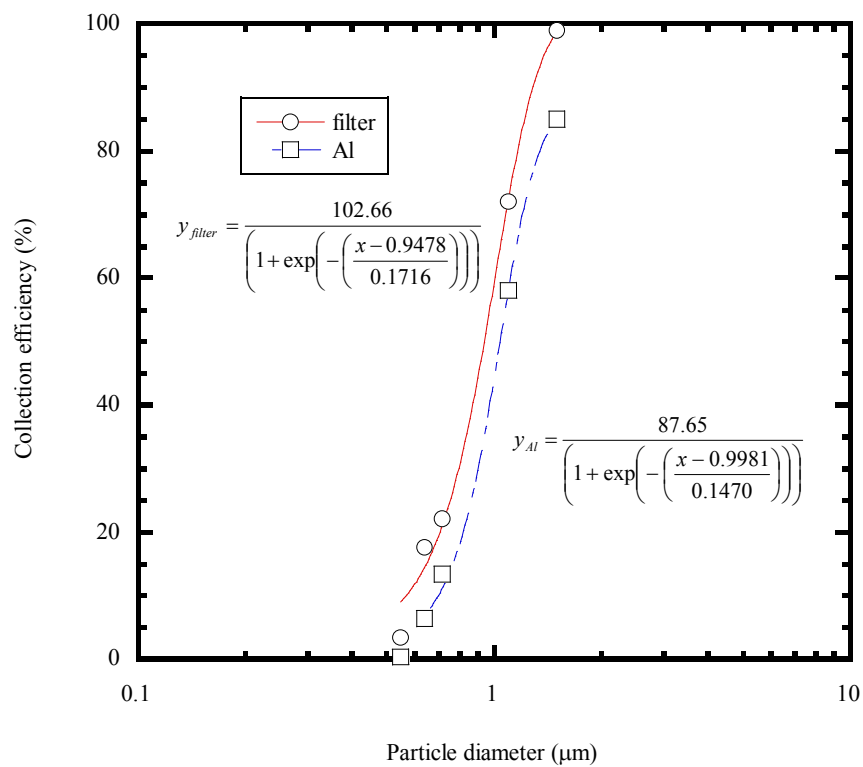


Figure 4-13 Collection efficiency of stage 3 (1 μm).

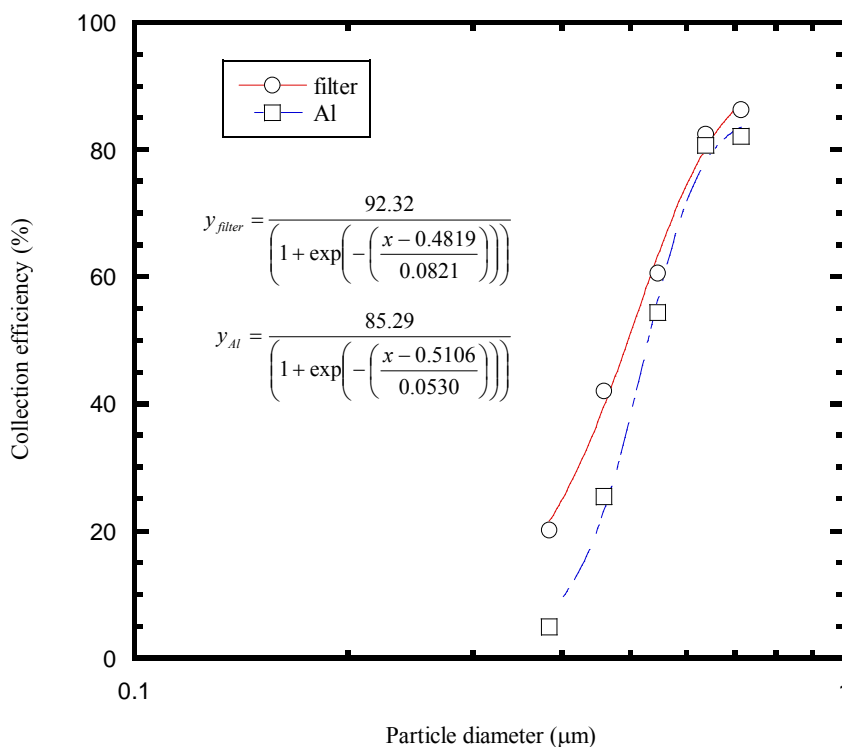


Figure 4-14 Collection efficiency of stage 4 (0.5 μm).

From the experimental collection efficiency data of stage 3 and 4 indicated that the 50% collection efficiency cut-point for filter and aluminum are closed to the design cut-point. Particle collection efficiency of aluminum substrate also decreased for particles smaller than 0.5 μm when compared with GF/F filter substrate, probably due to some particle bounce on that surface. This phenomenon is more likely to occur in the aluminum substrates because of the higher surface hardness of aluminum compared to filter paper.

The sharpness of the collection efficiency curve of an impactor can be defined in terms of the geometric standard deviation (σ_g), which is the square root of the ratio of the aerodynamic particle diameter corresponding to 16% collection efficiency to that corresponding to 84% efficiency [67]. Based on this principle, the values of σ_g for each stage and substrates were estimated and listed in Table 4-6.

Generally, lower σ_g values indicate the higher precision in particle separation characteristics of a given impaction stage, which is highly desirable feature of an impactor as it leads to a finer resolution in the size distribution of an aerosol. The

value of σ_g is approximately about 1.7–1.9 for filter and aluminum substrates, thereby indicating reasonably sharp particle separation characteristics when these two substrates were used.

Table 4-6 Sharpness of the collection efficiency for stage 3rd and 4th of the portable impactor as a function of substrate

Impactor stage (cut point diameter; μm)	Substrate type	σ_g
3 (1)	filter	1.37
	Al	1.37
4 (0.5)	filter	1.38
	Al	1.30

Unfortunately, we could not check the cut point diameter of stage 1st (10 μm) and stage 2nd due to limitation of aerosol generation system at NIRS which could not generated aerosol size bigger than 1.3 μm .

Taking into consideration of all the above experimental conditions, it could be assumed that the 50% collection efficiency cut-point for stage 1st and 2nd are also closed to the design cut-point of 10 and 2.5 μm , respectively.

4.3 Evaluation parameter that might affect the sensitivity of developed technique

In order to evaluate parameter that might affect sensitivity of the developed technique, radon chamber of NIRS was used. The radon concentration was maintained at about 5 kBq m^{-3} . For ambient aerosols, a condensation monodisperse aerosol generator Model 3472S was used; aerosol particles were generated by the evaporation-condensation method and supplied into the chamber through the sampling port. Carnauba wax was used as the aerosol material to generate a targeted aerosol size around 0.3 - 1 μm . The ambient aerosol concentration depends on the particle size and became constant 2 h after aerosol particles were injected into the chamber. The continuous particle size distribution was monitored by an ELPI. The developed technique was used for size measurement. The sampling and measuring time were 5 min and 4 h, respectively.

The CR-39 detectors were etched for 24 hours at 60° C in 6.25 N NaOH solution. The etch-pits were counted by a microscope. The Equilibrium Equivalent Radon concentration (EERC) and Equilibrium Equivalent Thoron concentration (EETC) were calculated theoretically from the etch-pit counts on the CR-39 detector that divided in to four channels by the equations 3.5 and 3.6, respectively.

The example of etch pit on the surface of CR-39 at each detection channel were shown in Figure 4-15.

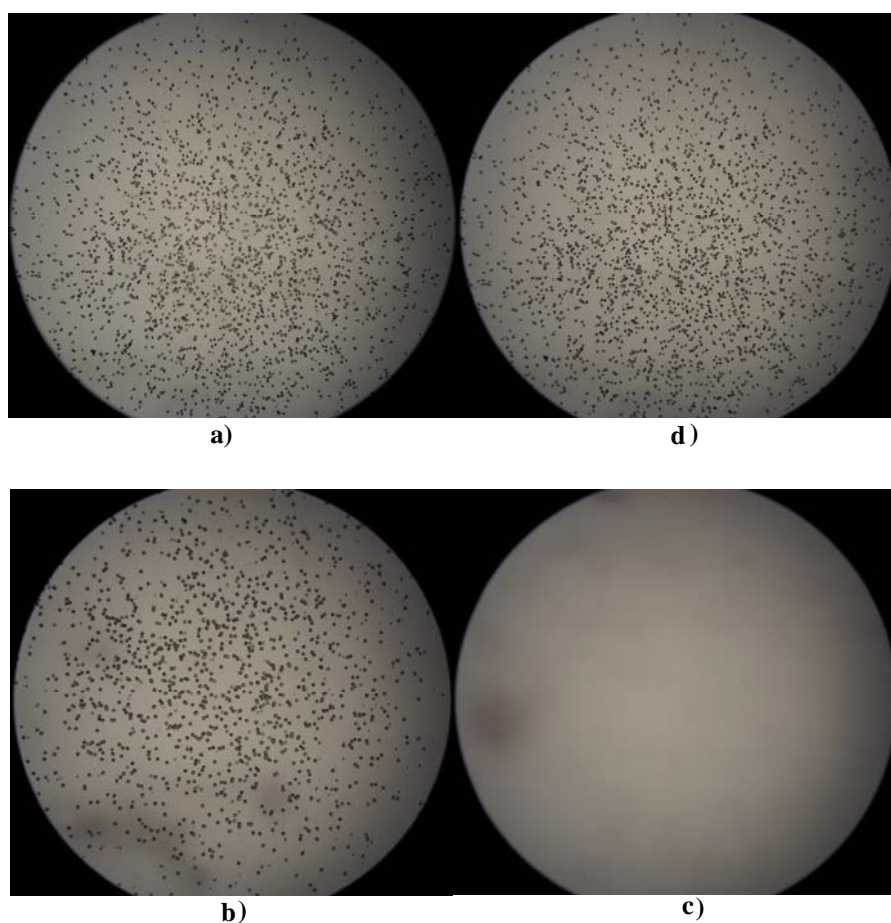


Figure 4-15 The illustration of etch pits on the surface of CR-39 at each detection channel of stage 3rd (Magnification: 100×). Sampling at radon concentration 5 kBqm⁻³ and aerosol size 1 μm was generated: a) CH1, b) CH2, c) CH3 and d) CH4.

Calculation method of EERC and EETC for portable impactor

For radiation protection purposes, the potential alpha energy concentration (PAEC) is usually the quantity of interest and it often measured in unit of Working

Level (WL). Another quantity of interest is the equilibrium equivalent concentration (EEC) measured in units of activity per unit volume.

A working level, WL, was originally defined as any combination of short-lived radon progeny (^{218}Po , ^{214}Pb , ^{214}Bi , ^{214}Po), and later by extension any combination of short-lived thoron progeny (^{216}Po , ^{214}Pb , ^{212}Bi , ^{212}Po), in 1 liter of air at normal temperature and pressure that had the potential to release 1.3×10^5 MeV of alpha particle energy in their ultimate radioactive decay.

The potential alpha energy concentration in air, is the sum of the potential alpha particle energy of all the short-lived radon or thoron progeny in a unit volume of air. The unit of potential alpha energy concentration defined as J m^{-3} or MeV m^{-3} .

The equilibrium-equivalent concentration, EEC, of a non-equilibrium mixture of radon or thoron progeny is the activity concentration of the parent radon or thoron gas in equilibrium with its short-lived progeny that has the same potential alpha energy concentration as the actual non-equilibrium mixture.

Therefore, EERC and EETC are theoretically calculated by the equation as follows;

$$EERC = \frac{(E_{Po-218} \times N_{Po-218 \text{ in } CH1}) + ((E_{Po-214} - E_{Po-218}) \times N_{Po-214 \text{ in } CH2})}{\eta \times T \times V} \times 2.846 \times 10^{-5} \quad (4-5)$$

$$EETC = \frac{[(E_{Bi-212} \times 0.561) + E_{Po-212}] \times N_{CH3}}{\eta \times T \times V} \times 0.215 \times 10^{-5} \quad (4-6)$$

where the counts of etch-pits on all channels are obtained with E_i , $N_{i\text{-ch}}$, T , V , and η .

E_i is alpha energy of i -nuclide in (MeV),

$N_{i\text{-ch}}$ is number of alpha tracks due to i -nuclide in the detection area of i -channel,

T is collecting period in (min),

V is flow rate in ($\text{m}^3 \text{ min}^{-1}$),

η is the CR-39 collection efficiency,

The collection efficiency was estimated deriving from the experiment and found 2.846×10^{-5} and 0.215×10^{-5} ($\text{Bqm}^{-3} (\text{MeV m}^{-3})^{-1}$) as the conversion constant for calculation of EERC and EETC from PAEC of radon and thoron progeny, respectively.

$N_{Po-218 \text{ in CH1}}$ and $N_{Po-214 \text{ in CH2}}$ are obtained by the following equations 3-7 and 3-8, respectively;

$$N_{Po-218 \text{ in CH1}} = N_{CH1} - \left(\frac{1}{0.6406} \right) N_{CH3} \quad (4-7)$$

$$N_{Po-214 \text{ in CH2}} = N_{CH2} - N_{CH3} \quad (4-8)$$

where N_{CH1} , N_{CH2} and N_{CH3} mean the alpha track count on CH1, CH2 and CH3, respectively. Therefore, $N_{Po-218 \text{ in CH1}}$ and $N_{Po-214 \text{ in CH2}}$ are counts per unit area of alpha track by $^{218}\text{Po} + ^{214}\text{Po}$ and ^{214}Po only, respectively.

The particle size distributions were described in terms of a log-normal distribution, defined by the activity median aerodynamic diameter (AMAD) and geometric standard deviation (σ_g). In addition to this numerical evaluation, the impactor data were also evaluated by a graphical method (Cumulative method) [64].

Detection limit

Detection limits in a measurement process can be explained as an analytical process leads to a quantitative detection and decides the results of analysis between a radioactive or non-radioactive. This is particularly relevant when the sample counts are very close to background and accurate measurements of sample counts and background counts must be made to distinguish the difference within reasonable error limits. The longer the counting time, the lower is detection level or minimal detectable activity (MDA). The MDA also referred to as the lower limits of detection (LLD) in Bq m^{-3} that yields a net count of above background with a 95% probability. In this case, LLD [68] can be expressed as:

$$LLD = \frac{2.706}{t} + 4.653 \sqrt{\frac{R_{bg}}{t}} \quad (4-9)$$

where t is collecting period in (min),

R_{bg} is the number of background alpha tracks on CR-39,

LLD is the lower limit of detection in track count.

The LLD can be converted to activity through the detector efficiency factor and a measured volume. Therefore, the LLD for EERC and EETC (LLD_{RnP} and LLD_{ThP} in Bq m^{-3}) are calculated by the following questions:

$$LLD_{RnP} = 0.09V_{total}^{-1} \quad (4-10)$$

$$LLD_{TnP} = 0.01V_{total}^{-1} \quad (4-11)$$

Where V_{total} is the total air volume passing through the impactor in (m^3),

For a period of 6 h continuous sampling 4 L min^{-1} , we have obtained 0.13 Bq m^{-3} and 0.02 Bq m^{-3} for EERC and EETC, respectively. The LLD will improve with longer sampling.

4.3.1 Humidity

In order to investigate the effect of humidity on the developed technique, the following environmental parameters in the radon chamber were set: temperature at 20°C and at different relative humidity e.g. 20, 60 and 90%. Two to three air samples were taken under each of environment conditions.

The data obtained in this experiment is shown in Table 4-7.

In this study, the influence of relative humidity on activity median aerodynamic diameter (AMAD) of particle size 0.3 and $1 \mu\text{m}$ using the developed technique was investigated. It was found that relative humidity had no effect on AMAD of particle size 0.3 and $1 \mu\text{m}$ using the developed technique. The aerosol material in this study was carnauba wax, which is insoluble in water. On the other hand, the size effect can be found, while increasing of relative humidity on fine salt aerosols such as NaCl, Na_2SO_4 and NaNO_3 [69].

Table 4-7 AMAD and σ_g at various relative humidity

Aerosol condition	Relative humidity (%)	AMAD(μm)	σ_g	Average AMAD (μm)
0.3 μm	30	0.433	2.08	0.431 \pm 0.003
		0.429	1.89	
	60	0.417	2.63	0.429 \pm 0.016
		0.440	1.91	
	90	0.383	2.94	0.415 \pm 0.045
		0.446	1.92	
1 μm	30	1.037	1.94	1.127 \pm 0.121
		1.264	1.92	
		1.079	1.78	
	60	1.129	1.97	1.100 \pm 0.028
		1.099	2.07	
		1.073	1.81	
	90	1.100	2.06	1.075 \pm 0.099
		1.159	1.99	
		0.966	1.97	

4.3.2 Temperature

In order to investigate the effect of temperature on the developed technique, the following environmental parameters in the radon chamber were set at 60 % relative humidity and temperature set at 10°C, 20°C and 30 °C. Two air samples were taken under each of environment conditions.

The data obtained in this experiment is shown in Table 4-8.

Table 4-8 AMAD and σ_g at various temperatures

Aerosol condition	Temperature °C	AMAD (μm)	σ_g	Average AMAD (μm)
1 μm	10	0.983	2.21	0.960±0.030
		0.971	1.88	
		0.926	1.94	
	20	0.989	2.32	0.944±0.040
		0.913	1.86	
		0.931	2.19	
	30	1.111	2.34	1.022±0.087
		0.937	1.81	
		1.017	1.84	

In this study, the influence of temperature on activity median aerodynamic diameter (AMAD) of particle size 1 μm using the developed technique was investigated. It was found that temperature had no effect on AMAD of particle size 1 μm . The aerosol material in this study was carnauba wax which melts at 80°C.

4.3.3 Unattached progeny

In order to investigate the effect of unattached progeny on the developed technique, with and without a 400-mesh metal wire screen (TETKO Inc., USA) was set at the top of the impactor sampler. The 400-mesh wire screen can prevent invasion of unattached progeny (1 - 10 nm) by diffusion with collection efficiency about 99.9%, while minimizing the collection by impaction and interception of attached progeny (0.1 – 10 μm) to less than 5%. These based on fan model filtration theory. Three different unattached fractions were tested. Table 4-9 shows experimental results for the effect of unattached progeny.

Table 4-9 Experimental results for the effect of unattached progeny

Test ID	Unattached fraction (f_u)	Track density (tracks/mm ²)							
		Stage 1		Stage 2		Stage 3		Stage 4	
		W	WO	W	WO	W	WO	W	WO
1	0.010	0.02±0.01	0.02±0.01	0.03±0.01	0.04±0.01	0.18±0.03	0.17±0.03	6.70±0.16	7.04±0.17
2	0.041	0.02±0.01	0.05±0.01	0.12±0.02	0.18±0.03	7.44±0.17	7.05±0.16	0.64±0.05	0.53±0.05
3	0.107	0.03±0.01	0.11±0.02	0.03±0.01	0.08±0.02	0.19±0.03	0.20±0.03	0.65±0.05	0.68±0.05

W =with 400-mesh wire screen

WO=without 400-mesh wire screen

The track density in test ID2 and 3 were observed higher about 2.5 and 3.7 times for stage 1 and 1.5 and 2.7 times for stage 2, respectively on unused the 400-mesh wire screen. This is due to the unattached radon progeny deposited on the CR-39 surface. To reduce this effect, the 400-mesh wire screen should be used in the sampling system of impactor sampler.

4.3.4 Changing of air sampling flow rate

In order to investigate the effect of air flow rate change on the developed technique, six different airflow rates were tested (1, 2, 3, 3.5, 4, and 4.5 Lm⁻¹). One or Two air samples were taken under each of airflow rate. Table 4-10 shows experimental results for the effect of airflow rate change.

In this study, the influence of airflow rate on activity median aerodynamic diameter (AMAD) of particle size 1 μm was investigated. It shows that the airflow rate change about 50-75% had more effect on AMAD about 20-40%. This effect due to the particle cut off diameters of each stage was changed according to airflow rate change. In the case of airflow rate change from 4 to 1 Lm⁻¹, the cut off diameter of stage 1st to 4th were calculated and found that it changed to 20, 5, 2 and 1 μm , respectively.

Table 4-10 Experimental results for the effect of airflow rate change

Aerosol condition	Airflow rate (Lm ⁻¹)	AMAD (μm)	σ_g	Average AMAD (μm)	
1 μm	1	0.611	2.30	0.611	
	2	1.284	2.19	1.284	
	3		1.094	2.25	1.108±0.019
			1.121	2.22	
	3.5		1.031	2.32	1.097±0.093
			1.163	2.10	
	4*		1.046	2.01	1.042±0.006
			1.037	1.94	
	4.5		0.980	2.08	1.089±0.156
			1.197	2.17	

* The proper airflow rate for portable impactor in this study.

4.4 Validation of developed technique

The AMAD of attached radon progeny in this study was verified using ELPI and MOUDI. Three aerosol particles with peak diameter of 0.3, 0.5 and 1 μm were tested.

In this study, the impactor sampler and measuring technique described earlier. It was operated at a flow rate of 4 Lmin^{-1} for a period of 5 min. After sampling, it was left for 4 hour to allow all ^{214}Bi decay to ^{214}Po .

The equilibrium-equivalent ^{222}Rn concentration (EERC) from each CR-39 was calculated theoretically by the equation 3-5. In this equation, η is the collection efficiency of CR-39, that was estimated to be 11.84% for measuring the alpha particles emitted from aerosols and impinge on CR-39 through the proper Al film and 10.01% for measuring the alpha particles emitted from the surface of the glass fiber filter and impinge on the CR-39 through an air layer of 22.5 mm and the proper Al film.

In case of ELPI, the attached radon progeny was collected on the aluminum foil as a material substance at a flow rate of 29.4 Lmin^{-1} for 5 minutes. After sampling, activity on the aluminum foil from stages 3rd -7th (for 0.3 μm), 4th-8th (for 0.5 μm), 6th-10th (for 1 μm), were simultaneously measured using ZnS(Ag) scintillation detectors. The tests were also conducted with MOUDI to verify the size distribution of the developed technique with a diameter of 1 μm ., Attached radon progeny were collected on the removable impaction plates in MOUDI, which used grease coating on each plate at a flow rate of 30 Lmin^{-1} for 5 minutes. After sampling, activity on the removable impaction plates from stages 5rd -9th (for 0.3 μm), 5th-9th (for 0.5 μm), 4th-7th (for 1 μm), were simultaneously measured with ZnS(Ag) scintillation detectors. The activity concentrations of radon progeny for ELPI and MOUDI at each stage were analyzed by using the decay method.

During the sampling period of ELPI, MOUDI and 4-stages impactor, a 400-mesh metal wire screen was set at the inlet of each sampler to prevent invasion of unattached progeny, and the collection efficiency was estimated to be 92.4%, 92.2%, and 99.9%, respectively based on fan model filtration theory. Two or Three air samples were taken under each condition.

Verification experimental results are shown in Table 4-11 and the example of activity size distribution of radon progeny from each impactor is shown in Figure 4-16.

To validate the developed technique with the commercial devices e.g. ELPI and MOUDI was conducted to obtain activity size distribution of radon progeny of particular particle size. Results have been given in Table 4-11 that the activity median aerodynamic diameters (AMAD) calculated by developed technique are corresponding with commercial devices from the range of 0.5 to 1 μm . However, AMAD from our technique was 43 % less effective than commercial devices at 0.3 μm . Due to our cut off diameter in last stages of impactor (0.5 μm) is bigger than 0.3 μm . In this case, the dose conversion factor was calculated using a dosimetric approach seemed to increase about 6% (Table 4-12). Moreover, the dose conversion factor of our technique at AMAD about 0.5 and 1 μm seemed to increase with σ_g (Table 4-12) but less than 30%. Thus, for the measurements with particle size 0.3, 0.5 and 1 μm , this technique (4-stage impactor) was an alternative to ELPI and MOUDI from the viewpoint of dosimeter.

Table 4-11 Verification results of developed technique.

Test ID	AMAD(μm)		σ_g		Average AMAD (μm)	
	ELPI/MOUDI	4-stage impactor	ELPI/MOUDI	4-stage impactor	ELPI/MOUDI	4-stage impactor
0.3 μm ; Test with ELPI/MOUDI						
1	0.312	0.440	1.35	1.91	0.302 \pm 0.013	0.431 \pm 0.013
2	0.292	0.422	1.35	1.89		
0.5 μm ; Test with ELPI(1,2)/MOUDI(3)						
1	0.496	0.542	1.36	1.96	0.453 \pm 0.043	0.495 \pm 0.064
2	0.451	0.520	1.36	1.91		
3	0.411	0.422	1.43	2.01		
1 μm ; Test with ELPI(1-3)/MOUDI(4,5)						
1	0.995	0.942	1.29	1.77	1.076 \pm 0.083	1.035 \pm 0.089
2	1.168	1.073	1.43	1.81		
3	0.982	0.938	1.32	1.94		
4	1.108	1.125	1.46	1.93		
5	1.125	1.099	1.46	2.07		

Table 4-12 A comparison of dose conversion factor from dosimetric approach

ELPI/MOUDI		4-stage impactor		Dose conversion factor (nSv/(Bq h m ⁻³))		Difference value of dose (%)
Average AMAD (μm)	σ _g	Average AMAD (μm)	σ _g	ELPI/MOUDI	4-stage impactor	
0.302	1.35	0.431	1.90	9.41	9.93	6
0.453	1.38	0.495	1.96	7.82	10.12	26
1.076	1.39	1.035	1.90	14.73	16.43	11

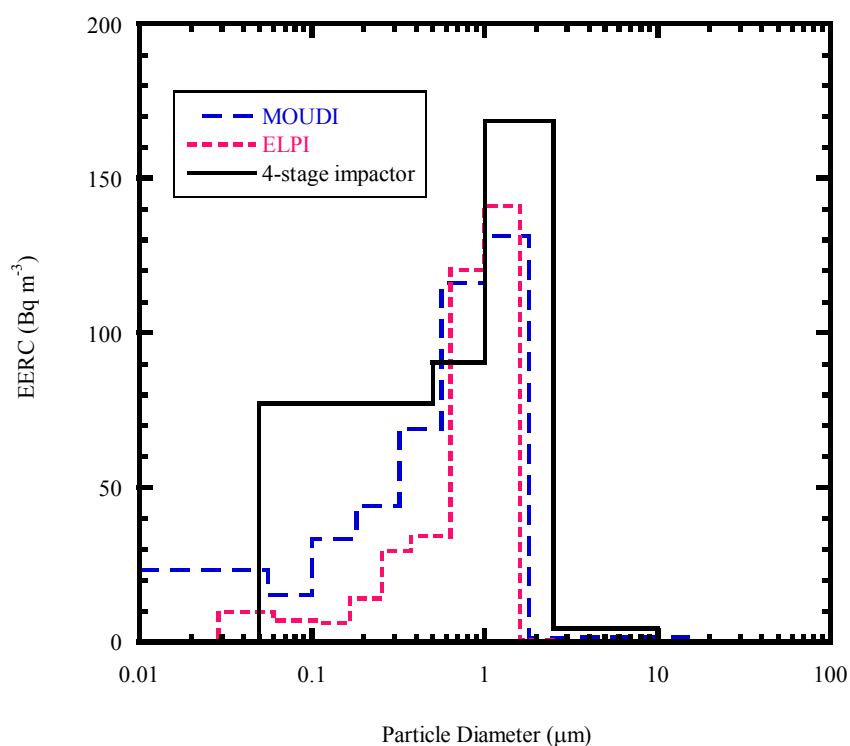


Figure 4-16 The activity size distribution of radon progeny: a) ELPI, b) MOUDI and c) 4-stage impactor. Sampling at radon concentration 5 kBq m⁻³ and aerosol size 1 μm was generated.

Chapter V

MEASUREMENT OF ATTACHED RADON AND THORON PROGENY SIZE DISTRIBUTION AND ESTIMATION OF DOSE ASSESSMENT IN THE MINERAL TREATMENT INDUSTRY

In this chapter, the main focus has been given to the temporal and spatial variation of attached radon and thoron progeny activity size distribution by developed technique and estimation of effective dose. The particle size distribution characterized by activity median aerodynamic diameter (AMAD) is a dominant parameter for dose assessment. At the very onset of the study, a field survey was conducted to speculate the spatial variations of attached radon and thoron progeny activity size distributions at a workplace in Phuket, Thailand. Final goal of this study was to estimate dose for worker.

5.1 Study location

Mineral treatment industry is located at Tambon Vichit, Amphur Muang Phuket, Thailand. The attached radon and thoron progeny activity size distributions were measured by developed technique at three areas such as health and safety office (HSE), ore sampling area and production storage area. The studies took place from 16th to 18th February, 2010. Figure 5-1 shows the location of measurement points.

5.2 Method and measurement set up

5.2.1 Determination of attached radon and thoron progeny activity size distribution

Measurements for the attached radon and thoron progeny activity size distribution have been performed using our modification portable cascade impactor consisting of four stages with a backup filter holder. The air flow rate through the impactor is 4 L min⁻¹ by a mini-pump (Sibata, MP-Σ500, Japan). The 50% efficiency aerodynamic cut-off diameters for the stages are 10, 2.5, 1, and 0.5 μm. Attached radon and thoron progeny aerosol particles were collected and measured. The unattached particles were separated at the entrance of impactor using a 400-mesh wire

screen. The aerosol collection time was 6 h and the cooling time was 4 d. The cooling time was set long enough to decay out ^{212}Pb (Thoron progeny) that has a half life of 10.64 h. After that, all the exposed CR-39 chips were chemically etched for 24 h in 6.25 N NaOH solution at 60 °C. The track densities were counted using an optical microscope.

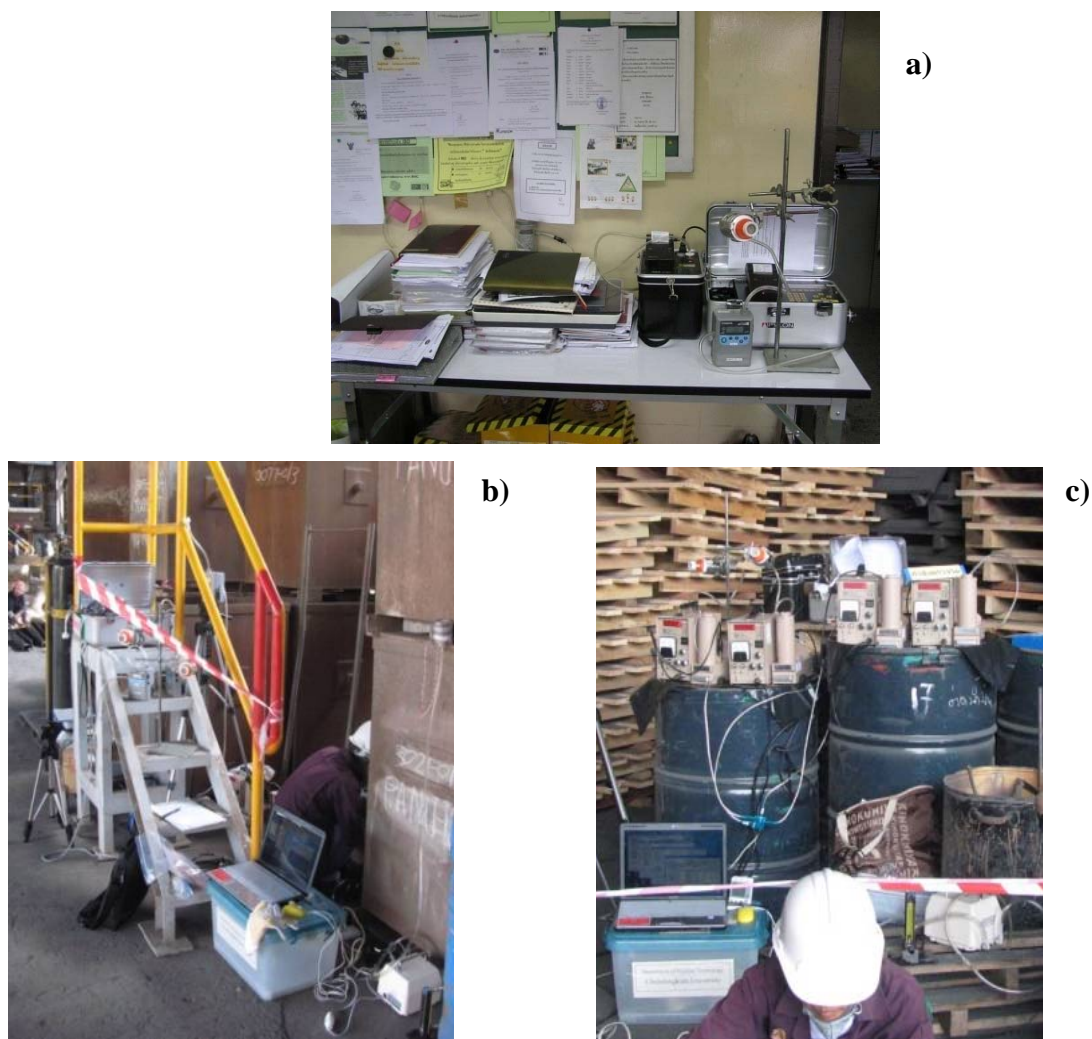


Figure 5-1 Location of measurement points at Mineral treatment industry, Phuket, Thailand: a) HSE office, b) Ore sampling area, and c) Production storage area.

5.2.2 Determination of radon, thoron and their progeny concentration

RAD-7 (DurrIDGE Co, Let., USA) was employed to monitor radon and thoron concentration. In this study, RAD-7 was employed for a minimum of 12 h to a maximum of 24 h to measure the activity concentration of radon and thoron at every 5 min interval by sniffer mode. During this period, setup of impactor and air sampling operates for a period of 6 h. The WLx portable working level radiation monitor (Pylon Electronics Inc., Model 147, and Canada) was operated for the same period of RAD-7 with a continuous sampling mode. This monitor uses 0.8 μm pore size and 25 mm diameter mixed cellulose-ester membrane filter (Millipor, USA) to estimate the activity concentration of radon and its progeny. After sampling, the total alpha activity on the membrane filter was measured by solid state detector and the working level (WL) concentration was calculated and recorded automatically.

Thoron progeny concentration was employed using CR-39 technique. The method used for this purpose is sampling air through an open-faced high efficiency filter paper (Whatman, \varnothing 25 mm, USA) at flow rate of 0.5 Lmin^{-1} for 24 h. In order to determine thoron progeny concentration, the registration on thoron progeny has to be distinguished from that of radon progeny. After air sampling is over, the filter is left for more than 6 h to allow radon progeny to completely decay. An aluminum foil with a thickness of 15 μm (4.0 mg.cm^{-2}) is then placed on the filter to reduce alpha particle energy emitted from ^{212}Po and to increase the detector effectiveness. Afterward, CR-39 detector is placed directly on the aluminum foil and left for about 2 d to allow registration of alpha tracks on the detector. All the detectors exposed were chemically etched for 24 hr in 6.25 N NaOH solution at 60°C and track density was counted by an optical microscope. From these data, EETC can be obtained with a proper calculation procedure [70].

The equilibrium factor “F” was determined from the ratio of the obtained equivalent equilibrium concentration of radon and thoron progeny to the concentration of radon and thoron.

5.3 Results of field survey

5.3.1 Attached radon and thoron progeny activity size distribution

The activity median aerodynamic diameter (AMAD) and geometric standard deviations (σ_g) of attached radon and thoron progeny in all experimental areas for Thaisarco is presented in Table 5-1 and the illustration of the particle size distribution is depicted in Figure 5-2.

Table 5-1 Size information of AMAD and σ_g of attached radon and thoron progeny at different places in Mineral treatment industry.

Study Areas	Radon progeny		Thoron progeny	
	AMAD (μm)	σ_g	AMAD (μm)	σ_g
1.HSE Office	0.469	2.19	0.451	2.20
2.Sampling area	0.527	2.39	ND	ND
3.Production storage area	0.722	2.47	0.420	2.27

ND: non-detectable (Lower than the detection limit: 0.13 Bq m⁻³ for radon progeny and 0.02 Bq m⁻³ for thoron progeny)

It could be observed from Table 5-1 that, AMAD at three areas' indoor environment in Mineral treatment industry for attached radon progeny varies from 0.469~0.722 μm with σ_g of 2.19~2.47 whereas for attached thoron progeny less variation from (0.420~0.451 μm) with σ_g of 2.20~2.27. It can be noticed in Table 5-1 that AMAD of attached radon progeny varied with location. On the other hand, similar size values are obtained in the case of attached thoron progeny. The different size of attached radon and thoron progeny may affect due to different aerosol sources and environment conditions: in the case of HSE office used air conditioner during the sampling period.

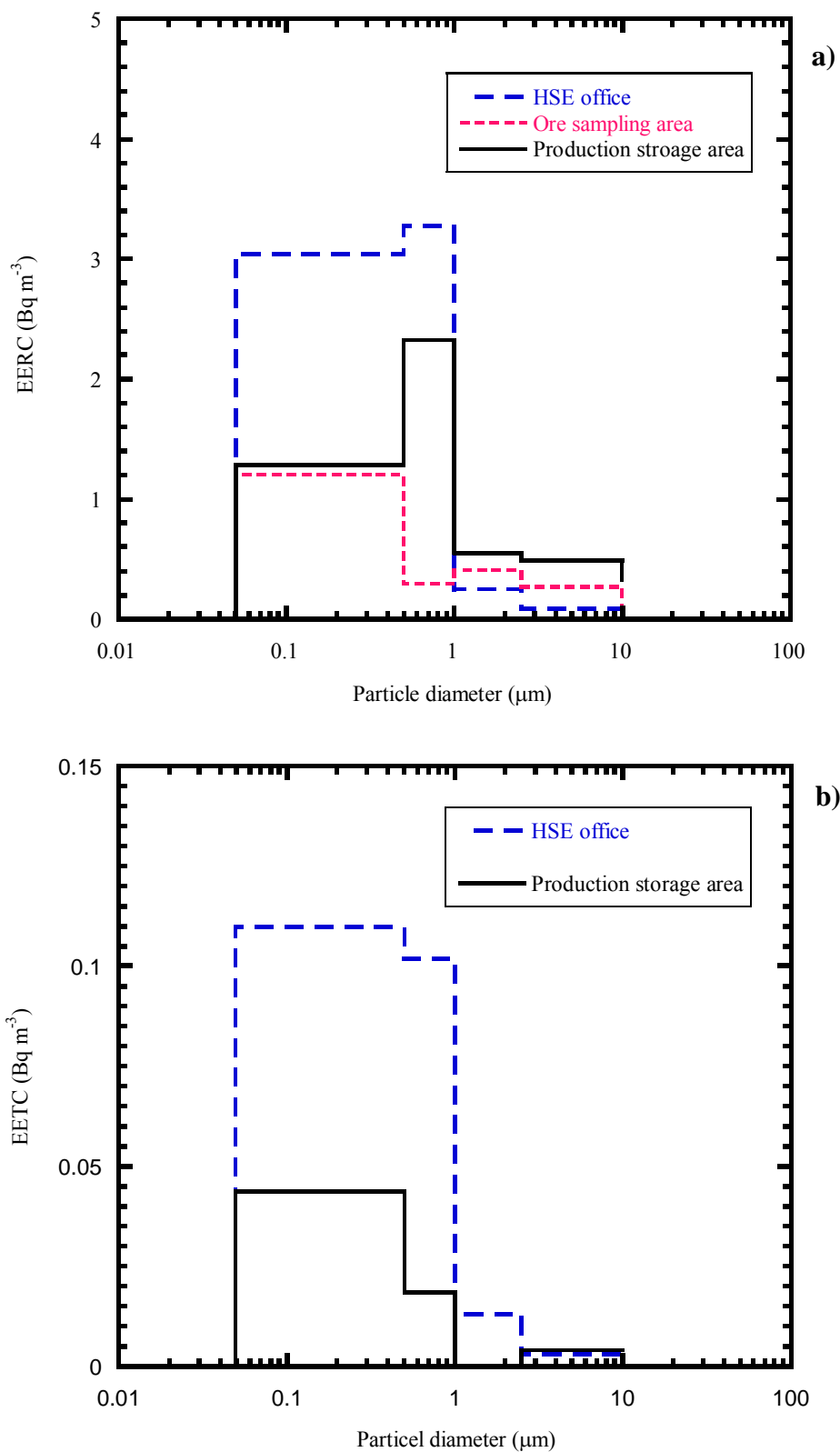


Figure 5-2 Illustration of the particle size distribution: a) attached radon progeny size distribution b) attached thoron progeny size distribution.

5.3.2 Determination of Equilibrium factor

The estimated activity concentrations of radon, thoron and their progeny corresponding to equilibrium factor “F” are represented in Table 5-2.

Table 5-2 Activity concentration of radon, thoron, their progeny concentration

Study area	Radon concentration (Bqm ⁻³)	Radon progeny Concentration (Bqm ⁻³)	F _{Rn}	Thoron concentration (Bqm ⁻³)	Thoron progeny Concentration (Bqm ⁻³)	F _{Tn}
1.HSE Office	12.73±1.79	6.66±0.27	0.52	12.01±4.76	0.43 ± 0.02	0.04
2.Ore Sampling area	4.74±2.25	4.24±0.74	0.89	20.65±4.49	0.14 ± 0.01	0.01
3.Production storage area	3.47±1.39	2.76±0.17	0.79	14.09±7.18	0.07 ± 0.01	0.01

F_{Rn}: Equilibrium factor of radon

F_{Tn}: Equilibrium factor of thoron

The activity concentration of radon, thoron and their progeny in workplace environment largely exhibits the indoor air quality. We have observed the average activity concentration of radon and thoron is almost equal at HSE office. On the other hand, thoron concentration was higher than radon concentration at ore sampling area as well as production storage area. That can be attributed to higher thorium than uranium concentration in ore and products [71]. In case of progeny concentrations, it is noticed that average radon progeny concentration is higher than average thoron progeny concentration at all study areas. Since uranium concentration is much higher than natural environmental samples, may be the reason why radon progeny is predominant over thoron progeny though thorium concentration is also high.

5.4 Dose assessment

For dose calculation of inhaled radon and thoron progeny, UNSCEAR [72] has come up with a very simple expression for calculating effective dose, E as follows:

$$E = C \times F \times T \times DCF \quad (5-1)$$

where, C = Rn/Tn concentration (Bq m⁻³)

F = Equilibrium factor of Rn/Tn

T = Occupancy factor (2000 h y⁻¹ for workplace and 7000 h y⁻¹ for home)

DCF = Dose conversion factor of Rn/Tn progeny (mSv (Bq m⁻³ h)⁻¹)

In this study, dose conversion factor of attached radon and thoron progeny were assessed using a computer program name LUDEP (Lung Dose Evaluation Program, distributed by NRPB) based on the ICRP 66 model. The input values for major parameters used for the calculation are listed in Table 2-1. It is considered that AMAD as one of the most important input parameter. Dose Conversion Factor (DCF) of attached radon and thoron progeny from LUDEP program are shown in Table 5-3.

Table 5-3 Dose Conversion Factor (DCF) of attached radon and thoron progeny by LUDEP.

Study areas	Dose Conversion Factor (DCF) nSv (Bq h m ⁻³) ⁻¹	
	Radon progeny	Thoron progeny
1.HSE Office	11.23	56.36
2.Sampling area	12.25	-
3.Production storage area	15.20	58.57
Average	12.89±2.06	57.47±1.56

Initially the radon and thoron progeny are formed as the unattached particles. Most of these unattached nuclei attach themselves to aerosol particles immediately after formation to produce attached radon and thoron progeny. Table 5-3 shows the particle size distribution of aerosol attached progeny influences the dose in the airways as particles of different size deposit.

In this study, measurement on unattached fraction of radon and thoron progeny size distribution has not been carried out. Dose conversion factor for unattached radon and thoron progeny by LUDEP has been suggested that AMAD and σ_g of a typical particle size distribution for the unattached are 1 nm and 1.3, respectively [45]. Therefore, DCFs of unattached radon and thoron progeny was calculated to be 8.66 and 21.91 nSv (Bq h m⁻³)⁻¹, respectively. Thus, the dose conversion factor of radon and thoron progeny for mineral treatment industry were calculated to be 21.55 and 79.38 nSv (Bq h m⁻³)⁻¹, respectively. It shows that dose conversion factor of thoron progeny is about 3.5 times higher than dose conversion factor of radon progeny. In addition, dose conversion factors from this study are consistent with earlier studies [43] on the radon (ranging from 9-22 nSv (Bq h m⁻³)⁻¹)

and thoron progeny (ranging from 51 – 114 nSv (Bq h m⁻³)⁻¹) dose conversion factors using the ICRP-66 human respiratory tract model [32].

It is a general practice in radon and thoron dosimetry to measure radon and thoron concentration and then translate their concentrations into individual radon and thoron progeny concentrations using equilibrium factor “F”. The factor “F” for this study were experimentally determined by measuring radon and thoron concentration using RAD-7, WLx portable working level radiation monitor and CR-39 technique to obtain the values of potential alpha energy concentration of radon and thoron progeny, respectively. The experimentally obtained equilibrium factors have already been presented in Table 5-2. Consequently, the rough dose assessment for study areas at mineral treatment industry were calculated from equation 5-1 with relates parameters. The effective dose for radon, thoron and their progeny is presented in Table 5-4.

Table 5-4 Annual effective doses at Mineral treatment industry due to exposure of radon, thoron and their progeny

Study areas	Annual effective dose (mSv y ⁻¹)		
	E_{Rn}	E_{Tn}	<i>total</i>
1.HSE Office	0.29	0.08	0.37
2.Sampling area	0.18	0.03	0.21
3.Production storage area	0.12	0.02	0.14

E_{Rn} and E_{Tn} is annual effective dose from radon, thoron and their progeny, respectively.

It is observed from Table 5-4 that effective dose for the three areas of mineral treatment industry, varies from 0.14 mSvy⁻¹ to 0.37 mSvy⁻¹, which is in the acceptable range resulting in equivalent dose to a single public member (lower than 1 mSvy⁻¹). In addition, most of effective dose for workers at mineral treatment industry are due to the inhalation of radon and thoron.

5.5 Conclusions

The field survey on attached radon and thoron progeny size distribution assess dose in working environment. The experimental sites were selected at the Mineral treatment industry. The following conclusion can be made from the experimental findings:

The mean radon and thoron concentration at three usual experimental sites ranges from 3.47±1.39 to 12.73±1.79 Bq m⁻³ and 12.01±4.76 to 20.65±4.49 Bq m⁻³,

respectively. It was found that thoron concentration was higher than radon concentration.

The AMAD of attached radon size distribution varied in between 0.469 μm ~0.722 μm at three locations. On the other hand, AMAD of attached thoron size distribution are 0.420 μm and 0.451 μm at HSE office and production storage area, respectively.

The ICRP 66 dosimetric approach through the use of LUDEP to estimate the effective dose of radon and thoron in three sites of Mineral treatment industry and was found to be 4-6 times higher radon dose than thoron. The implementation of particle size distribution, exposure time, breathing rate, equilibrium factor and the activity concentration of radon, thoron and their progeny altogether in LUDEP are required to make a significant dose assessment procedure. Such information will reflect about the actual situation and could be considered more compatible with the ambient environment to assess the effective dose due to inhalation of radon thoron and their progeny. These studies have impact on human health. Thus, a comparison has been made to visualize the workplace environment of Mineral treatment industry.

Chapter VI

SUMMARY AND CONCLUSIONS

In case of radiation protection two distinct objectives are identified; exposure assessment for individual worker to ensure compliance with exposure limit and area monitoring to maintain a safe working place and prevent high exposure. By deciding a monitoring program which takes these differences into account cost effectiveness can be increased and manpower requirement reduced. The main objective of this dissertation is to characterize radon, thoron and their progeny and estimate dose to the public since these are the most significant sources of natural radiation. In order to accurately estimate dose due to radon and thoron; not only the radon and thoron concentration is essential but also requires the activity median aerodynamic diameter (AMAD) derived from the activity-weighted size distribution of attached radon and thoron progeny on the particulate matters. In the case of both occupational and domestic exposure to thoron progeny are less well know but aerosol AMAD is probably larger than for radon progeny. Cascade impactor is well known as a tool to study airborne particles, because it provides means for direct determination of the distribution of aerodynamic diameter.

6.1 Conclusions and discussion

This study presents the successful development of the portable and economical technique for measuring the activity size distribution of attached radon and thoron progeny for dose assessment. In development of technique, performance test, effect of some parameters on sensitivity, validation and field test for dose assessment were studied. Results suggest about future improvements and to use successfully in field survey. It could be concluded as per following:

6.1.1 The 4-stages portable impactor has been designed and constructed according to the basic principles. Laboratory tests have been carried out in a standard laboratory of NIRS, Japan where radon and thoron chambers are calibrated with other international laboratories. Developed technique results are comparable with successfully with standard ones. Impactor could separate particles in the diameter ranges: <0.5, 0.5-1, 1-2.5, 2.5-10 and >10 μm , at an operation flow-rate of 4 L min^{-1}

by a battery-operated mini-pump. The collection efficiency as a function of particle size for the 0.5 and 1 μm cut-point stages were determined using monodisperse carnauba wax aerosols using glass fiber filter and aluminum-vaporized Mylar film disk as the substrate on impactor plate. Both substrates have the same 50 % collection efficiency cut-point (within experimental uncertainty of 95% confidence interval) at stage 3rd (1 μm) and stage 4th (0.5 μm), approximately at 0.95 ± 0.04 to 1.00 ± 0.03 μm and 0.50 ± 0.17 to 0.53 ± 0.06 μm , respectively. Thus, they are very close to the cut-point diameters those suggested by Rader et al [74]. The square root of the Stokes number at a 50% collection efficiency was found to 0.54 and this was comparable with reported value [63, 74]. The advantages of developed impactor are :

- It is suitable for using in the field where direct electric power supply is not available.

- It has a reasonable price (130,000 baht) in comparison with commercial items (870,000-3,000,000 baht).

The disadvantage is only a small amount of particle would be collected due to the limitation of 4 liter/min flow rate of DC pump that present available in the market. However, it is not much a significant factor.

6.1.2 Simultaneous measurement of radon and thoron progeny technique was developed using the combination of CR-39 detector and aluminum-vaporized Mylar film for the activity size distribution. The following findings were obtained from the experiment studies;

6.1.2.1 The proper aluminum-vaporized Mylar film density for cutoff alpha energy about 4.2, 6.1 and 7.7 MeV of uranium-thorium, ^{214}Po and ^{214}Pb , respectively was confirmed by track density on CR-39 detector at 2 geometries; a) the collection media side and b) the opposite side of backup filter.

6.1.2.2 The counting efficiencies of radon and thoron progeny alpha particles on CR-39 were estimated to be about 12 % and 10% at 2 geometries; a) the collection media side and b) the opposite side of backup filter, respectively. The detected efficiency of CR-39 detector found to be lower than a traditional ZnS (Ag) scintillation detector ($\approx 30\%$). This might be due to factors such as, background effects, losses due to the backward movement of the alpha particles, personnel error etc.

However, the obtained efficiency of the CR-39 is considered to be reasonable within the acceptable range. Nevertheless, CR-39 has other advantages comparing to a ZnS(Ag) detector, for instant: CR-39 has no mechanically affected by humidity and temperature, and it has lower price (144 chips \approx 10,000 Baht) than ZnS (Ag) scintillation detector (60,000 Baht).

6.1.3 Influence of sensitive parameters such as relative humidity (30-90%), temperature (5-30 °C), unattached progeny, changing of air sampling flow-rate (\approx 12-75%), were investigated. It was found that high- unattached radon progeny (at radon concentration \approx 10 kBq m⁻³) enhanced deposition effect on impactor stage 1st (10 μ m) and stage 2nd (2.5 μ m) about 4 and 3 times, respectively in comparison to normal condition. In addition, the changing of activity median diameter (AMAD) could not be observed at different relative humidity, temperature and changing of air flow-rate at about 20-40%.

6.1.4 Validation of developed technique with the commercial devices was performed at aerosol sizes 0.3, 0.5 and 1 μ m and radon concentration of 5,000 Bq m⁻³. ELPI and MOUDI instruments were used as references of particle sizes and ZnS(Ag) scintillation counters was used as alpha detectors. It is found that AMAD measured by the developed technique can be compared with commercial devices in the range of 0.5 to 1 μ m. However, developed technique shows smaller AMAD of 43% at 0.3 μ m than the commercial devices. When the dose conversion factor was considered, it seemed to increase by 6 %. This technique can demonstrate as an alternative to commercial devices from the viewpoint of dosimeter. Thus, the developed technique could be employed in determining size distribution characteristics of attached radon and thoron progeny aerosols for dose assessment study.

6.1.5 The developed technique was tested in field for dose assessment. The experimental results in dose calculations by LUDEP showed that AMAD play a significant role on the particle size distribution of attached radon and thoron progeny. The dose conversion factor from short term measurement due to exposure from inhalation of radon and its progeny shows high dose conversion factor of thoron 4 times than dose conversion factor from radon and its progeny. This study can be

compared with previous reports published elsewhere [43] and effective dose for the workers exposed to radon is about 4-6 times higher than thoron.

Thus, it concludes that this new finding technique and device is suitable for measuring of attached radon and thoron progeny size distribution in the viewpoint of the dosimeter because

- 1) It is a passive device that is easily to handle and operate with DC power,
- 2) It has low cost consumption,
- 3) It is simple to carry for a field measurement,
- 4) It has efficiency good enough to detect radon and thoron progeny alpha particles.

6.2 Suggestions and future studies

Suggestions and future studies are as follow;

6.2.1 There are some experiments that could not be completed during this investigation due to limitation of laboratory facilities such as collection efficiency of impactor stage 1st (10 μm) and stage 2nd (2.5 μm).

6.2.2 The effect of relative humidity, temperature on the measuring sensitivity should be studied in laboratory with hygroscopic aerosols in the future. These factors might play an important role in activity size distribution of attached radon and thoron progeny as well as the mass size distribution studies [73].

6.2.3 In case of using this developing technique to measure attached radon and thoron progeny at different aerosol size conditions smaller than 0.2 μm , the impactor system should have the lowest cutpoint diameter smaller than 0.5 μm to be more effective on AMAD.

6.2.4 The radon and thoron related radiation dose varies considerably. The factors that influence the variability are manifold and not well understood. Among them are radioactive source, particle characteristics, its transport, and behavior patterns on movement. Further studies should be focused to assess the temporal and spatial variation of activity size distribution on seasonal basis of attached radon and

thoron progeny. The particle size distribution characterized by AMAD is a dominant parameter for dose assessment.

6.2.5 For proper dose assessment by LUDEP, the actual parameters, such as unattached fraction, equilibrium factor, AMAD of attached and unattached radon and thoron progeny should be measured at in-situ.

6.2.6 The objective of measurement and monitoring must be to achieve and maintain safe working conditions for occupationally exposed groups and safe environmental conditions for members of the general public. Monitoring must also demonstrate compliance with national dose standards. It should enable the effectiveness of environmental control measures to be evaluated and also provide estimates of exposure suitable for future analysis of epidemiological data. Considering these objectives, monitoring for occupational exposure should combine operational monitoring for control of the workplace with individual monitoring of high risk workers. For non-occupational exposure it is first necessary to identify areas or types of housing with enhanced levels of radon and thoron progeny exposure, for which individual measurements in selected dwellings are required. Subsequent monitoring must then be concerned with achieving or demonstrating compliance with national standards.

Regulation of NORM has not been implemented yet in Thailand. Such type of studies is important to support while preparing guideline of NORM and radiological impact assessment by NORM to industry workers and the public.

6.3 List of publications

6.3.1 Kranrod, C., Tokonami, S., Ishikawa, T., Sorimachi, A., Janik, M., Shingaki, R., Furukawa, M., Chanyotha, S., Chankow, N. "Mitigation of the effective dose of radon decay products through the use of an air cleaner in a dwelling in Okinawa, Japan" Applied Radiation and Isotopes, Volume 67, Issue 6, June 2009, Pages 1127-1132.

6.3.2 Kranrod, C., Chanyotha, S., Chankow, N., Tokonami, S., Ishikawa, T., Sahoo, S.K. "Simple Technique for Determining the Equilibrium Equivalent Thoron Concentration Using a CR-39 Detector: Application in Mineral Treatment Industry" Radioprotection, Volume 44, Number 5, June 2009, Pages 301-304.

6.3.3 Kranrod, C., Ishikawa, T., Tokonami, S., Sorimachi, A., Chanyotha, S., Chankow, N. “Comparative dosimetry of radon and thoron” Radiation Protection Dosimetry 141 (2010) : 424-427.

6.3.4 Kranrod, C., S., Sorimachi, A., Tokonami, S., Ishikawa, T., Chanyotha, S., Chankow, N., Pattarasumunt A., “A Simple Technique for Measuring the Activity Size Distribution of Attached Radon and Thoron Progeny” The 5th International Symposium on Radiation Safety and Detection Technology (ISORD-5), 15-17 July 2009. Kitakyushu International Conference Center, Kitakyushu, Japan.

REFERENCES

- [1] United Nations Scientific Committee on the Effects of Atomic Radiation. Sources and effects of ionizing radiation. Report to the General Assembly of the United Nations with Scientific Annexes. New York : United Nations publication, (2000).
- [2] World Health Organization. WHO handbook on indoor radon. A public health perspective. Geneva : WHO, (2009).
- [3] Shimo, M., Torii, T., and Ikebe, Y. Measurements of unattached and attached RaA atoms in atmosphere and their deposition in human respiratory tract. Journal of the Atomic Energy Society of Japan 23 (1981) : 851-861.
- [4] Ito, N., and Mizohata, A. Concentration variation of atmospheric sulfate observed at Sakai, Osaka from 1986 to 1995. Journal of Aerosol Research 13 (1998) : 343-353. (in Japanese).
- [5] Butterweck, G., Porstendörfer, J., Reineking, A., and Kesten, J. Unattached fraction and aerosol size distribution of the radon progeny in a natural cave and mine atmospheres. Radiation Protection Dosimetry 45 (1992) : 167-170.
- [6] Tsujimoto, T., and Miyake, H. Continuous measurement of the size distribution of radon progeny using drum impactor. KURRI Progress Report 1995 (1995) : 220-230.
- [7] Tu, K.W., Fisenne, I., and Hutter, A. Short and long-lived radionuclide particle size measurements in a Uranium mine. EML. U.S. DOE Report EML-588, 1997.
- [8] Yamasaki, K. Size selective performance of low pressure Andersen sampler and its application to activity size distribution radon progeny. In Katase, A. and Shimo, M. (eds.), Radon and Thoron in the human environment. pp.73-78. Singapore : World Scientific Publishing Co. Pre. Ltd. 1998.
- [9] Iimoto, T., Kawashima, K., and Kasako, T. Using an Imaging plate to measure the concentration of radon progeny in Air. Radioisotopes 53 (2004) : 461-468.
- [10] Danis, A., Oncescu, M., and Ciubotariu, M. System for calibration of track detectors use in gaseous and solid alpha radionuclides monitoring. Radiation Measurements 34 (2001) : 155-159.

- [11] Abdel-Naby, A., Pálfalvi, J., and Durrani, S.A. Alpha-particle spectrometry with CR-39 using combined chemical and electrochemical etching. Nuclear Tracks 12 (1986) : 205–210.
- [12] Khayrat, A.H., and Durrani, S.A. Variation of alpha-particle track diameter in CR-39 as a function of residual energy and etching conditions. Radiation Measurements 30 (1999) : 15-18.
- [13] Amero, C., Golzarri, J.I., Izerrouken, M., and Espinosa, G. ^{148}Gd , ^{238}U , ^{239}Pu and ^{244}Cm alpha particle energy analysis using tracks in solids. Radiation Measurements 34 (2001) : 341-343.
- [14] Espinosa, G., Golzarri, J.I., and Bogard, J.S. Radon and progeny alpha-particle energy analysis using nuclear track methodology. Journal of Radioanalytical and Nuclear Chemistry 277 (2008) : 131-135.
- [15] Pressyanov, D.S., Guelev, M.G., and Pentchev, O.J. Integrated measurements of short-lived ^{222}Rn progeny by rotating filters. Health Physics 64 (1993) : 522-527.
- [16] Zhuo, W., and Iida, T. An instrument for measuring equilibrium-equivalent ^{222}Rn and ^{220}Rn concentrations with etched track detectors. Health Physics 77 (1999) : 365–370.
- [17] Zhuo, W., and Iida, T. Estimation of thoron progeny concentrations in dwellings with their deposition rate measurements. Health Physics 35 (2000) : 365-370.
- [18] Friedlander, S.K. The characterization of aerosols distributed with respect to size and chemical composition. Journal of Aerosol Science 1 (1970) : 295-307.
- [19] Martin, J.E. Physics for radiation protection. 2nd. Germany : Wiley-VCH, 2006.
- [20] Porstendörfer, J., Zock, Ch., and Reineking, A. Aerosol size distribution of the radon progeny in outdoor air. Journal of Environmental Radioactivity 51 (2000) : 37-48.
- [21] Knutson, E., and Whitby, K. Aerosol classification by electric mobility: apparatus, theory, and applications. Journal of Aerosol Science 6 (1975) : 443-451.
- [22] Wang, S., and Flagan, R. Scanning electrical mobility spectrometer. Aerosol Science and Technology 13 (1990) : 230–240.

- [23] Becker, K.H., Reineking, A., Scheibel, H.G., and Porstendörfer, J. Radon daughters' activity size distributions. Radiation Protection Dosimetry 7 (1984) : 147-150.
- [24] Yamada, Y., Tokonami, S., and Yamasaki, K. Applicability of the electrical low pressure impactor to size determination of aerosols attached to radon decay products. Review of Scientific Instruments 76 (2005) : 065102-065104.
- [25] Rahman, N.M., et al. Evaluation of aerosol sizing characteristic of an impactor using imaging plate technique. Radiation Protection Dosimetry 123 (2007) : 171-181.
- [26] Mohamed, A. Activity size distribution of short-lived radon progeny in indoor air. Radiation Protection Dosimetry 86 (1999) : 139-145.
- [27] Tu, K.W., and Knutson, E.O. Size distribution of radon progeny aerosol in the working area of a dry former uranium mine. Environmental Interactions 22 (1996) : S617-S622.
- [28] Tokonami, S., Takahashi, F., Iimoto, T., and Kurosawa, R. A new device to measure the activity size distribution of radon progeny in a low level environment. Health Physics 73 (1997) : 494-497.
- [29] Bohr, N. On the theory of the decrease of velocity of moving electrified particles on passing through matter. Philosophical Magazine 25 (1913) : 10-31.
- [30] Bethe, H. Zur Theorie des Durchgangs schneller Korpuskularstrahlen durch Materie. Annual Physic 5 (1930) : 325-400. (in German)
- [31] Bloch, F. Bremsvermögen von Atomen mit mehreren Elektronen. Zeitschrift für Physik 81 (1933) : 363-376. (in German)
- [32] Ziegler, J.F., Biersack, J.P., and Littmark, U. The Stopping and Ranges of Ions in Solids. Oxford : Pergamon Press, 1985. (The code is available on <http://www.srim.org>)
- [33] International commission on radiological protection (ICRP). Human respiratory tract Model for radiological Protection. ICRP Publications 66. Annual ICRP 24. Oxford : Pergamon Press, 1994.
- [34] Birchall, A. A demonstration of LUDEP. 2nd Reprinted. The Assessment of doses from occupational intakes of radionuclides, 6-10. Mol, Belgium, 1997.

- [35] International commission on radiological protection (ICRP). Limits for Intakes of radionuclides by Worker. ICRP Publications 30. Part 1. Annual ICRP 2. Oxford : Pergamon, 1979.
- [36] International commission on radiological protection (ICRP). Report of Committee II on permissible Dose for Internal radiation (1959), Health Physics 3 (1960) : 1-380.
- [37] Harvey, R.P., and Hamby, D.M. Uncertainty in particulate deposition for 1 μ m AMAD particles in an adult lung model. Radiation Protection Dosimetry 95 (2001) : 239-247.
- [38] Ishikawa, T., Tokonami, S., Yonehara, H., Fukutsu, K., and Yamada, Y. Effects of activity size distribution on dose conversion factor for radon progeny. Japanese Journal of Health Physics 36 (2001) : 329-338.
- [39] Ishikawa, T., Tokonami, S., and Nemeth, C. Calculation of dose conversion factors for thoron decay products. Journal of Radiological Protection 27 (2007) : 447-456.
- [40] Porstendörfer, J., and Reineking, A. Radon: characteristics in air and dose conversion factors. Health Physics 76 (1991) : 300-305.
- [41] Porstendörfer, J. Physical Parameters and Dose Factors of the Radon and Thoron Decay Products. Radiation Protection Dosimetry 94 (2001) : 365-373.
- [42] Marsh, J.W., et al. Uncertainty analysis of the weighted equivalent lung dose per unit exposure to radon progeny in the home. Radiation Protection Dosimetry 102 (2002) : 229-248.
- [43] Nuccetelli, C., and Bochicchio, F. The thoron issue: monitoring activities, measuring techniques and dose conversion factors. Radiation Protection Dosimetry 78 (1998) : 59-64.
- [44] Kranrod, C., Ishikawa, T., Tokonami, S., Sorimachi, A., Chanyotha, S., and Chankow, N. Comparative dosimetry of radon and thoron. Radiation Protection Dosimetry 141 (2010) : 424-427.
- [45] Kranrod, C., et al. Mitigation of the effective dose of radon decay products through the use of an air cleaner in a dwelling in Okinawa, Japan. Applied Radiation and Isotopes 67, (2009) : 1127-1132.

- [46] Sanada, T., Fujimoto, K., Miyano, K., Doi, M., Tokonami, S., Uesugi, M., and Takata, Y. Measurement of nationwide indoor Rn concentration in Japan. Journal of Environmental Radioactivity 45 (1999) : 129–137.
- [47] Thomas, J.W. Measurement of radon daughters in air. Health Physics 23 (1972) : 783–792.
- [48] Tokonami, S. Determination of the diffusion coefficient of unattached radon progeny with a graded screen array at the EML radon/aerosol chamber. Radiation Protection Dosimetry 81 (1999) : 285–290.
- [49] Tokonami, S., Ichiji, T., Imoto, T., and Kurosawa, R. Calculation procedure of potential alpha energy concentration with continuous air sampling. Health Physics 71 (1996) : 937–943.
- [50] Cliff, K.D. The measurement of low concentrations of radon-222 daughters in air, with emphasis on RaA assessment. Physics in Medicine and Biology 23 (1978) : 25–65.
- [51] Virgil, A.M., Kenneth, L.R., and Stephen, M.B. A micro orifice uniform deposit impactor (MOUDI): Description, calibration and use. Aerosol Science and Technology 14 (1991) : 434–446.
- [52] Cheng, Y.S., and Yeh, H.C. Theory of a screen-type diffusion battery. Journal of Aerosol Science 11 (1980) : 313–320.
- [53] McLachlan, G., and Krishnan, T. The EM Algorithm and Extensions. Wiley series in probability and statistics, New York : John Wiley & Sons, 1997.
- [54] Nagda, N.L., Rector, H.E., and Koontz, M.D. Guidelines for Monitoring Indoor Air Quality. New York : Harper & Row, 1987.
- [55] Li, C.S., and Hopke, P.K. Efficiency of air cleaning systems in controlling indoor radon decay products. . Health Physics 61 (1991) : 785–789.
- [56] Maher, E.F., Rudnick, S.N., and Moeller, D.W. Effective removal of airborne ²²²Rn decay products inside buildings. . Health Physics 53 (1987) : 351–356.
- [57] Ruzer, L.S., and Harley, N.H. Aerosol Handbook : Measurement, Dosimetry and Health Effects. New York : CRC Press, 2005.
- [58] Hinds, W.C. Aerosol Technology, Properties, Behavior and Measurement of Airborne Particles. New York : Wiley & Sons, 1982.

- [59] Trust Science Innovation (TSI) Incorporated. Mechanisms of Filtration for high Efficiency Fibrous Filters. Application Note ITI-041 [Online]. 2008. Available from : <http://www.tsi.com/documents/ITI-041.pdf> [May 2008]
- [60] Hopke, P.K., Montassier, N, and Wasiolek, P. Evaluation of the effectiveness of several air cleaners for reducing the hazard from indoor radon progeny. Aerosol Science and Technology 19 (1993) : 268–278.
- [61] Tokonami, S., Matsuzawa, T., Ishikawa, T., Iimoto, T., Yonehara, H, and Yamada, Y. Changes of indoor aerosol characteristics and their associated variation on the dose conversion factor due to radon progeny inhalation. Radioisotopes 52 (2003) : 285–292.
- [62] Marple, V.A., and Liu, B.Y.H. Characteristics of lamina jet impactors. Environmental Science and Technology 8 (1974) : 648-654.
- [63] Marple, V.A., and Willeke K. Impactor design. Atmospheric Environment 10 (1976) : 891-896.
- [64] Hinds, W. C., Aerosol Technology: Properties, Behavior, and Measurement of Airborne Particles. 2nd Edition. New York : John Wiley & Sons, 1999.
- [65] Rao, N.P., and Navascues, J., Fernandez de la Mora, J. Aerodynamic focusing of particles in viscous jets. Journal of Aerosol Science 24 (1993) : 879-892.
- [66] Tremblay, R.J., Leclerc, A., Mathieu, C., Pepin, R., and Townsend, M.G. Measurement of radon progeny concentration in air by alpha-particle spectrometric counting during and after air sampling. Health Physics 36 (1979) : 401-411.
- [67] Marple, V.A., and Willeke, K., Inertial impactors: theory, design and use. B.Y.H. Liu, Editor, Fine particles: Aerosol generation, measurement, sampling, and analysis. 411-416. New York : Academic Press, 1976.
- [68] Currie, L.A. Limits for qualitative detection and quantitative determination : Application to radiochemistry. Analytical Chemistry 40 (1968) : 586-593.
- [69] Dawei, H., et al. Hygroscopicity of Inorganic Aerosols: Size and Relative Humidity Effects on the Growth Factor. Aerosol and Air Quality Research 10 (2010) : 255-264.

- [70] Kranrod, C., Chanyotha, S., Chankow, N., Tokonami, S., Ishikawa, T., and Sahoo, S.K. Simple Technique for Determining the Equilibrium Equivalent Thoron Concentration Using a CR-39 Detector: Application in Mineral Treatment Industry. Radioprotection 44 (June 2009) : 301-304.
- [71] Kranrod, C., Kritsanawanat, R., Chanyotha, S., Tokonami, S., and Sahoo, S.K. Measurement of uranium and its activity ratio in some selected Thailand TENORM samples. Proceedings of 3rd Asian and Oceanic Congress on Radiation Protection. Tokyo, Japan, 2010.
- [72] United Nations Scientific Committee on the Effects of Atomic Radiation (UNSCEAR). Report sources and effects of ionizing radiations. Report to the General Assembly with Scientific Annexes. New York : United Nations, 2006.
- [73] Varuntida, V. Ambient and laboratory studies of aerosol size distributions and hygroscopicity. Doctoral degree thesis, Chemical Engineering, California Institute of Technology, 2006.
- [74] Rader, D.J., and Marple, V.A. Effect of ultra-stokesian drag and particle interception on impaction characteristics. Aerosol Science and Technology 4 (1985) : 141-156.
- [75] May, K.R. Calibration of a modified Anderson Bacterial aerosol Sampler. Applied Microbiology 12(1964) : 37-43.
- [76] Picknett, R.G. A new method of determining aerosol size distributions from multistage sampler data. Journal of Aerosol Science 3 (1972) : 185-198.
- [77] American Industrial Hygiene Association. Particle sampling using cascade impactors: Some practical application notes. Fairfax, VA, USA : AIHA Publications, 1995.
- [78] Marple, V.A., Olson, B.A., Santhanakrishnan, K., Roberts, D. L., Mitchell, J.P., and Hudson-Curtis, B. Drug Delivery to the Lungs –XIV. The Aerosol Society, 37-40. London, UK, 2003.
- [79] Rader, D.J., and Marple, V.A. Effect of gravitational forces on the calculation of impactor efficiency curves. B.Y.H. Liu, D.Y.H. Pui and H.J. Fissan, Editors, Aerosols, 123-126. New York, USA : Elsevier, 1984.

- [80] Fang, C.P., Marple, V.A., and Rubow, K.L. Influence of Cross-flow on Particle Collection Characteristics of Multi-nozzle Impactors. Journal of Aerosol Science 22 (1991) : 403-415.
- [81] Anderson, A. New sampler for the collection, sizing and enumeration of viable airborne particles. Journal of Bacteriology 76 (1958) : 471-484.
- [82] Mc Farland, A.R., Wedding, J.B., and Cermak, J.E. Wind tunnel evaluation of a modified Anderson impactor and an all weather sampler inlet. Atmospheric Environment 11 (1997) : 535-539.
- [83] Yamasaki, K., Yamada, Y., Miyamoto, K., and Shimo, M. Responses of low pressure Andersen sampler for collecting substrate. Proceeding of 10th International Congress of. IRPA. Hiroshima, Japan, 2000.

APPENDICES

APPENDIX A

Particle Sizing Method

There are various methods used in particle sizing. The most widely used techniques are discussed below:

A-1 Techniques for Measuring Natural Radioactive Aerosol

Sieves: Sieve is an old fashioned, but cheap and readily usable technique for large particles such as those found in mining and some food processing applications. It allows separation into some size bands if required. Using this technique it is not possible to measure sprays or emulsions and dry powders under 38mm. The longer the measurement times the smaller the answer, as particles orient themselves to fall through the sieve. A true weight distribution is not produced as the method relies on measuring the second smallest dimension of the particle. It is a low-resolution method.

Sedimentation: In Sedimentation, the speed of particles falling in a suspension liquid is determined with the help of light or X-ray beams. The particle size is then expressed in terms of the equivalent spheres which have the same settling speed in laminar flow conditions. Centrifuges are sometimes used to accelerate sedimentation process. This technique has a resolution that is many times that of Dynamic Light Scattering (DLS) and also has excellent reproducibility. But sedimentation technique has a limited range, with particular difficulties below 2 mm and above 50 mm. Moreover this method depends on the ambient temperatures that affect viscosity. Other disadvantages include slowness of measurement, which makes repeat measurements tedious. Irregularly shaped particles, such as disc-shaped, take even longer to settle due to their increased drag compared with spherical particles.

Electrozone Sensing: Electrozone sensing technique was originally developed for sizing blood cells. It is difficult to measure emulsions and impossible to measure sprays. This method is slow for materials of relatively wide particle size and it is not easy to measure particles below 2 mm. Optical and Electron Microscopy is an excellent technique that allows direct examination of the particles, and one that is relatively cheap. However, it is not suitable for measuring airborne particles. A quick look with a microscope applying this technique often gives a great deal of information that other methods are unable to give. The method inspires great confidence in the results. However, the number of particles measured applying this technique is usually

small compared to other particle sizing methods, so representative sampling becomes critical. And also the sample preparation for electron microscopes is slow, expensive, and requires considerable technical expertise.

Microscopy: This is an excellent technique that allows direct examination of the particles in question, and one that is relatively cheap. However, it is not suitable as a precise measurement technique beyond the level of simple judgment. Also, as relatively few a particles are examined, there is a real danger of unrepresentative sampling and if weight distribution is measured results are magnified. Missing one 10 mm particle has the same effect as missing one thousand 1mm particles. Sample preparation for electron microscopy is laborious and slow, and for manual methods fewer particles are examined.

Laser Diffraction: Laser diffraction method utilizes a laser beam (a source of coherent, intense light of a fixed wavelength) that passes through a sample of particles, and light intensity data is collected at different (low) scattering angles away from the axis of the laser beam. The method relies on the fact that diffraction angle is inversely proportional to particle size. Laser diffraction method can measure dry powders and liquid suspensions and emulsions, as well as sprays and aerosols. It is very fast in data collection with proper sample preparations, high reproducibility and precision; it is relatively simple to use. But this method is based on the assumption of sphericity of the measured particles. The laser diffraction method is precise but for particles with low aspect ratio, the results are inherently non-accurate, regardless of the definition of a “true” particle size. The measurement depends on the optical parameters (refractive index, light absorption) used to calculate the scattering properties of the particles. Light absorption characteristics are often unknown and must be "estimated". In addition, no multiple, or subsequent, scattering is considered. Resolution is limited by the number of detectors. The larger the measured particles, the lower the resolution of laser diffraction systems are.

Dynamic Light Scattering (DLS): Dynamic Light Scattering (DLS) or Photon Correlation Spectroscopy (PCS) technique monitors the doppler shifts in reflected laser light created by the Brownian motion of submicron fine particles. A minimum amount of information about the sample is needed to run an analysis. But this

measuring technique has extremely low resolution; The method does not really provide much "size distribution" data, only a mean size and estimate of standard deviation.

Time of Flight Mass Spectrometry (TOFMS): Time of Flight Mass Spectrometry (TOFMS) technique works with dry powders. It has broad total measurement range, -0.2 to 700 μm . The technique also has fast analysis time, normally about 1 minute. Although by this technique, liquid suspensions of particles may be difficult or impossible to measure. Particles $<0.2 \mu\text{m}$ can't be measured; measurements below 0.5 μm will likely be low resolution. High resolution analysis is not possible due to physical limitations of the method.

Focused-Beam Reflectance Measurement (FBRM): Focused-Beam Reflectance Measurement (FBRM) is a particle size determination technique based on a laser beam focusing in the vicinity of a probe sapphire window. The beam follows a circular path at speeds of up to 6 m s⁻¹. When it intersects with the edge of a particle passing by a window surface, an optical collector records a backscatter signal. The time interval of the signal multiplied by the beam speed represents a chord length between two points on the edge of a particle. The chord length distribution (CLD) can be recalculated to represent either a number or volume weighted particle size distribution. And this method provides on-line and in situ information about the chord length distribution (CLD) of a population of particles in dispersion. But a measured CLD does not directly represent a particle size distribution (PSD). Conversion of CLD to PSD is not straightforward and requires sophisticated mathematical software that is not easy to validate.

Laser Obscuration (Time-of-Transition): Laser Obscuration (Time-of- Transition), the Ankersmid systems are based on well-founded principles of the Laser Obscuration, or Time of Transition (TOT) theory. A sample containing moving or stationary particles is scanned with a focused He-Ne laser beam, rotating with a constant frequency by a wedge prism. Since the angular velocity is known, the size of each individual particle can be calculated from the duration and form of the beam obscuration signal. This has got a very fast data collection with proper sample preparations, very high reproducibility. The TOT method refers directly to particle

size rather than to any secondary properties. This eliminates inconsistencies due to refractive index, density and viscosity variations, Brownian motion, thermal convection and other physical phenomena. But measurement minimum of 0.5 μm . Need to change lenses (once) to cover the whole distribution from 0.5 to 3600 μm .

Inertial Impactors: Inertial impactors are devices widely used for the sampling and size selective collection of aerosol particles. Their principal of operation is simple: an aerosol stream passes through a nozzle and impinges upon a collection plate. Particles in the aerosol stream having large enough inertia will impact upon the collection plate while the other particles will follow the airflow out of the impaction region. There are two classes of inertial impactors: single stage impactors and multiple stage impactors (also called cascade impactors). The cascade impactors are commonly used to determine the aerosol size distribution. They have sharp cut-point characteristics, low internal particle holdup, and are easy to operate. Particles can be collected on substrates for microscopic analysis or additional measurements of mass or composition. They are designed for applications where wide size-range coverage and fast response are required.

APPENDIX B

Impactors in Particle Size Distribution

Impactors are simple devices, consisting of air flowing around a body or an impaction plate. Particles with sufficient inertia will slip across the air streamlines and impact on the impaction surface. Particles with less inertia will not slip across the streamlines sufficiently to strike the surface and will instead follow the airflow from the impaction area. In the impactor air is drawn through a series of orifices of decreasing size; the air flow is normal to collecting surfaces on which aerosols are collected by inertial impaction. The particles, separated stepwise by their momentum differences into a number of size ranges, are collected simultaneously.

B-1 Constructional Details

Typically, cascade impactors are consists of a number of impactor stages connected in series. Each stage of a cascade impactor is made up of a number of nozzles and an impaction plate arranged perpendicular to the flow of sampled air stream as shown in Figure B-1.

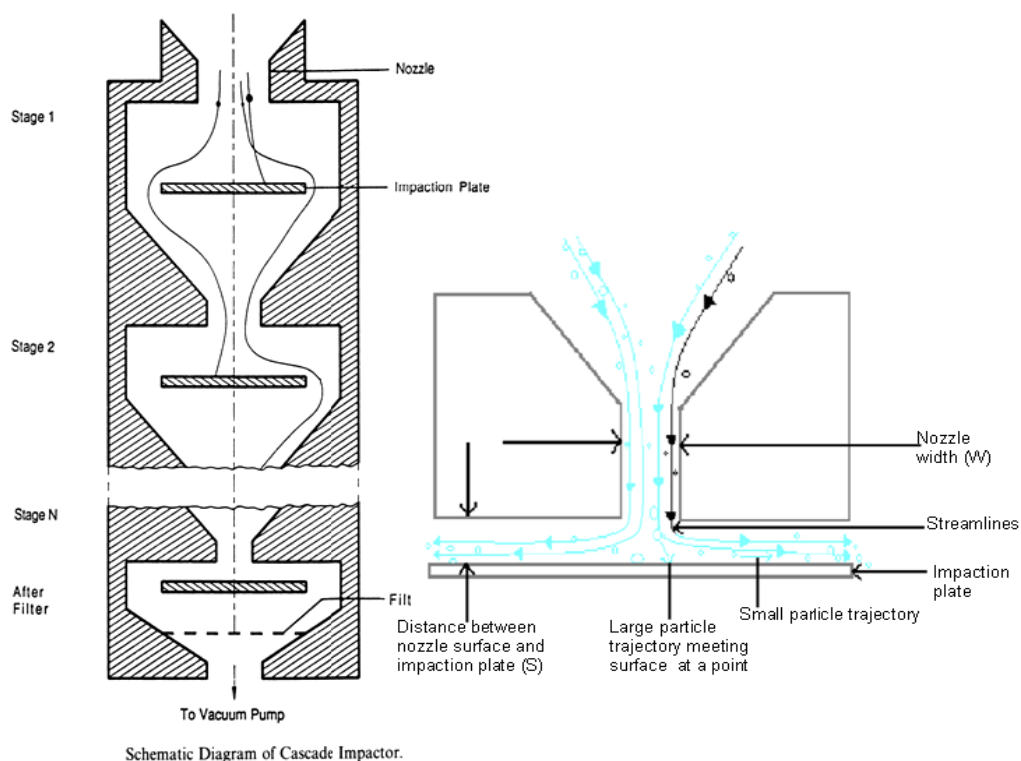


Figure B-1 Schematic projection of one single stage within impactor, showing divergent streamlines in flow approaching collection surface.

Nozzle plate of each stage of the impactor comprises of circular shaped nozzles of diameter W and the flat circular impaction plate is placed at a fixed distance S from the nozzle plate. In each stage an aerosol stream passes through the nozzle and impinges upon the plate. Particles in the aerosol stream having a large enough inertia will impact upon the plate, and smaller particles will pass as an aerosol onto the next stage. The magnitude of this differing inertia reflects the resistance to a change in direction of the laminar flow streamlines [45, 46]. As the incoming flow passes through the nozzle plate, the impaction plate deflects the flow to form an abrupt 90° bend in the streamlines.

By designing each successive stage with higher aerosol velocities in the nozzle, smaller diameter particles will be collected at each stage. Particles too small to be collected in the last stage are generally collected on an after-filter. The particulate mass deposited on each stage is determined using well-established techniques such as gravimetric or atomic absorption spectrometry (AAS) or by any other radiation detector. For associated radioactivity, the deposits are analyzed for alpha or beta-gamma activity.

B-2 Principle of Impactor

The theory of impactors has been well developed by Marple and colleagues over several years, based on a two-dimensional solution of the Navier-Stokes equations defining the gas flow field in the absence of particles, and then using Newton's equation of motion to model the passage of different sized particles through various stage geometries [62, 63, 74].

Good understanding of the design basis has been achieved on the subject of impactors since they were first introduced by May [75]. Computer-based analysis for prediction of fluid flow and particle trajectories has enabled the development of design guidelines. These have helped in enabling the impactors to operate according to specific requirements with sharp cut-off characteristics.

An impactor is composed of a nozzle plate bearing N number of nozzles, each of diameter W , an impaction plate and a stage wall. Among these, the nozzle plate plays the most important role in determining the particle collection efficiency. Impactors that have a 'sharp cut-off' collection efficiency curve approach the ideal step-function in which all particles greater than a certain aerodynamic size are

collected and all particles less than that size pass through. This size is called the cut-off diameter of the stage. The response of an impactor is characterized by the dimensionless parameter, the Stokes number S_{tk} , defined as:

$$S_{tk} = \frac{\rho_p V_0 C D_p^2 18 \mu}{W/2} \quad (\text{B-1})$$

where, ρ_p is the density of particles, V_0 the flow velocity through the nozzle, D_p the diameter of particles, μ the dynamic viscosity of the fluid medium, W the nozzle diameter and

The Cunningham slip correction factor C , given by the following expression:

$$C = 1 + \frac{0.163}{D_p P} + \left[\frac{0.054}{D_p P} \times e^{(-6.66 D_p P)} \right] \quad (\text{B-2})$$

where, P is the absolute atmospheric pressure (atm) upstream of the nozzle and D_p is specified in units of mm. The quantity of interest while designing an impactor is the S_{tk50} , which is the Stokes number that gives 50% collection efficiency. This is equivalent to assuming that the mass of particles larger than the cut-off size that get through equals that of the particles below the cut-off size that are collected.

The standard value for S_{tk50} calculated for a circular jet impactor is 0.25, while that for a rectangular jet is 0.59. As it is more convenient to make circular nozzles with precision, it was decided to develop the impactor with circular jets and hence all further design parameters were estimated using the value of 0.25 for S_{tk50} .

The particle collection efficiency (E) of an ideal impactor stage, expressed as a percentage, will increase in a step-wise manner between limits of zero to 100% at a critical value of S_{tk} . In practice, for a well designed stage, E is a monotonic sigmoidal function of S_{tk50} or d_p that increases steeply from $E \sim 0\%$ to $>95\%$, typically reaching its maximum steepness when E is 50% that is represented in Figure B-2, corresponding to the stage effective cut-off diameter, also termed its d_{50} value.

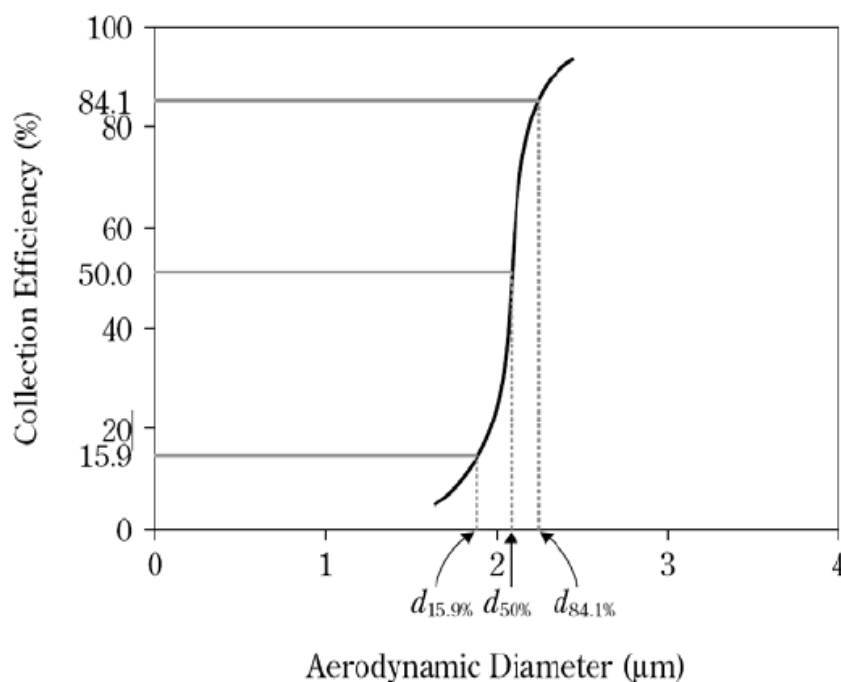


Figure B-2 Idealized collection efficiency curve for a single round-nozzle impactor stage.

It is possible to take into account the shape of the actual collection efficiency curve of the stage in the analysis of impactor data [76], but this refinement is rarely done for measurements of inhaler performance. Instead, the assumption is made that the mass of particles larger than d_{50} that penetrate the stage, is exactly compensated by the mass associated with particles finer than this size, that are collected [77]. Thus the d_{50} value is a constant for a given stage at a fixed flow rate. Marple et al. [78] and more recently Rader et al. [79], with an improved theory taking into account the effect of ultra-Stokesian drag, have identified that $\sqrt{S_{tk}}$ at E_{50} ($\sqrt{S_{tk50}}$) should be close to 0.49 for well-designed round-nozzle impactors as shown in Figure B-2, where differences in particle inertia dominate the size separation process. The $\sqrt{S_{tk50}}$ remains close to this value when the flow Reynolds number is within the range from 500 to 3000 [62].

The sharpness of cut of a given stage is defined in terms of the geometric standard deviation (GSD) of the collection efficiency curve, derived from the expression:

$$GSD_{stage} = \left(\frac{d_{84.1}}{d_{15.9}} \right)^{\frac{1}{2}} \quad (\text{B-3})$$

where, $d_{84.1}$ and $d_{15.9}$ are the sizes corresponding to the 84.1 and 15.9 percentiles of the curve by analogy with the log-normal distribution function expressed in cumulative form, to which the shape of the collection efficiency curve approximates as is seen in Figure B-2. GSD for a well functioning stage should ideally be <1.2 (the GSD for an ideal size fractionator would be 1.0) [78].

However, in practice, values in many designs of commercial impactor can exceed this limit, especially with stages that classify particles larger than 5 μm aerodynamic diameters, where gravitational sedimentation significantly contributes to the size separation processes [79]. The influence of gravity becomes especially evident at low flow rates with impactors such as the NGI that are designed to operate over a range of flow low rates [78].

For multi-orifice impaction stages, Fang et al. [80] also identified the importance of the cross-flow parameter (X_c), as a parameter that affects stage GSD. X_c is defined as:

$$X_c = \frac{nW}{4D_c} \quad (\text{B-4})$$

where, D_c is the diameter of a cluster of nozzles on the stage and n is the total number of nozzles on a stage. If the value of this dimensionless parameter is greater than 1.2, the potential exists for spent air leaving the orifices closer to the centre of the nozzle plate to interfere with the flow exiting the outer orifices, thereby preventing their flow from reaching the collection surface.

B-3 Chronicle of Impactor

There have been numerous impactor designed, built and described in various reports and in the open literature. Many impactors have been built for special studies, but only a few of the impactors have been widely distributed. Of the impactors that have been widely used, there are many writings in the literature describing variations and modifications made to these more “standard” impactors.

Of all the impactors, Anderson Cascade impactors have gained its enormous popularity. In 1956 the Anderson impactor was developed at Dugway Proving Ground for the specific purpose of determining the size distribution of viable airborne particles [81].

The impactor was consisted of six stages having 400 nozzles and impaction plates which were Petri dishes containing agar culture medium. The original prototype design used four stages consisted of 340 nozzles and impaction plate. After a sampling period, the Petri dish impaction plates were incubated and the viable deposits counted. May [75], did a redesign of the Anderson viable impactor after doing an extensive calibration and evaluation of stage deposit. In 1966 the Anderson viable impactor was modified for respiratory health hazard assessment of any airborne particles by substituting stainless steel impaction plates for the Petri dishes. The number and size of the nozzles per stage remained unchanged from the original viable sampler and this version was known as the nonviable Anderson impactor.

An MKI version of the impactor was introduced in about 1970 with the addition of two upper stages to make an eight-stage impactor with a larger cut size than the original. Later, the top two stages were modified and a pre-impactor was added in the MKII version following the work of Mc Farland et al. [82].

High Volume Cascade Impactors are commercially available to measure the size distribution and respirable mass fraction of airborne particles in outdoor and indoor environments. Compared to multiple circular jet designs, it has eight times the sensitivity, the sharpest cut-off, the lowest internal losses, and is easiest to use. They are designed to minimize particle reintrainment (or blow-off), to minimize inter-stage losses, and to maximize sharpness of cut-off.

MOUDI™¹ –micro-orifice, uniform-deposit impactor is a precision cascade impactors that provide high sampling flow rate, sharp cut-point, and low-loss characteristics. In the rotating version, the nozzle plates are rotated relative to the impaction plates to obtain near uniform particle deposit on the collecting substrate over the 25 mm impaction area. The aerosol particles are size-fractionated by the MOUDI™ into four equal geometrical increments per decade of particle size, making data interpretation simple and easy.

From 1970 forward, the design of impactors became rather routine work, and numerous impactors of all shapes and sizes for all manner of purposes now a day are designed and built.

B-4 The Low Pressure Andersen Cascade Impactor

Cascade impactors that are used in normal pressure suffer from the drawback of minimum size selection of 0.4 μm in diameter. The low pressure cascade impactors are thus in-use for the reason to have a choice of minimum size range from 0.02 to 0.06 μm in diameter along with the operating ability at the reduced pressure of a few tens of kilo-Pascals (kPa) [83]. Measurement of activity size distribution of radon decay products using several kinds of low pressure cascade impactors (e.g. Andersen, Berner, Davis, MOUDI etc) were reported in the literatures [4, 5, 6, 83]. Although several types of impactors have been designed and operated over the past few decades, the most widely used commercially available instrument is the Andersen impactor from Andersen Graseby Inc, USA. This is considered a standard instrument and has been widely tested and used in aerosol studies.

APPENDIX C

Radiation Detectors

1. Charcoal Canisters - Charcoal Canisters (CC) are passive devices requiring no power to function. The passive nature of the activated charcoal allows continual adsorption and desorption of radon. During the measurement period, the adsorbed radon undergoes radioactive decay. Therefore, the technique does not uniformly integrate radon concentrations during the exposure period.

2. Scintillation Counter- The scintillation counter is a solid state radiation detector which uses a scintillation crystal (phosphor) to detect radiation and produce light pulses. Scintillation counters are constructed by coupling a suitable scintillation phosphor to a light sensitive photomultiplier tube. This device is portable and easy to handle. There are three classes of solid state scintillation phosphors: organic crystals, inorganic crystals, and plastic phosphors. Inorganic crystals include lithium iodide (LiI), sodium iodide (NaI), cesium iodide (CsI), and zinc sulfide (ZnS). Inorganic crystals exhibit high efficiency for detection of gamma rays and are capable of handling high count rates. Organic scintillation phosphors include naphthalene, stilbene, and anthracene. This type of crystal is frequently used in the detection of beta particles. Plastic phosphors are made by adding scintillation chemicals to a plastic matrix. The plastic has high hydrogen content; therefore, it is useful for fast neutron detectors.

3. Solid State Nuclear Track Detector or SSNTD- is a sample of a solid material (photographic emulsion, crystal, glass or plastic) exposed to nuclear radiation, chemically etched, and examined microscopically. The basis of solid state nuclear track detection is that charged particles damage the detector within nanometers along the track in such a way that the track can be etched many times faster than the undamaged material. The size and shape of these tracks yield information about the mass, charge, energy and direction of motion of the particles. The main advantages over other radiation detectors are the detailed information available on individual particles, the persistence of the tracks allowing measurements to be made over long periods of time, and the simple, cheap and robust construction of the detector.

Alpha Track Detectors - An alpha track detector (ATD) consists of a small piece of plastic or film enclosed in a container with a filter-covered opening. Radon diffuses through the filter into the container and alpha particles emitted by the radon and its

decay products strike the detector and produce submicroscopic damage tracks. At the end of the measurement period, the detectors are returned to a laboratory and placed in a caustic solution that accentuates the damage tracks so they can be counted using a microscope or an automated counting system. The number of tracks per unit area is correlated to the radon concentration in air, using a conversion factor derived from data generated at a calibration facility.

CR-39, or Allyl di-glycol polycarbonate - is a piece of plastic material, which can register alpha particles that hit it. This alpha radiation, which comes from radon and its progeny, does microscopic damage to the surface of the plastics. After chemical etching the damaged area is enlarged and seen as tracks. The tracks can be counted and related to the radon concentration in the air in which the detector was exposed. *CR-39*, has exceptionally few background tracks and it is protected from electrostatic influence and optimally sensitive (may be used over 14 days and up to 1 year).

4. Liquid Scintillation Counters (LSC) - are traditional laboratory instrument with two opposing Photo multiplier Tubes (PMT) that view a vial that contains a sample and liquid scintillator fluid, or cocktail. When the sample emits a radiation (often a low energy beta) the cocktail itself, being the detector, causes a pulse of light. If both PMTs detect the light in coincidence, the count is tallied. This type of detector is very expensive and not portable. The benefit of this type of detector is that it can detect many different types of isotopes. Most modern LSC units have multiple sample capability and automatic data acquisition, reduction, and storage.

5. Proportional Counter- is a common laboratory instrument with sample counting tray and chamber and argon/methane flow through counting gas. Most units employ a very thin ($\mu\text{g cm}^{-2}$) window, while some are windowless. Shielding and identical guard chambers are used to reduce background and, in conjunction with electronic discrimination, these instruments can distinguish between alpha and beta radiation and achieve low MDAs. Similar to the LSC units, these proportional counters have multiple sample capability and automatic data acquisition, reduction, and storage.

6. Multi Channel Analyzer- Multi channel Analyzer System with a sodium iodide crystal and photo multiplier tube (PMT) is a solid-state germanium detector or a silicon-type detector can provide a powerful and useful capability for counting liquid

or solid matrix samples or other prepared extracted radioactive samples. Most systems are used for gamma counting, while some silicon detectors are used for alpha radiation. These MCA systems can also be utilized with well-shielded detectors to count internally deposited radioactive material in organs or tissue for bioassay measurements. In all cases, the MCA provides the capability to bin and tally counts by energy and thus identify the emitter. Again, most systems have automatic data acquisition, reduction, and storage capability.

Biography

Ms. Chutima Kranrod was born on April 1, 1976 at Samut parkan province. She graduated from Department of Applied Radiation and Isotopes, Faculty of Science, Kasetsart University in 1996 with a Bachelor of Science degree. Later, joined Department of Nuclear Technology, Faculty of Engineering, Chulalongkorn University and received Master of Science degree in Nuclear Technology in 2002. Then, continued in the same department as an assistant researcher under radionuclide analyses project for 3 years. In 2004, she was awarded a fellowship by Ministry of Education, Science and Technology (MEXT), Government of Japan to be trained in radon measurement techniques at National Institute of Radiological Sciences (NIRS), Japan. In 2006, she joined for a doctoral degree in nuclear technology at Department of Nuclear Technology, Chulalongkorn University. In 2007, she was awarded for the second time MEXT scholarship to undertake higher researches to facilitate her Ph.D. dissertation in NIRS for 11 months. In 2009, Prof. Dr. Shinji Tokonami invited her to continue her doctoral researches at NIRS for two more years. She presented her research papers at the international conference on Radioecology and Environmental Radioactivity at Bergen, Norway in June 2008 and in July 2009 presented another paper at 5th international Symposium on Radiation Safety and Detection Technology (ISORD-5) in Kitakyushu, Japan. These studies have resulted to three papers and have been submitted to Journal of Applied Radiation, Radioprotection and Isotopes and Radiation Protection Dosimetry.